

Conceptual Design Study

Designing a Next-Generation Radio Facility for Multi-Messenger Astronomy

Deliverable No: **D5.1**

Deliverable/Document Name: **D5.1 Report on RF simulations and results**

Version: **1.0**

Release date: **30/06/2024**

Dissemination level: **Public**

Status: **submitted**

Author: **UPRC**

Dr. Y. Stratakos

Dr. L. Marantis

V. Misirlis



This project has received funding from the European Union's Horizon Europe research and innovation programme under grant agreement **No 101094354**. The content of this material reflects the opinions of its authors and does not in any way represent the opinions of the European Union


Document history

Version	Date	Content and changes	Edited by
0.1	14/2/2023	Contents and Introduction	V. Misirlis
0.2	22/2/2024	Feed Design	Dr. Y. Stratakos
0.3	29/3/2024	Feed Simulations	Dr. Y. Stratakos
0.4	25/4/2024	Additional Plots	Dr. L. Marantis
0.5	20/6/2024	First review and Corrections	Prof. A. Kanatas
0.6	24/06/2024	Final corrections & modifications	Dr. L. Marantis
0.7	25/06/2024	Formatting corrections	V. Misirlis
0.8	26/06/2024	Final review	Prof. Kanatas

Peer reviewed by

Partner	Reviewer	Version Reviewed
FORTH	Dr. Stefanos Papadakis	0.8

Approved by

Partner	Name	Signature
UPRC	Dr. Leonidas Marantis	

Contents

Executive Summary 7

1 Introduction 8

1.1 Scope of the Deliverable8

2 Frontend Requirements..... 9

2.1 Antenna feed & reflector requirements.....11

3 Draft antenna-receiver scenarios..... 13

3.1 Introduction.....13

3.2 Antenna dish reflector structure13

 3.2.1 Case 1..... 14

 3.2.2 Case 2..... 15

3.3 Simulation setups15

4 Dual polarization feed horn antenna studies 17

4.1 Introduction.....17

 4.1.1 Straight flared horn feed 17

 4.1.2 Bell shaped flared horn feed 31

5 Antenna dish reflector studies..... 45

5.1 Antenna dish reflector calculation procedures comparisons.....45

 5.1.1 Antenna dish reflector with radiation source without blockage 46

 5.1.2 Antenna dish reflector with radiation source with blockage 49

 5.1.3 Antenna dish reflector including feeding antenna true geometry using SAM procedure (System Assembly modelling), unidirectional approach. 52

 5.1.4 Antenna dish reflector including feeding antenna true geometry using SAM procedure (System Assembly modelling), bidirectional approach. 55

5.2 Meshing approaches on SAM 3D EM Dish-Horn antenna simulations57

 5.2.1 Introduction 57

 5.2.2 Simulation results 59

5.3 Antenna dish reflector performance vs geometric anomalies.....71

 5.3.1 Introduction 71

5.4 Simulation results.....71

 5.4.1 Case 1..... 71

 5.4.2 Case 2..... 74

 5.4.3 Case 3..... 77

6 Additional Optimizations..... 80

6.1 K-type.....80

6.2 N-type.....81

6.3 Conclusions.....82

List of Figures

Table 2-1: Antenna System Requirements Table.10

Table 2-2: Antenna Feed & Reflector Requirements Table.12

Figure 3-1: Full parabolic reflector antenna system design.....13

Table 3-2: Draft specifications of the antenna system design.14

Figure 3-3: Full parabolic antenna system design with directional coupler.14

Figure 3-4: Full parabolic antenna system design without power splitter.15

Figure 4-1: Geometry of the straight flared horn feed.17

Figure 4-2: Far-field radiation patterns of horizontal polarization for 1 GHz.18

Figure 4-3: Far-field radiation patterns of vertical polarization for 1 GHz.18

Figure 4-4: Far-field radiation patterns of horizontal polarization for 2 GHz.19

Figure 4-5: Far-field radiation patterns of vertical polarization for 2 GHz.19

Figure 4-6: Far-field radiation patterns of horizontal polarization for 3 GHz.20

Figure 4-7: Far-field radiation patterns of vertical polarization for 3 GHz.20

Figure 4-8: Reflection coefficient.21

Figure 4-9: S parameters for design 1.22

Figure 4-10: Realized gain vs flare diameter.23

Figure 4-11: 3dB beamwidth (elevation) vs flare diameter.24

Figure 4-12: 3 dB beamwidth (azimuth) vs flare diameter.25

Figure 4-13: 12 dB beamwidth (elevation) vs flare diameter.26

Figure 4-14: 12 dB beamwidth (azimuth) vs flare diameter.27

Figure 4-15: Spill-over efficiency percentage vs flare diameter.28

Figure 4-16: 3D Radiation patterns port 1.29

Figure 4-17: 3D Radiation patterns port 2.30

Figure 4-18: Geometry of the feed.....31

Figure 4-19: Monopole Placement.....31

Figure 4-20: Far-field radiation patterns of horizontal polarization for 1 GHz.32

Figure 4-21: Far-field radiation patterns of vertical polarization for 1 GHz.32

Figure 4-22: Far-field radiation patterns of horizontal polarization for 2 GHz.33

Figure 4-23: Far-field radiation patterns of vertical polarization for 2 GHz.33

Figure 4-24: Far-field radiation patterns of horizontal polarization for 3 GHz.34

Figure 4-25: Far-field radiation patterns of vertical polarization for 3 GHz.34

Figure 4-26: Reflection coefficient.35

Figure 4-27: S parameters for design 2.36

Figure 4-28: Realized gain vs flare diameter.37

Figure 4-29: 3 dB beamwidth (elevation) vs flare diameter.38

Figure 4-30: 3 dB beamwidth (azimuth) vs flare diameter.39

Figure 4-31: 12 dB beamwidth (elevation) vs flare diameter40

Figure 4-32: 12 dB beamwidth (azimuth) vs flare diameter41

Figure 4-33: Spill-over efficiency percentage vs flare diameter.42

Figure 4-34: 3D Radiation patterns port 1.....43

Figure 4-35: 3D Radiation patterns port 2.....44

Figure 5-1: Gain variation over frequency.....46

Figure 5-2: 3dB beamwidth variation over frequency47

Figure 5-3: Radiation patterns over frequency.48

Figure 5-4: Gain variation over frequency.....49

Figure 5-5: 3dB beamwidth variation over frequency50

Figure 5-6: Radiation patterns over frequency.51

Figure 5-7: Gain variation over frequency.....52

Figure 5-8: 3 dB beamwidth variation over frequency.....53

Figure 5-9: Radiation patterns over frequency.54

Figure 5-10: Gain variation over frequency.....55

Figure 5-11: 3 dB beamwidth variation over frequency.....56

Figure 5-12: Radiation patterns over frequency.57

Figure 5-13: General dish-horn geometry.....58

Table 5-14: Simulation cases.....58

Figure 5-15: S_{11} , S_{22} simulation results over frequency, 5% convergence.....60

Figure 5-16: S_{11} , S_{22} simulation results over frequency, 1% convergence.....61

Figure 5-17: Dish antenna Gain over frequency, 5% and 1% convergence.....64

Figure 5-18: 3 dB beamwidth of dish antenna gain over frequency, 5% and 1% convergence.....66

Figure 5-19: Ultra-Low Mesh 5% Convergence67

Figure 5-20: Ultra-Low Mesh 1% Convergence67

Figure 5-21: Low Mesh 5% Convergence68

Figure 5-22: Low Mesh 1% Convergence68

Figure 5-23: High Mesh 5% Convergence69

Figure 5-24: High Mesh 1% Convergence69

Figure 5-25: 3D Radiation patterns of the Dish antenna70

Figure 5-26: Parabolic dish geometry.....71

Figure 5-27: Gain variation vs frequency72

Figure 5-28: 12 dB, 10 dB, 3 dB beamwidths variation vs frequency.....73

Figure 5-29: Parabolic dish geometry.....74

Figure 5-30a: Gain variation vs frequency75

Figure 5-30b: 12 dB, 10 dB, 3 dB beamwidths variation vs frequency.....76

Figure 5-31: Parabolic dish geometry77

Figure 5-32: Gain variation vs frequency77

Figure 5-33: 12 dB, 10 dB, 3 dB beamwidths variation vs frequency.....79

Figure 6-1: K-type Datasheet.....80

Figure 6-2: N-type Datasheet.....81

Executive Summary

The main target of this deliverable is to investigate and design the best possible feed and components for the ARGOS telescope antennas. Through the process, of creating a custom feed, low noise amplifiers, and filters, numerous of simulations are necessary to examine how different approaches behave in the system, and without breaking the borders of the ARGOS system requirements. The simulations also include alternative designs, to compare their pros and cons, and they made using the specifications of the reflector that ARGOS will use.

Two alternative dual polarization wideband horn feeds have been studied and optimized by means of 3D electromagnetic simulation using the commercial software tool CST Microwave Studio. Both alternative feeds show good performance but the bell-shaped flared horn is slightly better with respect to radiation pattern metrics. The bell-shaped flared horn has been chosen to be the ARGOS antenna feed, because of the better characteristics in comparison with the straight flared horn, as presented in this report.

Several 3D electromagnetic comparisons have been presented in this report vs numerous parameters that affect either simulation accuracy or simulation time efficiency for both feeds and the complete dish antennas. Also, simulations have been presented concerning the effects on dish antenna performance versus mechanical tolerances. Equipping an almost half-meter antenna such as ARGOS feed with the most suitable connector is crucial for ensuring reliable performance and long-term functionality. N-type connectors are specifically designed for achieving lower levels of losses than the K-type connectors. Furthermore, the robust build and weatherproof design of N-type connectors make them ideal for outdoor systems like ARGOS. Their secure threaded coupling mechanism ensures a vibration-resistant connection, a vital factor for maintaining signal integrity.

1 Introduction

Many of the most fundamental astronomical advances achieved in the past sixty years have been made through radio astronomy, and many more are expected in the following years, since the radio astronomical observations provide the only way to investigate some cosmic phenomena. ARGOS is a concept for a leading-edge, low-cost European astronomical facility that will directly address several fundamental scientific questions, from the nature of dark matter to the origin of Fast Radio Bursts and the properties of extreme gravity, thereby satisfying urgent needs of the community.

In order to observe what ARGOS is looking for, a complicated front-end RF chain is being developed, which will deliver the signal from each component making it available for capture. The very first stage of that chain is the reflector dish antenna with its feed, a seemingly simple device plays a pivotal role in receiving these faint signals, efficiently collecting them and funneling them into the receiver for further analysis. Through meticulous simulations and comparisons between different feed elements, we aim to identify the design that best satisfies the telescope's demanding requirements. Factors like beam pattern, illumination, and overall system efficiency will be thoroughly evaluated.

By optimizing the feed design, we try to unlock the full potential of the telescope. This translates to increased sensitivity, allowing us to detect fainter signals. A wider field of view enables us to observe a larger swathe of the sky, which is great for phenomena like Fast Radio Bursts. Ultimately, the perfect feed design empowers ARGOS to become a powerful tool for groundbreaking discoveries, pushing the boundaries of our cosmic knowledge.

Having a high-level feed antenna, that is able to collect the weak celestial signals, the rest of the signal chain plays an important role to improve and clean the signal, through the amplification and the filtering process. This process starts with the low noise amplifier which is responsible to amplify the signal improving the signal to noise ratio. At that step, it is important to have a clean gained signal, but not an overloaded or a supersaturated one, to avoid overflow in the dynamic range of the system.

At the stage of filters, a very specific part of the spectrum should pass this process, to remove all the unwanted signals that the feed will deliver to the system from frequencies that ARGOS is not interested in.

This report delves into the technical details of the RF front-end design for ARGOS. We will explore various feed element and components options through simulations, compare their performance, and ultimately identify the best possible feed design for ARGOS needs.

1.1 Scope of the Deliverable

The main scope of the deliverable is to report all the investigations about the RF front-end of the ARGOS radio-telescope. The RF front-end includes the important elements for the signal collection of the telescope. In order to achieve the most out of the instrument, it is necessary to have the best possible components, and the best possible combination of them. This leads in an extended analysis of them that is carried out in a series of simulation investigations. To determinate the gain, the losses and all the information regarding the RF chain of the telescope, several simulation processes were made on the feed design, the combination with the reflectors that are available in the market, and of course the rest of the electronic components of the RF chain such as the LNAs and the filters. All the above demonstrate specific gain and spectrum characteristics, and therefore should be thoroughly examined in order to select the best option for each part of the chain.

Through rigorous simulations, a performance comparison between two alternative feed elements is carried out, considering factors like the radiation pattern, the reflection coefficient, the illumination and the overall system efficiency. Our primary objective is to identify the optimal feed design that best satisfies the demanding requirements of the ARGOS system. This will involve a detailed evaluation ensuring the proposed design delivers the desired sensitivity, field of view and overall efficiency.

2 Frontend Requirements

The frontend subsystem encompasses several crucial components essential for the ARGOS system’s functionality. These include the parabolic dish and its steering mechanism, the feeder containing the antenna elements, as well as both passive and active analog signal components such as filters and amplifiers. Additionally, the frontend subsystem interfaces with the digitization system, facilitating the conversion of analog signals into digital format for further processing.

The following table provides a comprehensive summary of the requirements specifically pertaining to the parabolic dish and its associated steering mechanism. This table serves as a reference point for ensuring that these components meet the necessary specifications and performance criteria essential for the successful operation of the ARGOS system.

Requirement ID	Description	Parents	Issues / Notes
REQ-ARGOS-FE-01	ARGOS shall consist of at least 1200 parabolic reflectors (antennas)	L0_02, L0_22, L0_23, L0_30	
REQ-ARGOS-FE-02	The minimum distance between antennas shall be 23 m	L0_04	L0 requirement will likely be relaxed
REQ-ARGOS-FE-03	1024 of the antennas shall be arranged on a regular 32x32 grid, while the rest shall be randomly placed outside the grid	L0_08, L0_18	Under investigation
REQ-ARGOS-FE-04	The diameter of ARGOS antennas shall be 6m	L0_05, L0_30	
REQ-ARGOS-FE-05	The ARGOS antennas shall have a solid surface	L0_11	
REQ-ARGOS-FE-06	The surface of the ARGOS reflectors shall deviate from a perfect parabola by no more than 50mm	L0_11	
REQ-ARGOS-FE-07	The ARGOS receivers shall be positioned on the prime focus of the reflectors	L0_12, L0_13, L0_29	
REQ-ARGOS-FE-08	The antenna efficiency of the ARGOS reflectors shall be greater than 0.7	L0_02	
REQ-ARGOS-FE-09	The F/D ratio shall be 0.38	L0_05, L0_07, L0_15	Still under investigation, may change to 0.40
REQ-ARGOS-FE-10	The ARGOS feeds shall cover the frequency range from 1 to 3 GHz	L0_06, L0_09	

		L0_15	
REQ-ARGOS-FE-11	The ARGOS feeds shall capture vertical and horizontal polarizations	L0_16	
REQ-ARGOS-FE-12	The ARGOS feeds shall weight less than 10 kg	L0_02	Expected weight 3 - 4 kg
REQ-ARGOS-FE-13	The feed LNAs shall operate at ambient temperature	L0_02	
REQ-ARGOS-FE-14	The feed LNAs shall have a noise figure smaller than 35K	L0_02	
REQ-ARGOS-FE-15	The frontend shall offer a power attenuation mechanism	L0_17	
REQ-ARGOS-FE-16	The frontend shall offer an absolute calibration mechanism	L0_17, L0_18	
REQ-ARGOS-FE-17	The ARGOS antennas shall be mounted on altazimuth mounts	L0_04, L0_12	
REQ-ARGOS-FE-18	The ARGOS mounts shall be motorized	L0_12	
REQ-ARGOS-FE-19	The ARGOS mounts shall offer access to elevation angles between 0 - 90° and azimuth angles between 0 - 360°	L0_04, L0_12	
REQ-ARGOS-FE-20	The ARGOS antennas shall move with a velocity of up to 36° / minute	L0_04, L0_31	
REQ-ARGOS-FE-21	The ARGOS mounts shall position the antennas with an accuracy < 0.1°	L0_12, L0_13, L0_14	
REQ-ARGOS-FE-22	The ARGOS antennas shall operate under a wind load of at least 60 km/h	L0_23	
REQ-ARGOS-FE-23	The ARGOS antennas shall survive wind loads of at least 180 km/h	L0_01, L0_02, L0_03	

Table 2-1: Antenna System Requirements Table.

2.1 Antenna feed & reflector requirements

Starting the design of the RF chain, it is crucial to describe the system specification of the project, to use it as a guideline and as a limit controller. The RF chain starts with a parabolic mesh reflector antenna designed for operation within the 1-3 GHz frequency band. Due to budget constraints, a solid surface reflector has been declined. A cost-effective mesh reflector with mesh gap less than 0.9 cm ($\lambda/10$ allowance) can adequately operate up to 3 GHz. The operating frequency band (bandwidth) and polarization are also crucial for the feed design. Dual linear polarization is selected for the ARGOS feed antenna since it is often required in radio-telescopes and allows reception in both vertical and horizontal orientations.

A motorized azimuth-elevation (Az-El) mount is required in order to point the reflector antennas at each part of the sky, with a sidereal tracking that is not affected by Earth's rotation. The antenna's construction prioritizes sturdiness. A reinforced concrete support structure is employed to ensure the antenna can withstand strong winds, with a survival wind speed exceeding 150 km/h. Table 2-2 includes all the antenna system specifications (along with their specific values and critical comments) that were determined during the starting period of the ARGOS-CDS project.

<u>Antenna System Specification</u>	<u>Value</u>	<u>Comments</u>
No. of reflectors per antenna element	1	Due to budget constraints
Shape of reflector	Parabolic	
Type of reflector	Solid	Not applicable for Pathfinder due to budget constraints, Mesh will be employ for the Pathfinder with gap < 0.9 cm (3 GHz)
Feeder antenna position	Prime focus / axial – front fed	Due to budget constraints
Diameter of reflector	6 m	
F/D ratio	0.38	(or 0.40)
Frequency bandwidth	1-3 GHz	
Polarization	Dual linear polarization (Vertical - Horizontal)	
Dish gain	> 30 dBi (31.5 - 40.5 dB)	Depending on frequency
12dB feed taper angle	> 70° (75-95°)	Depending on frequency
Sidelobe level	< -25 dB	
Feeder horn gain	> 11 dBi (12-14 dBi)	
Polarization ports isolation	> 40 dB	Estimation
Return losses at both feeder ports	> 13 dB (min)	
Connector type	N-type	For low losses
Maximum power handling	10 W	Could be better if needed
Feeder antenna weight	< 10kg (expected 3-4kg)	
Type of mounting	Polar mount	Azimuth – elevation
Scanning abilities	Elevation range: 0-90°	

	Azimuth range: 0-360°	
Type of motion	Motorized motion	Too heavy antenna system for manual motion
Velocity	> 36°/minute	
Pointing accuracy	< 0.25°	
Operating wind speed	> 60 km/h	
Survival wind speed	> 150 km/h	
Antenna system support	Reinforced concrete support structure	In order to withstand strong winds and mechanical torque

Table 2-2: Antenna Feed & Reflector Requirements Table.

3 Draft antenna-receiver scenarios

3.1 Introduction

In this report, both the antenna feed simulations and the complete reflector dish antenna simulations will be presented along with their results. The antenna dish is a parabolic reflector with $F/D = 0.38$ and a diameter of 6 meters. The antenna feed is a custom microwave antenna horn which supports dual polarization in the frequency range of 1-3 GHz. The antenna feed has embedded N-type female coaxial ports which match accordingly the dual waveguide structure of the feed. In the next sections several simulation results will be shown of the feed and the reflector dish antenna as a whole. For the simulation purposes CST Microwave Studio software package is used.

3.2 Antenna dish reflector structure

In this section, system topologies of the parabolic dish antenna (with diameter 6 meters and $F/D = 0.38$) are presented. Two different scenarios of noise injection circuitry are also shown. In Figure 3-1 the whole antenna system is demonstrated, including the receiver at the feed position as well as the 6 m parabolic dish reflector along with all supporting mechanical structures. Based on the F/D ratio, the feed will be positioned 2.28 m away from the reflector center in order to exhibit an optimum performance. The feeder will be a dual linearly polarized wideband horn antenna which covers the frequency band of 1-3 GHz. The whole antenna dish reflector will be properly mounted on a reinforced concrete support structure in order to withstand winds and mechanical torque. The first draft antenna system specifications are shown in Table 3-2. These specifications were defined during the preliminary design stage of ARGOS and may slightly differ from the specification requirements of Table 2-1.

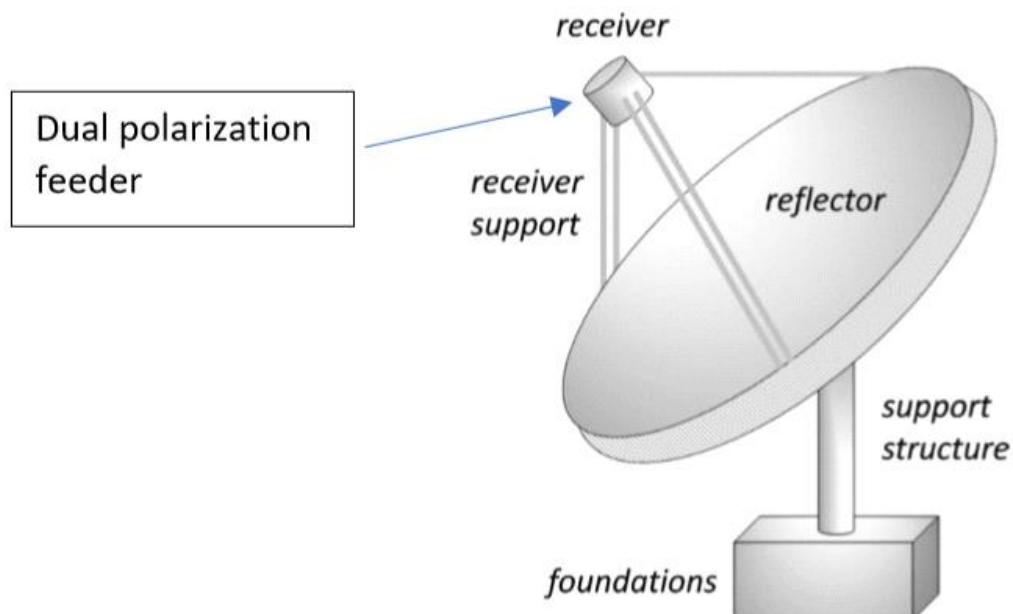


Figure 3-1: Full parabolic reflector antenna system design.

Specification	Value	Comments
Frequency bandwidth	1-3 GHz	
Dish gain	38-41 dBi	Depending on frequency
10 dB feed taper angle	~120 degrees	Typical value
Feeder horn gain	~10-12 dBi	
Polarization ports isolation	> 40 dB	Estimation
Return losses at both feeder ports	> 15 dB	Could be better if needed
Maximum power handling	10 W	Could be higher if needed

Table 3-2: Draft specifications of the antenna system design.

3.2.1 Case 1.

In this case the noise injection is performed through the use of a directional coupler. Thanks to the directional coupling, additional noise can be imported to the system that will be activated in the calibration stage of the system. In this case, there is no switch added to the chain. The system setup is shown in the Figure 3-3.

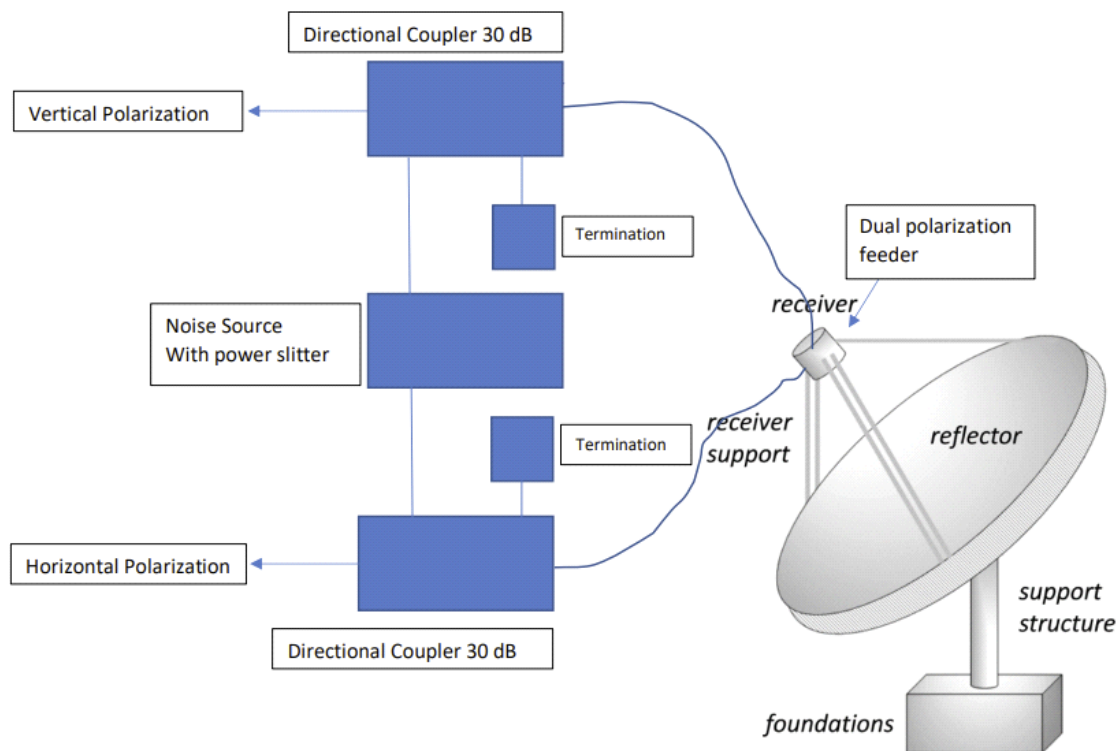


Figure 3-3: Full parabolic antenna system design with directional coupler.

3.2.2 Case 2.

In this case the noise injection is performed without the use of a power splitter at the noise source output. The single noise output is injected to the coupled port of the Horizontal polarization directional coupler and through its isolated port the noise is fed into the Vertical polarization directional coupler's coupled port. The system setup is shown in Figure 3-4.

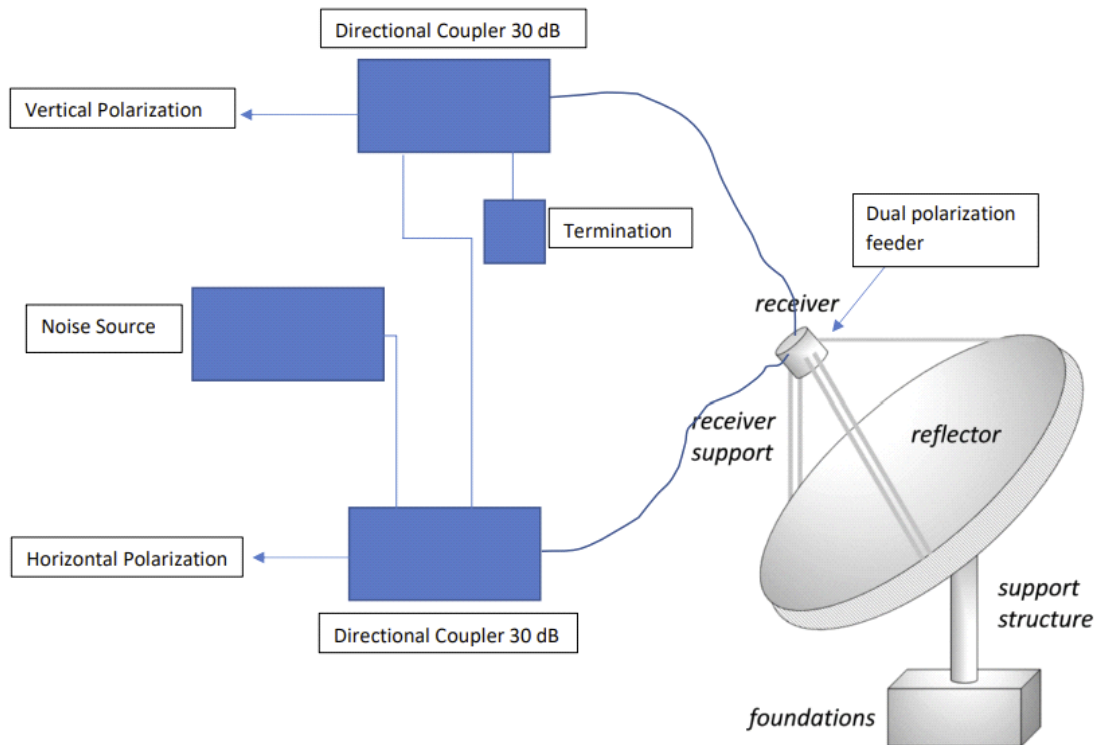


Figure 3-4: Full parabolic antenna system design without power splitter.

In both cases the directional coupler should be bidirectional for greater flexibility of assembly. The advantage of case 2 over case 1 is that there is no need for a power splitter to split the noise source power into the two directional coupler inputs.

3.3 Simulation setups

In CST there are several solvers available for simulating waveguide/antenna structures such as the Frequency Domain (FD), Time Domain (TD) and Integral Solver (IS). In large problems the structure to be studied can be separated in its ingredients in order to minimize the computer resources requirements. For the antenna feed only all the above solvers can deliver proper results in few hours' time. For the dish antenna though, since it is a quite large structure to analyze with respect to the wavelength (frequency 1-3 GHz), a different approach has been followed. The two main approaches that have been followed and give similar results are:

- Use of a radiation source which is linked to the data obtained from the simulation of the antenna feed alone. Then this radiation source is applied to the dish antenna geometry and run either Time domain or Integral solver analysis.
- Use of SAM (System Assembly Modeling) technique inside CST which in fact takes into account the full geometric model of the antenna dish and the feed and then solves each structure separately using the optimum solver for its case. Finally, it combines the results obtained in order to deliver the complete simulation outcome for the dish/feed antenna.

The computer used is an INTEL based multi-core (12 cores) one with graphics card accelerator capability and 64 GB of RAM.

4 Dual polarization feed horn antenna studies

4.1 Introduction

In this section two dual polarized feeds are analyzed in the CST 3D-Electromagnetic simulator. The first one is a straight flared horn and the second one is a bell-shaped flared horn. Both feeds are operating in the frequency range 1-3 GHz. Parametric results over the aperture size of each feed are presented with respect to gain, 3 dB beamwidth, 12 dB beamwidth and spill-over efficiency. For the spill-over efficiency the illuminated dish under consideration has a diameter of 6 m and $F/D = 0.38$.

4.1.1 Straight flared horn feed

The general geometry of the straight flared horn antenna is shown in the Figure 4-1. The swept geometric parameter is the flare diameter which ranges from 250 mm to 500 mm in five steps.

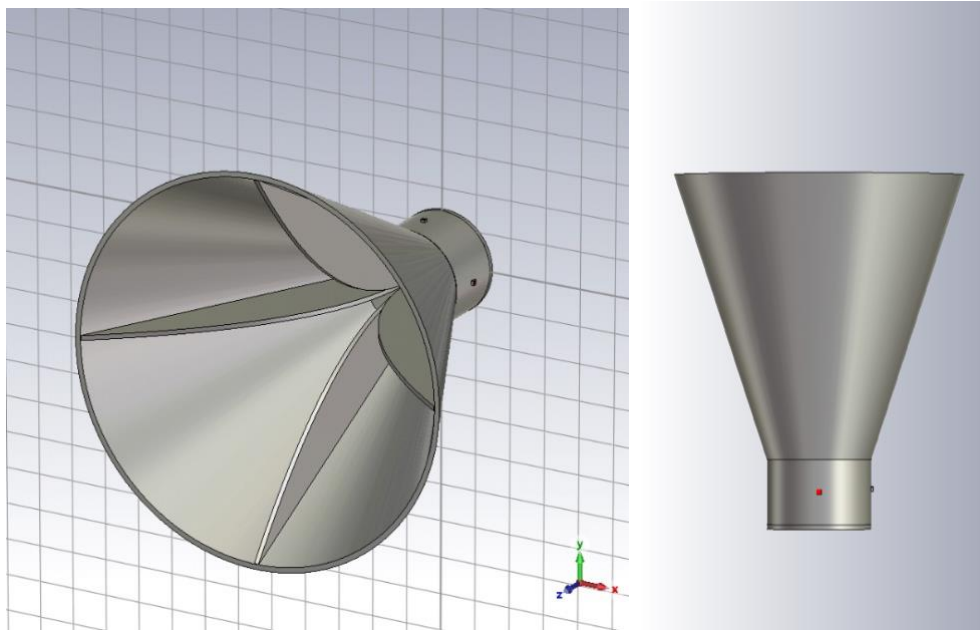


Figure 4-1: Geometry of the straight flared horn feed.

The far-field radiation patterns for this antenna at 1 GHz reveal some interesting characteristics. The patterns for both polarizations exhibit a degree of asymmetry, deviating from a perfectly circular beam. Additionally, there is a slight difference in gain between the two polarizations, indicating that one polarization might be slightly stronger than the other. Despite these observations, it's important to note that the sidelobe levels remain below -16 dB. This signifies a good level of control over unwanted radiated signals outside the main beam, ensuring efficient reception characteristics.

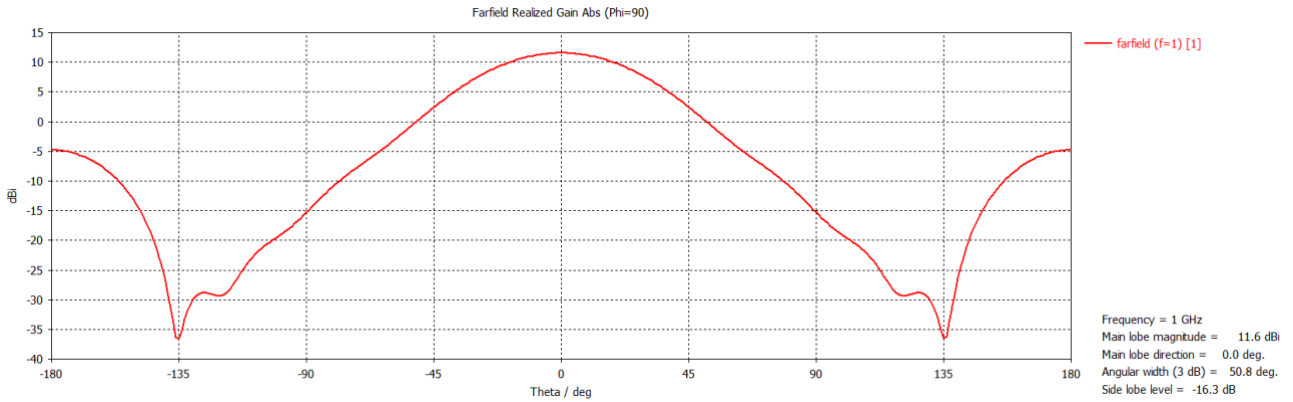


Figure 4-2: Far-field radiation patterns of horizontal polarization for 1 GHz.

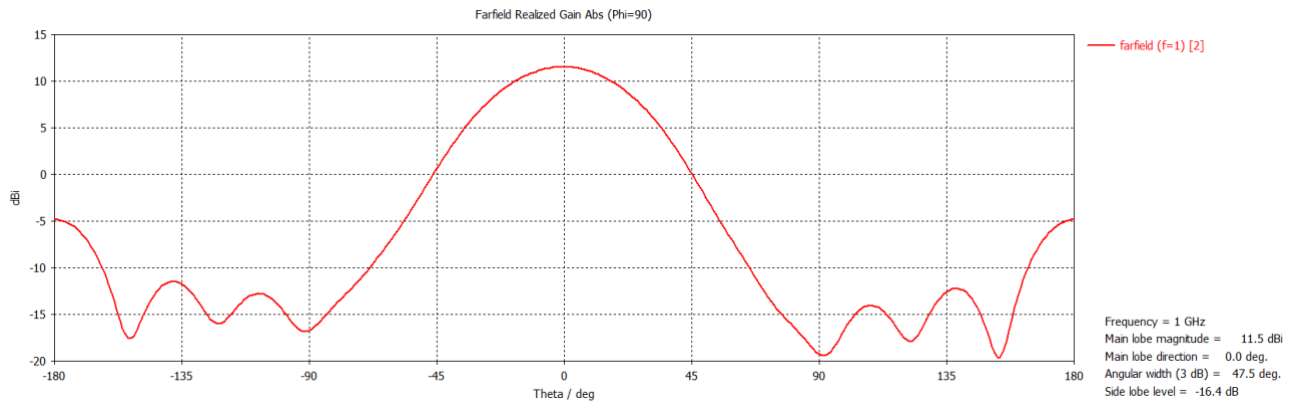


Figure 4-3: Far-field radiation patterns of vertical polarization for 1 GHz.

The far-field radiation patterns for the antenna at 2 GHz reveals a realized gain of 14.6 dBi. This indicates a good level of signal strength being directed in the main beam direction. However, the patterns exhibit a slight disturbance, deviating from a perfectly ideal shape. The sidelobe level of the vertical polarization increases at -8.5 dB. This suggests there might be some unwanted radiated energy outside the main beam compared to the observations at 1 GHz.

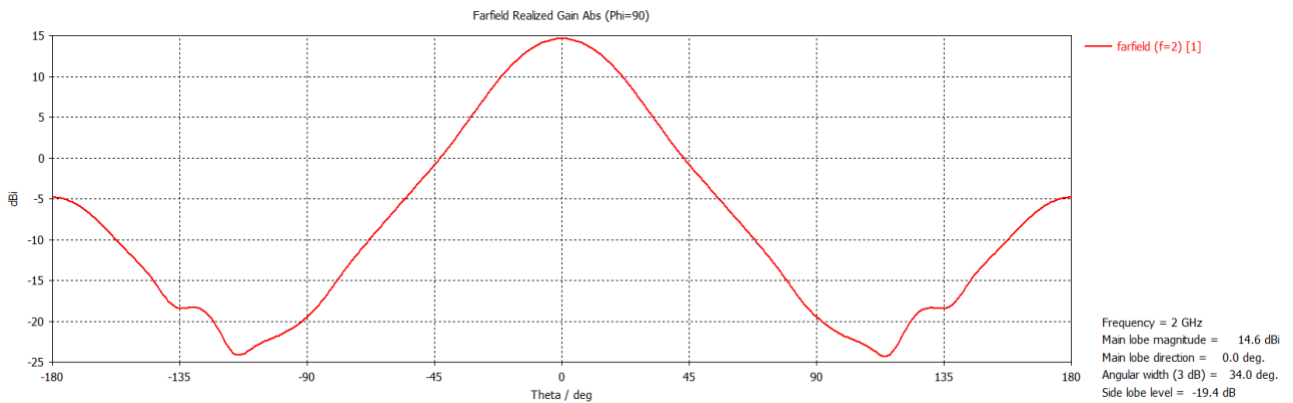


Figure 4-4: Far-field radiation patterns of horizontal polarization for 2 GHz.

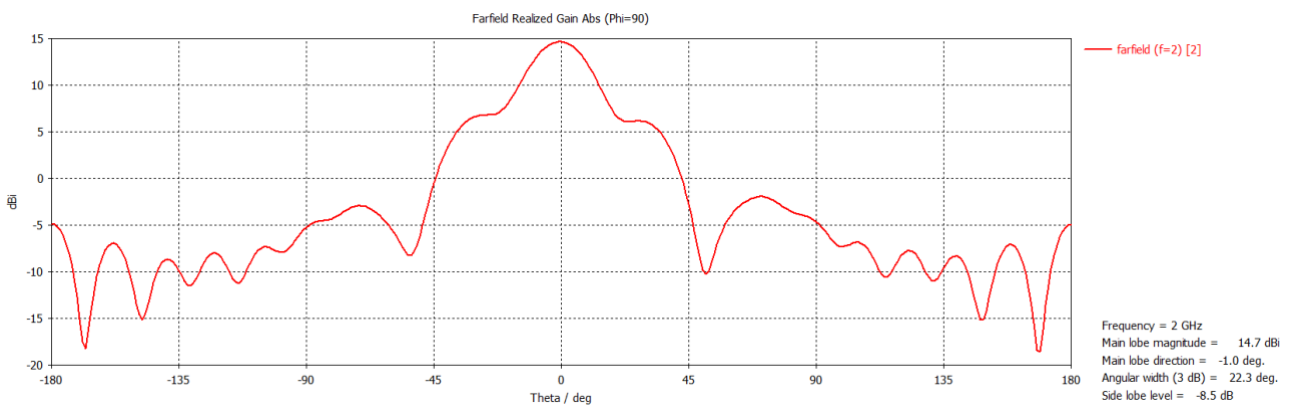


Figure 4-5: Far-field radiation patterns of vertical polarization for 2 GHz.

The far-field radiation patterns for the antenna at 3 GHz shows that while the sidelobe level remains unacceptable at -8.5 dB, indicating some unwanted radiated energy, both the realized gain and the overall pattern show cause for concern. Generally, this reflect to a poor realized gain suggesting the antenna is not efficiently directing signal strength into the main beam direction.

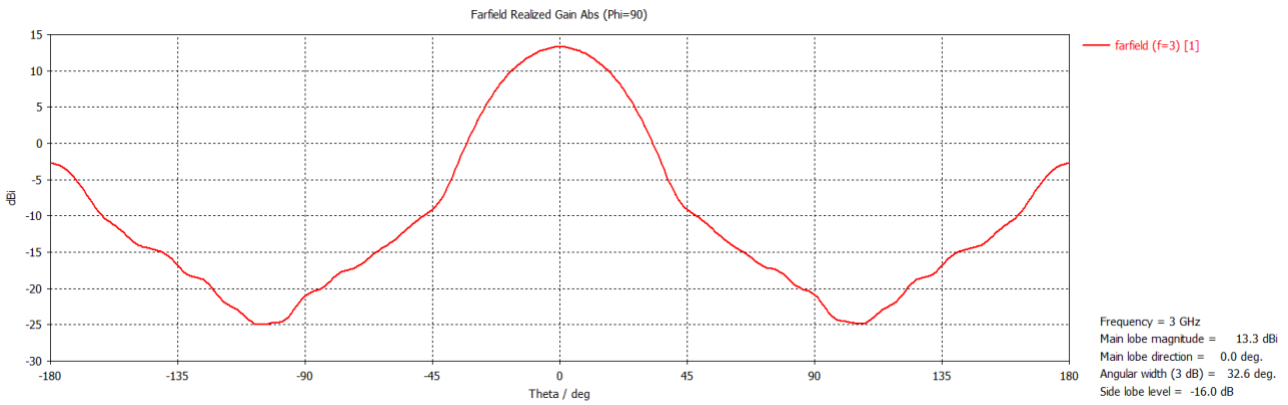


Figure 4-6: Far-field radiation patterns of horizontal polarization for 3 GHz.

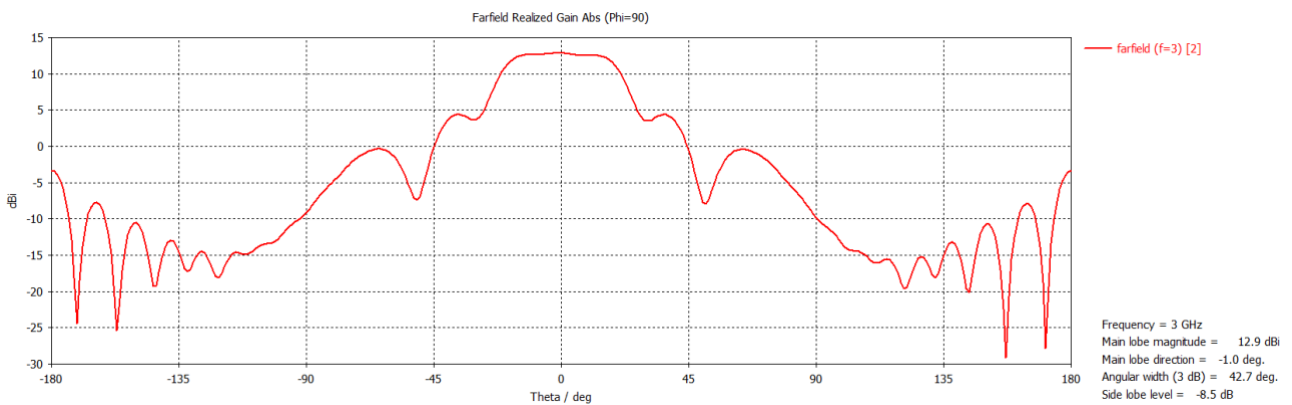


Figure 4-7: Far-field radiation patterns of vertical polarization for 3 GHz.

A parameter sweep simulation process was executed for the S_{11} vs frequency plot. The reflection coefficient of the horn is shown in Figure 4-8 for 5 different values of the flare diameter. We can see that an optimum value is for flare diameter = 370 mm approximately.

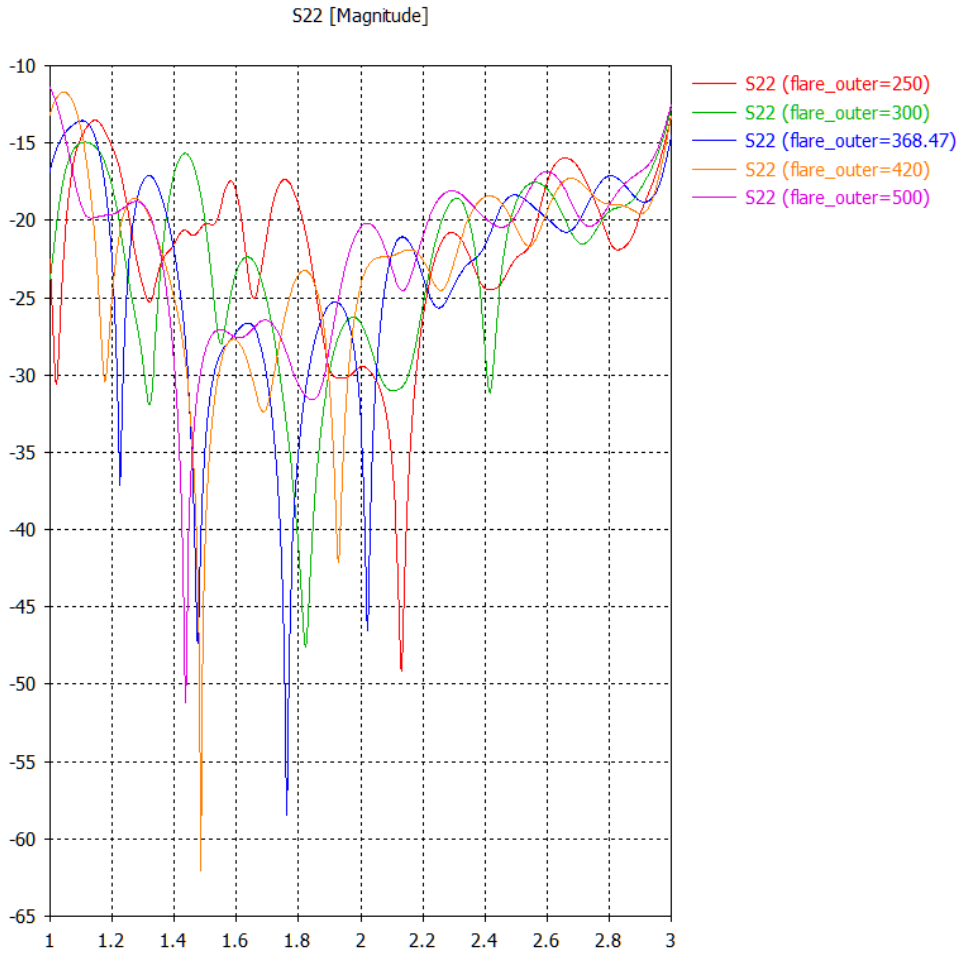


Figure 4-8: Reflection coefficient.

The following S-parameter plot (see Figure 4-9) demonstrates that the probes themselves are not perfectly symmetrical (since they do not coincide) and thus, they exhibit slightly different reflection coefficient responses. Additionally, the isolation between the ports is excellent, exceeding -40 dB, signifying minimal signal leakage between the two polarizations.

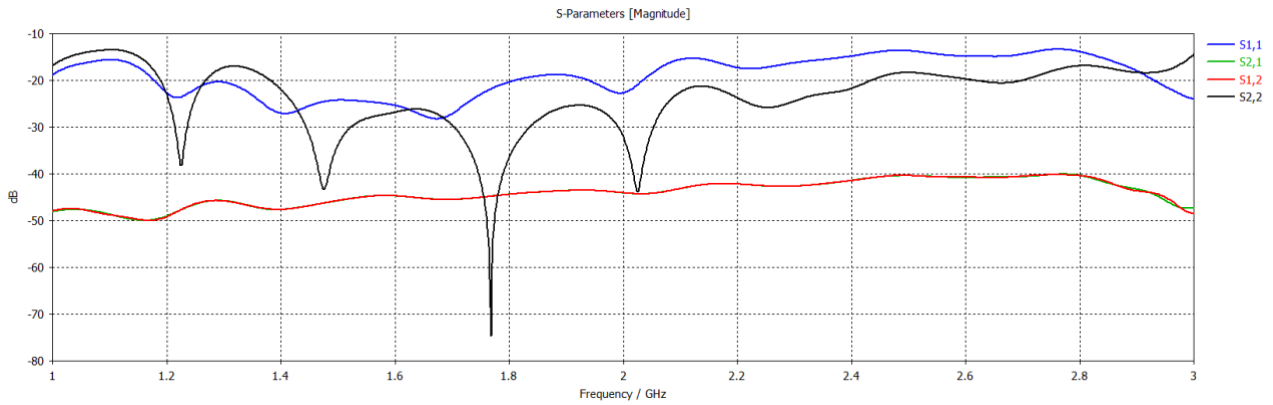


Figure 4-9: S parameters for design 1.

The realized gain vs frequency for the swept parameter of the flare diameter is shown in Figure 4-10. Again, the flare diameter = 370 mm provides the optimum gain performance over frequency since it demonstrates smaller value deviations (more flatness) combined with increased maximum realized gain value.

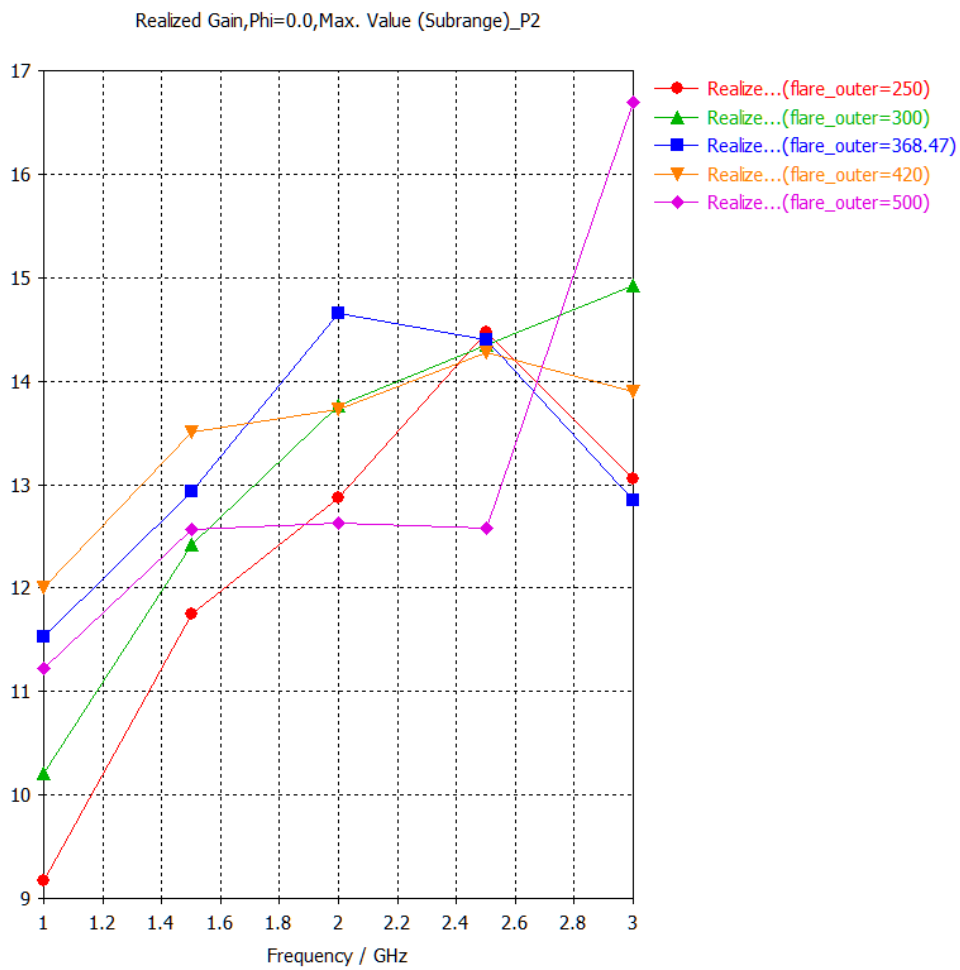


Figure 4-10: Realized gain vs flare diameter.

The 3 dB beamwidth of the radiation pattern (for the $\phi = 0^\circ$ cut) vs frequency for the swept parameter of the flare diameter is plotted in figure 4-11. Again, for flare diameter = 370 mm, a good gain performance over frequency is demonstrated.

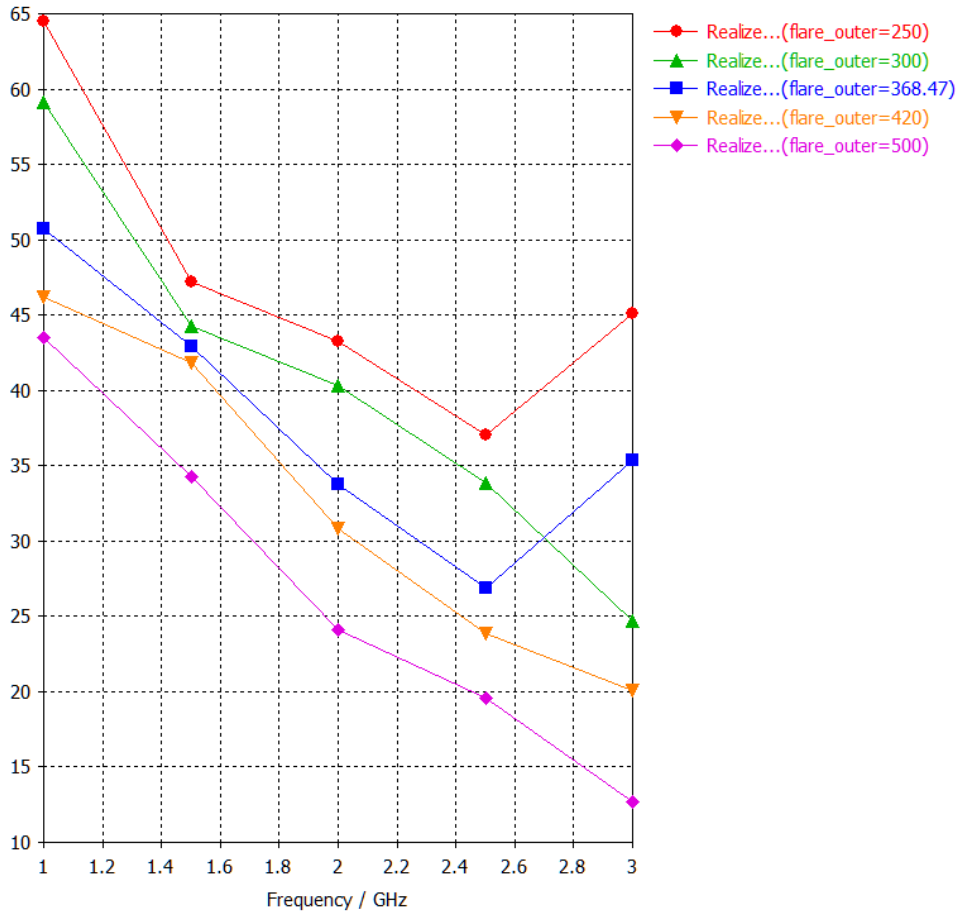


Figure 4-11: 3dB beamwidth (elevation) vs flare diameter.

The 3 dB beamwidth (for the $\phi = 90^\circ$ cut) vs frequency for the swept parameter of the flare diameter is shown in Figure 4-12. Again, for flare diameter = 370 mm, we have the optimum gain performance over frequency (smaller beamwidth indicated more directive beam).

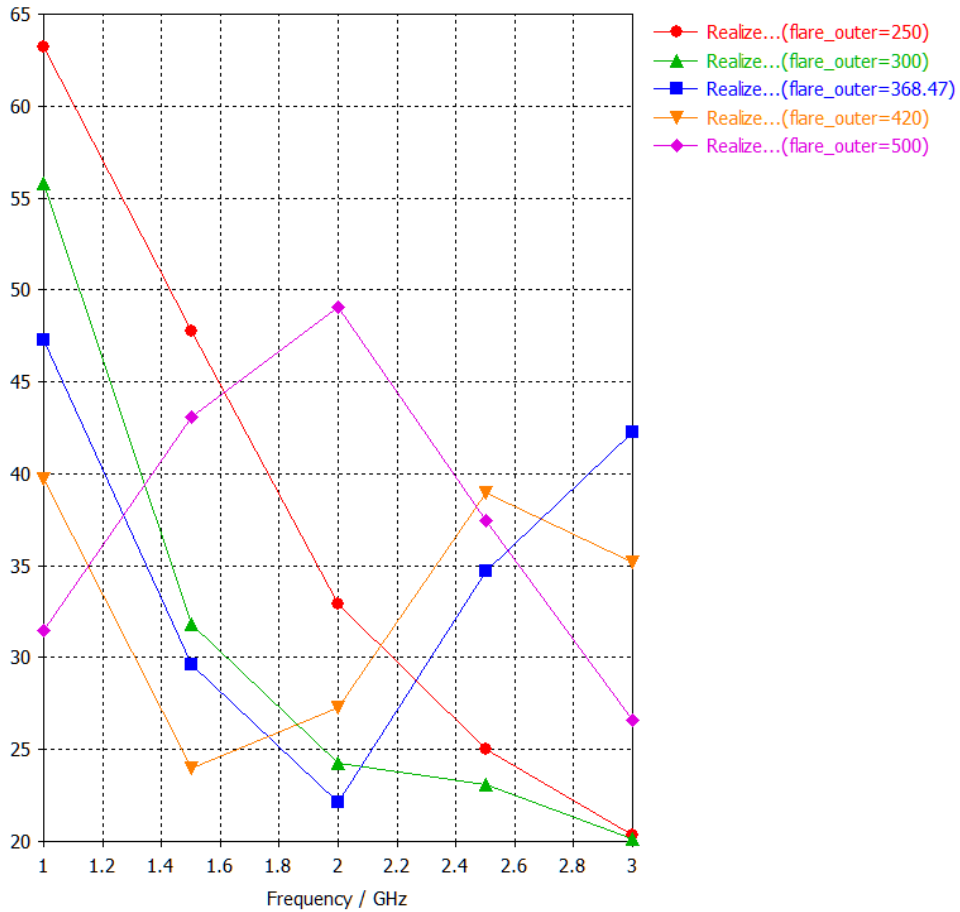


Figure 4-12: 3 dB beamwidth (azimuth) vs flare diameter.

The 12 dB beamwidth (for the $\phi = 0^\circ$ cut) vs frequency for the swept parameter of the flare diameter is shown in figure 4-13. The flare diameter = 370 mm still gives a good gain performance over frequency.

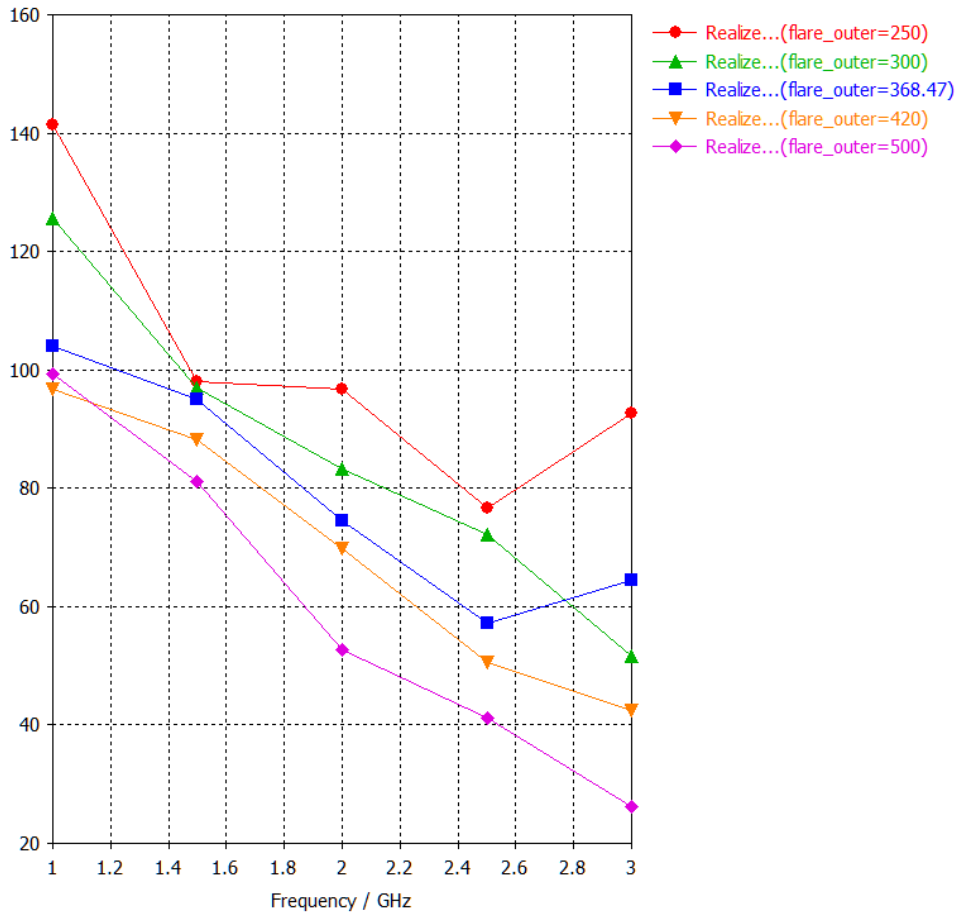


Figure 4-13: 12 dB beamwidth (elevation) vs flare diameter.

The 12 dB beamwidth for (for the $\varphi = 90^\circ$ cut) vs frequency for the swept parameter of the flare diameter is shown in Figure 4-14. Again, for flare diameter=370 mm we have the optimum gain performance over frequency (smaller beamwidth indicated more directive beam).

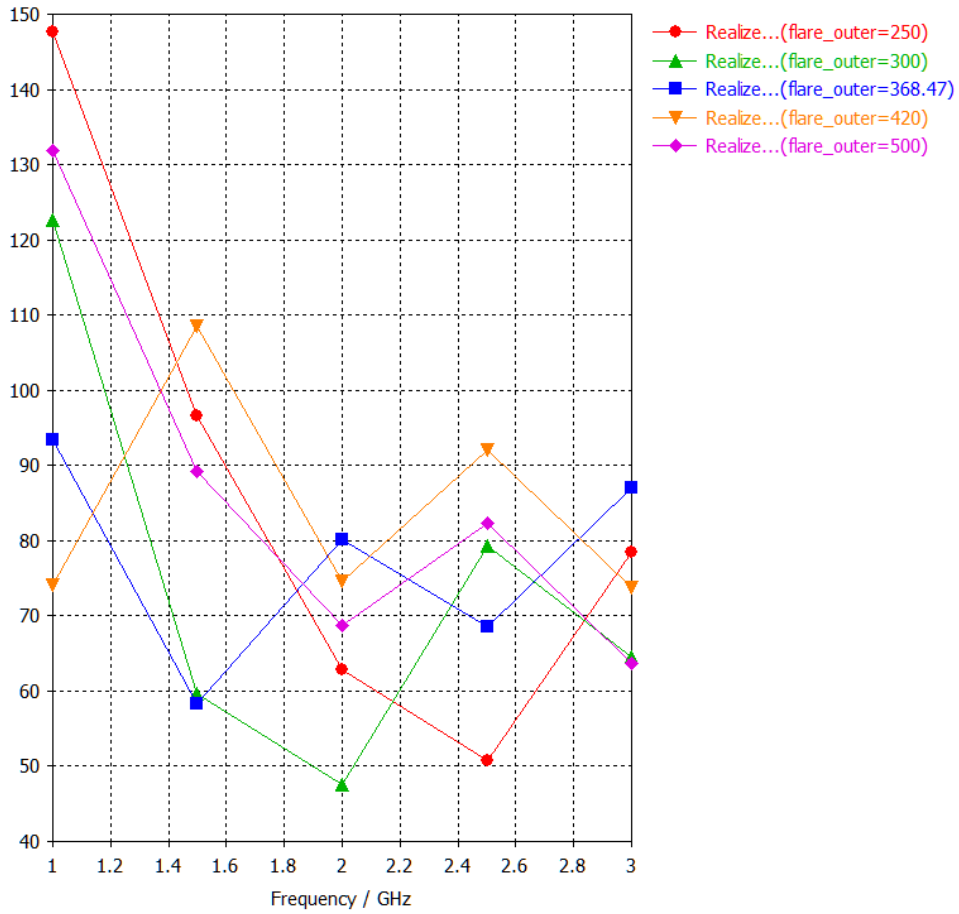


Figure 4-14: 12 dB beamwidth (azimuth) vs flare diameter.

The spill-over efficiency vs frequency for the swept parameter of the flare diameter is shown in Figure 4-15. The flare diameter = 370 mm provides the optimum performance over frequency (flatter). For the spill-over efficiency the illuminated dish under consideration has a diameter of 6 m and $F/D = 0.38$. In order to calculate the spill-over efficiency, firstly the calculation of the power flow inside the dish volume is done and secondly, the power flow over the whole spherical space. The spill-over efficiency is the percentage of the fraction of the difference of the total radiated power minus the power flow inside the dish volume over the total radiated power.

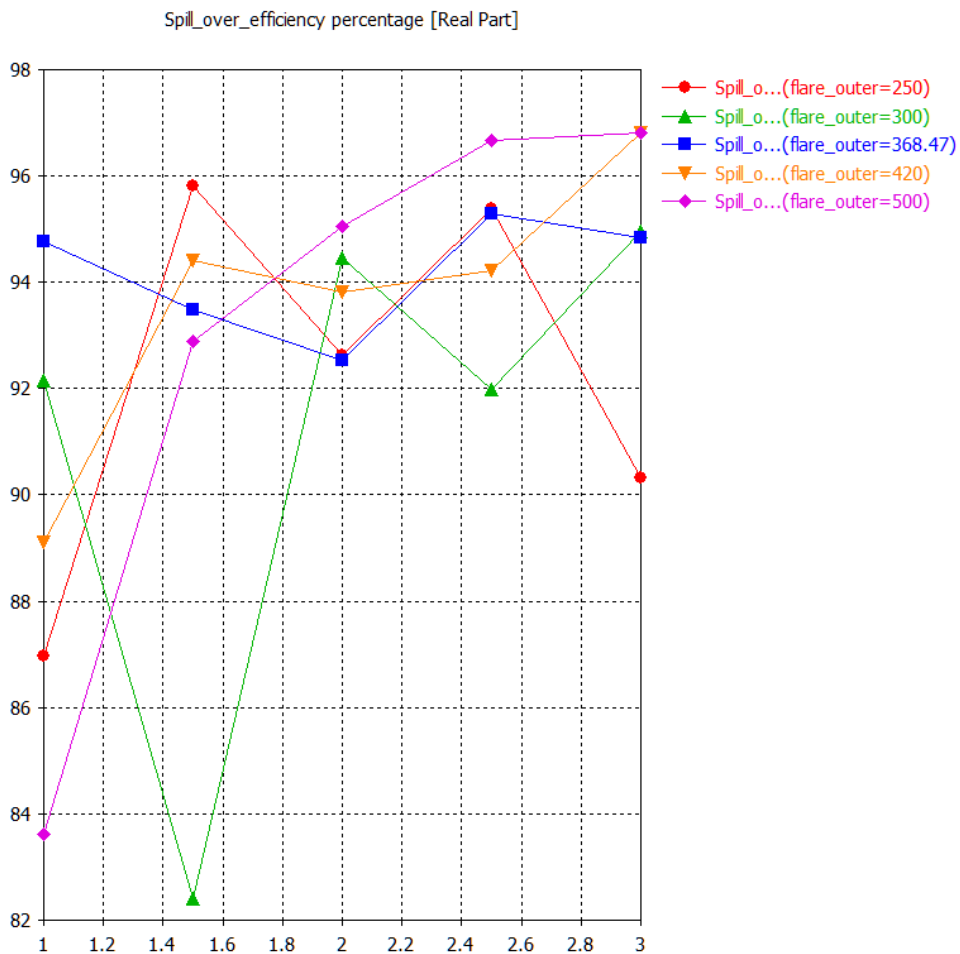


Figure 4-15: Spill-over efficiency percentage vs flare diameter.

Figure 4-16 and Figure 4-17 demonstrate the 3D radiation patterns for the realized gain over the frequency range 1-3 GHz (with 0.5 GHz step) for the simple straight flared horn antenna.

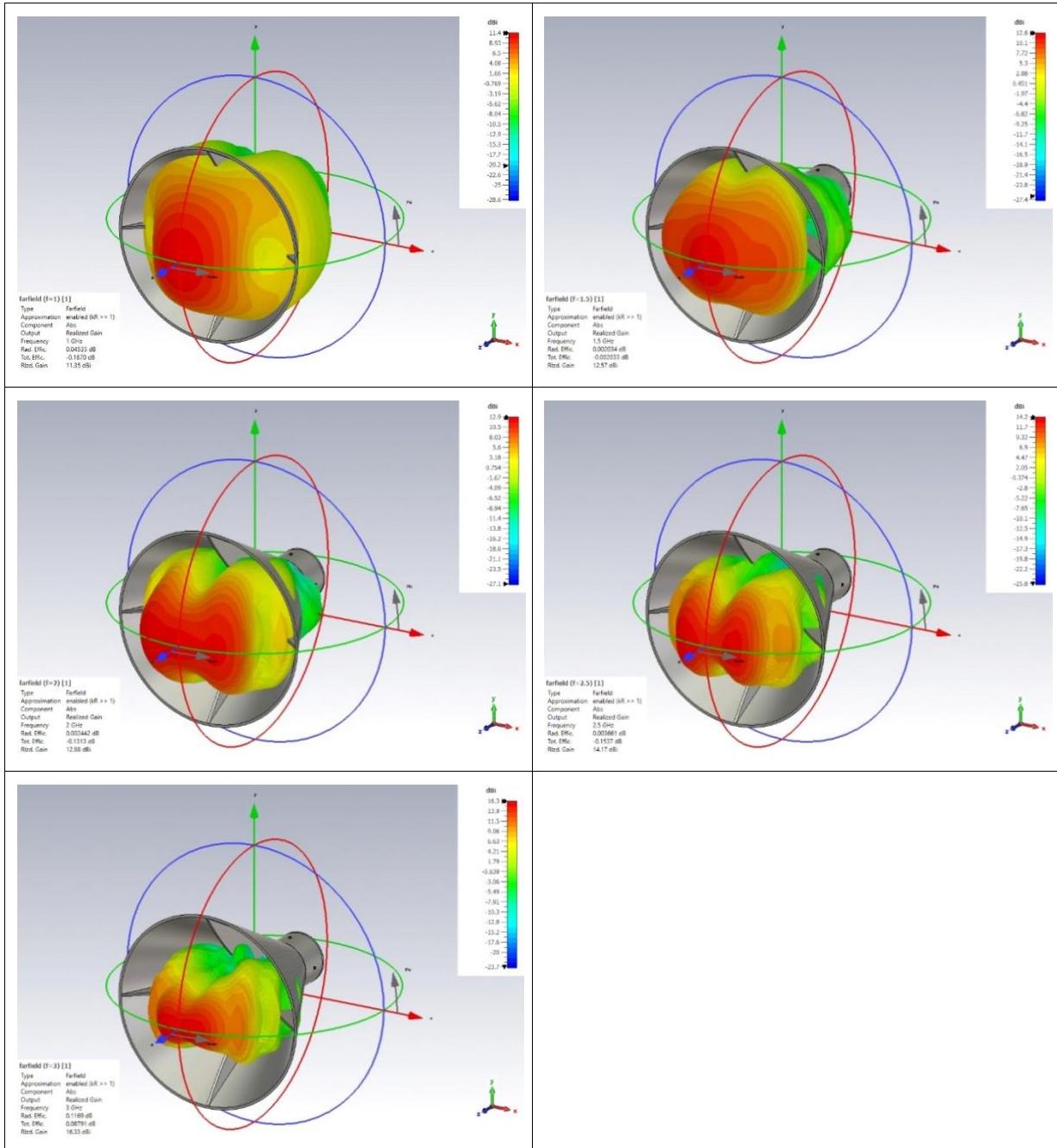


Figure 4-16: 3D Radiation patterns port 1.

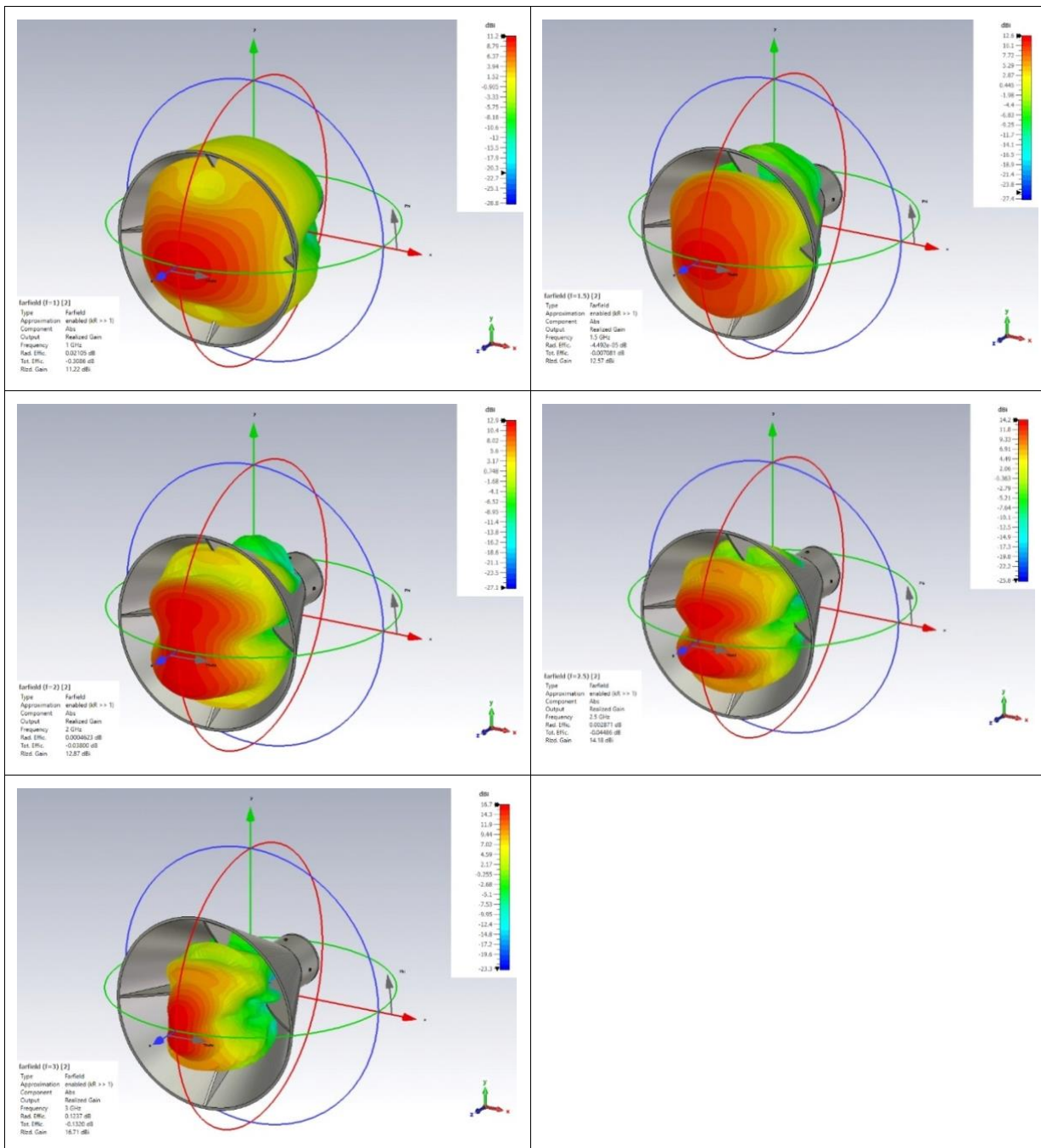


Figure 4-17: 3D Radiation patterns port 2.

4.1.2 Bell shaped flared horn feed

The geometry of the bell-shaped flared horn feed is shown in figure Figure 4-18. The swept geometric parameter is the flare diameter which ranges from 200 mm to 500 mm in five steps.

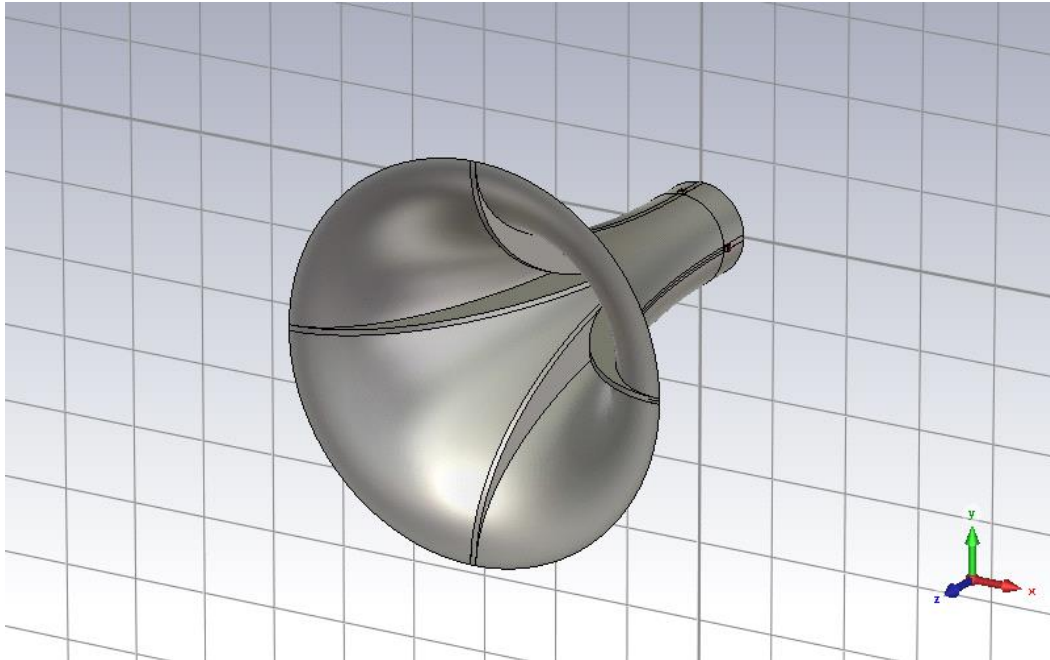


Figure 4-18: Geometry of the feed.

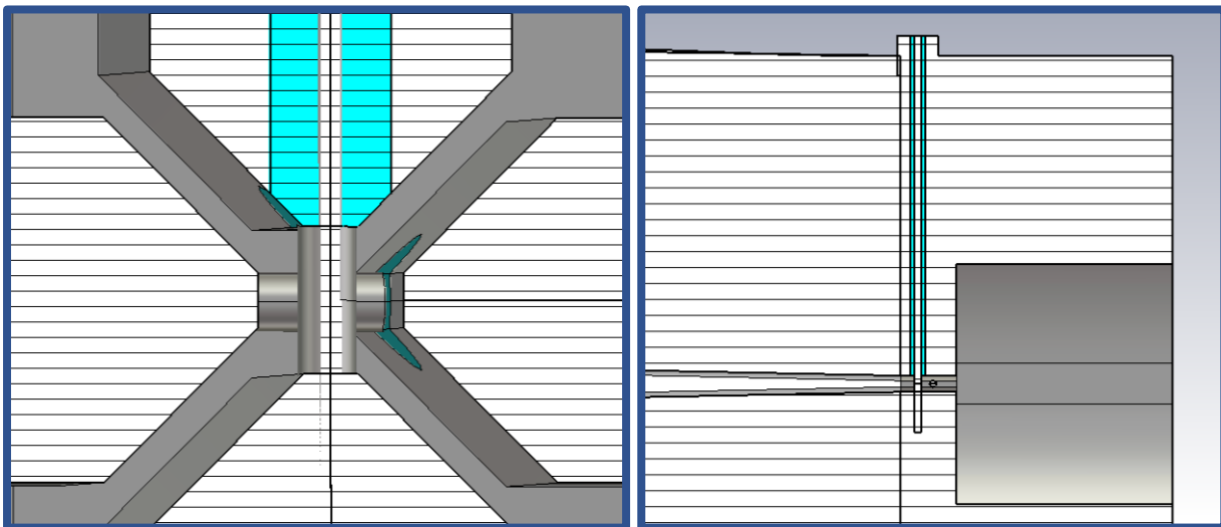


Figure 4-19: Monopole Placement.

Compared to the straight flare horn, the beam exhibits a more symmetrical shape, indicating a more ideal radiation pattern. This symmetry suggests the antenna is efficiently directing radio waves in a specific direction with minimal deviation. Additionally, the sidelobe level remains below -15 dB (at 1 GHz).

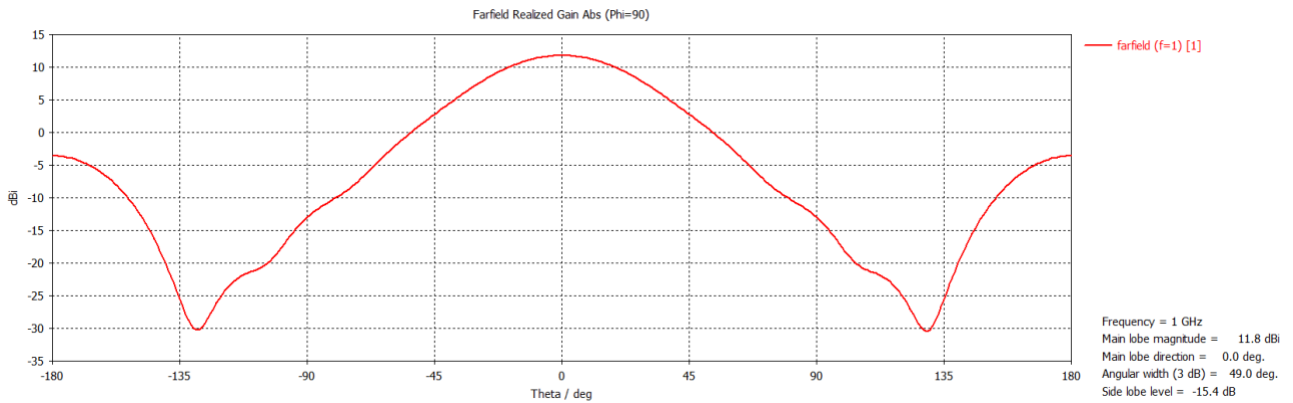


Figure 4-20: Far-field radiation patterns of horizontal polarization for 1 GHz.

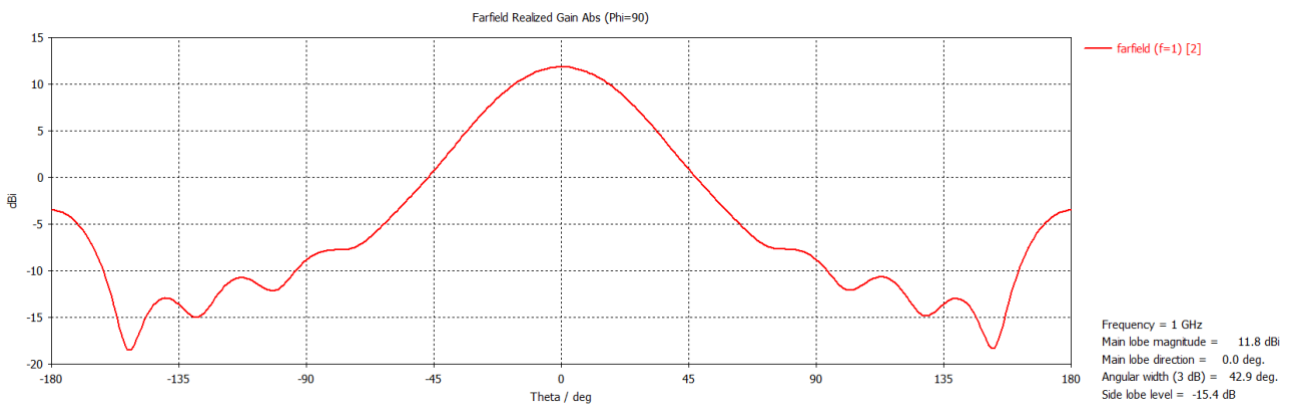


Figure 4-21: Far-field radiation patterns of vertical polarization for 1 GHz.

The far-field radiation patterns for the bell-shaped flared horn antenna at 2 GHz also demonstrate positive results. The measured realized gain of 14.0 dBi indicates a good concentration of signal strength in the main beam direction, ensuring efficient antenna reception. Even more encouraging is the sidelobe level that is significantly lower than -21 dB.

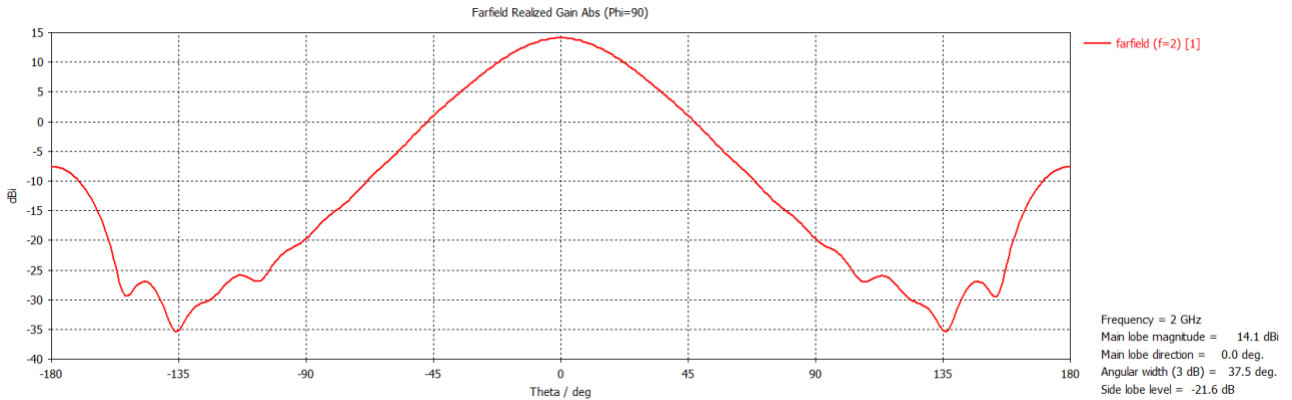


Figure 4-22: Far-field radiation patterns of horizontal polarization for 2 GHz.

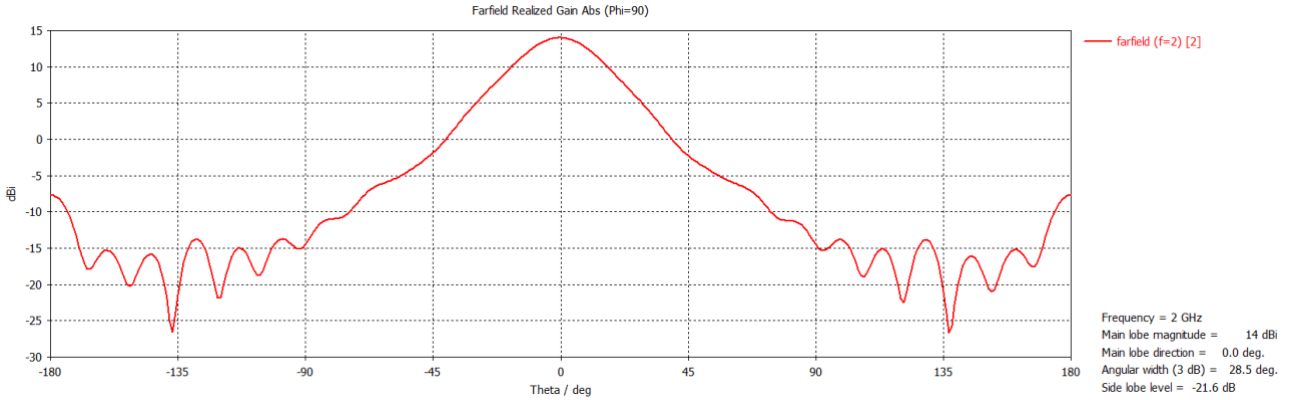


Figure 4-23: Far-field radiation patterns of vertical polarization for 2 GHz.

At 3 GHz, the far-field radiation patterns for the antenna provide an excellent sidelobe level of -25 dB.

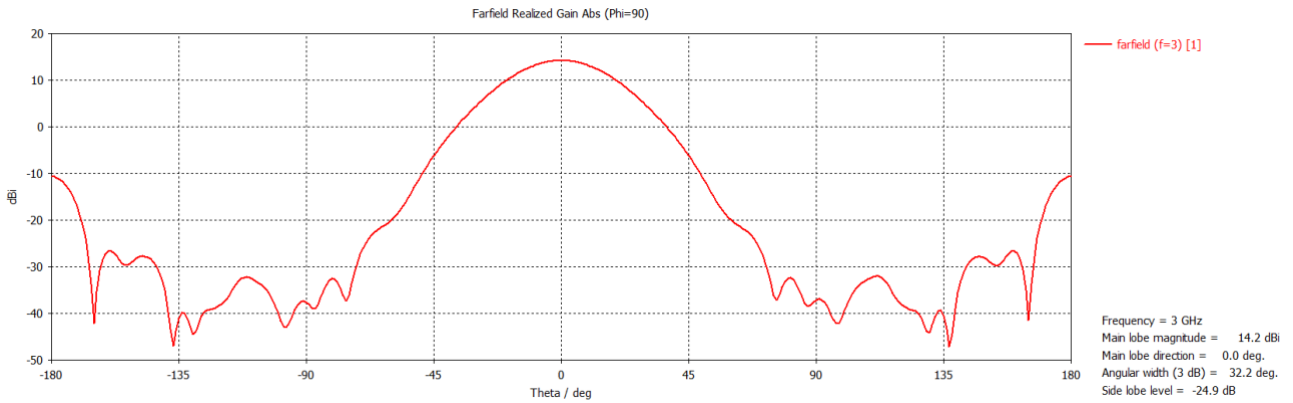


Figure 4-24: Far-field radiation patterns of horizontal polarization for 3 GHz.

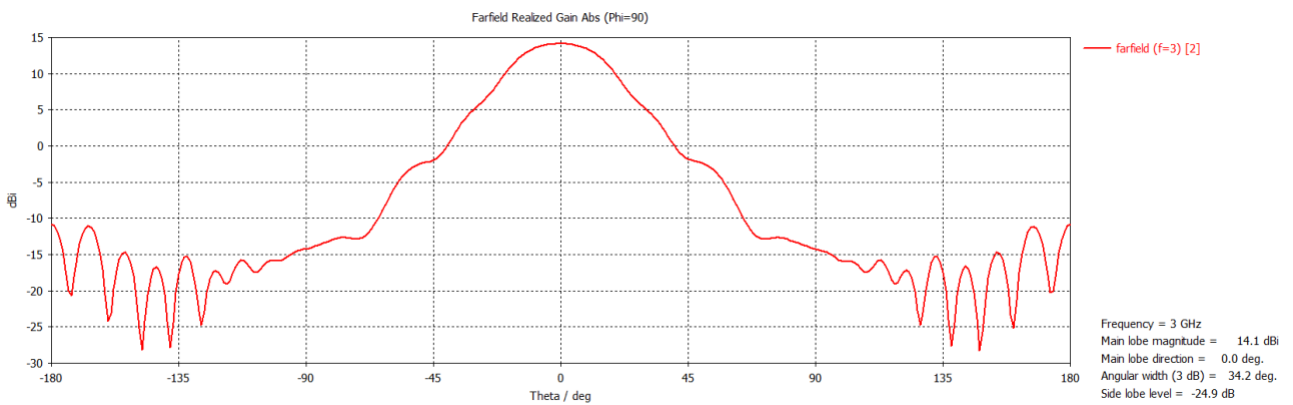


Figure 4-25: Far-field radiation patterns of vertical polarization for 3 GHz.

The reflection coefficient of the horn is shown in Figure 4-26. We can see that an optimum flat response over the 1-3 GHz frequency bandwidth is for flare diameter = 445 mm approximately.

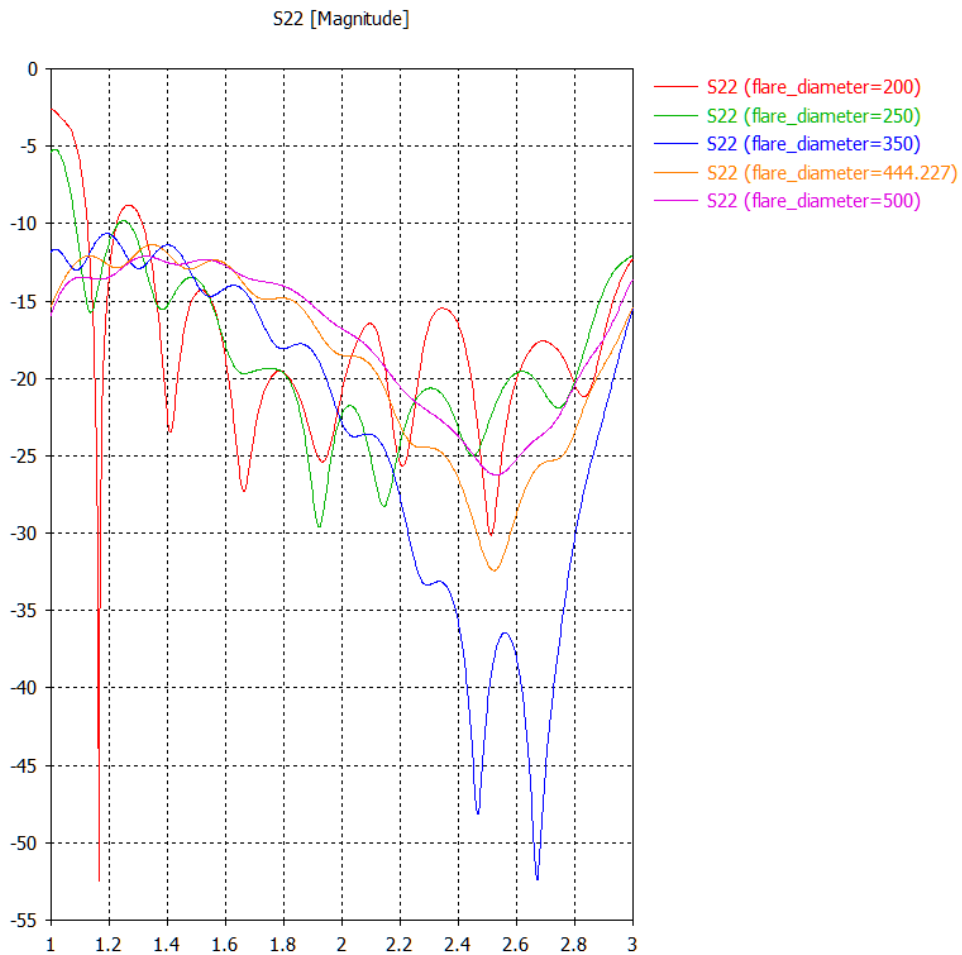


Figure 4-26: Reflection coefficient.

The following S-parameter plot, depicted in Figure 4-27, shows that the probes themselves are not perfectly symmetrical (do not coincide). The isolation between the ports is excellent, exceeding -40 dB, signifying minimal signal leakage between them. Additionally, the reflection coefficient (S_{11} and S_{22}) remains below -15 dB for most of the desired 1-3 GHz operational frequency range, indicating good impedance matching across the band.

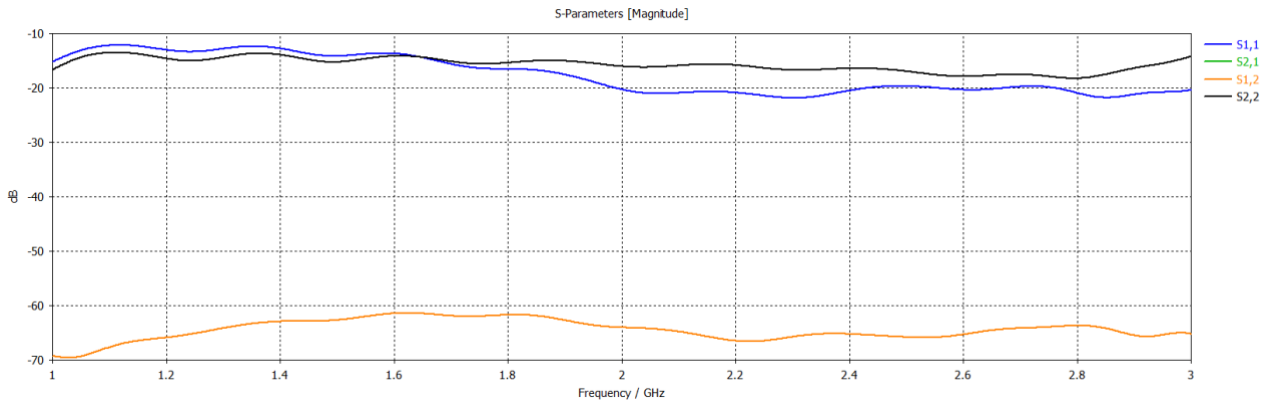


Figure 4-27: S parameters for design 2.

The realized gain vs frequency for the swept parameter of the flare diameter is shown in Figure 4-28. Again, for flare diameter = 445 mm we have the optimum gain performance over frequency (enhanced flatness – small gain deviation over frequency).

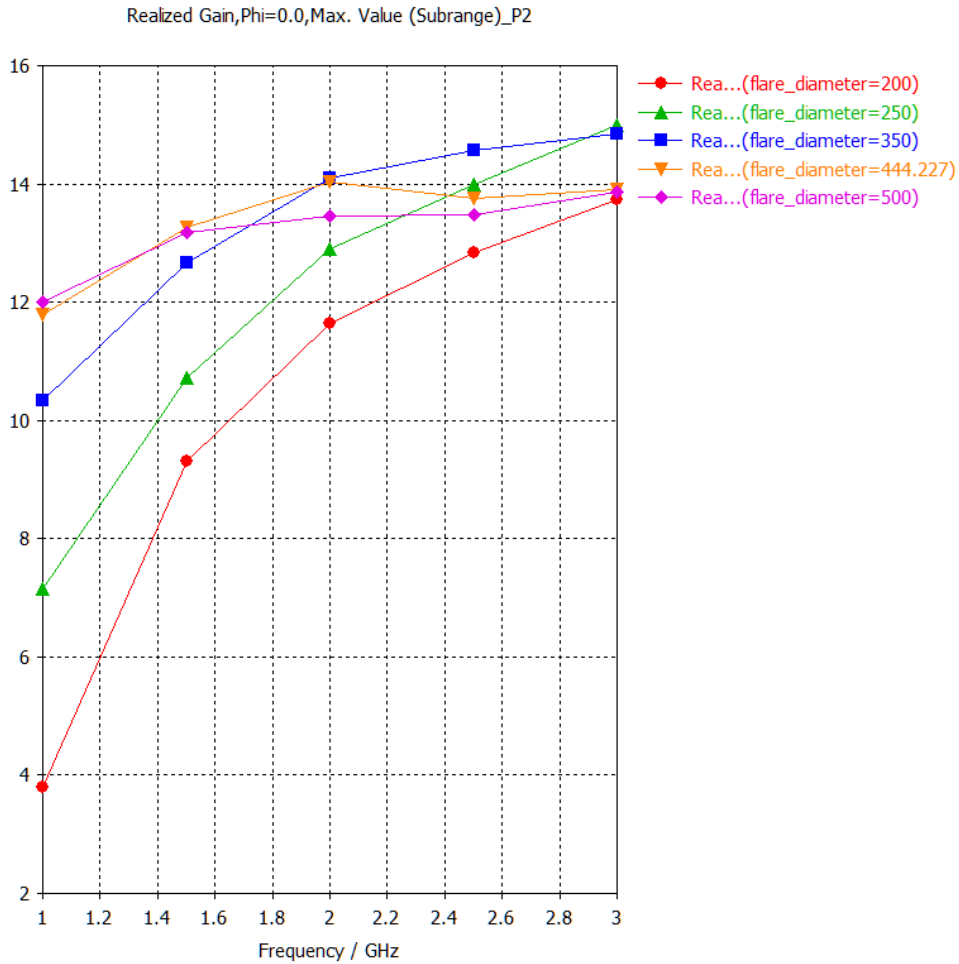


Figure 4-28: Realized gain vs flare diameter.

The 3 dB beamwidth (for the $\varphi = 0^\circ$ cut) vs frequency for the swept parameter of the flare diameter is shown in Figure 4-29. Again, for flare diameter = 445 mm we have the optimum gain performance over frequency.

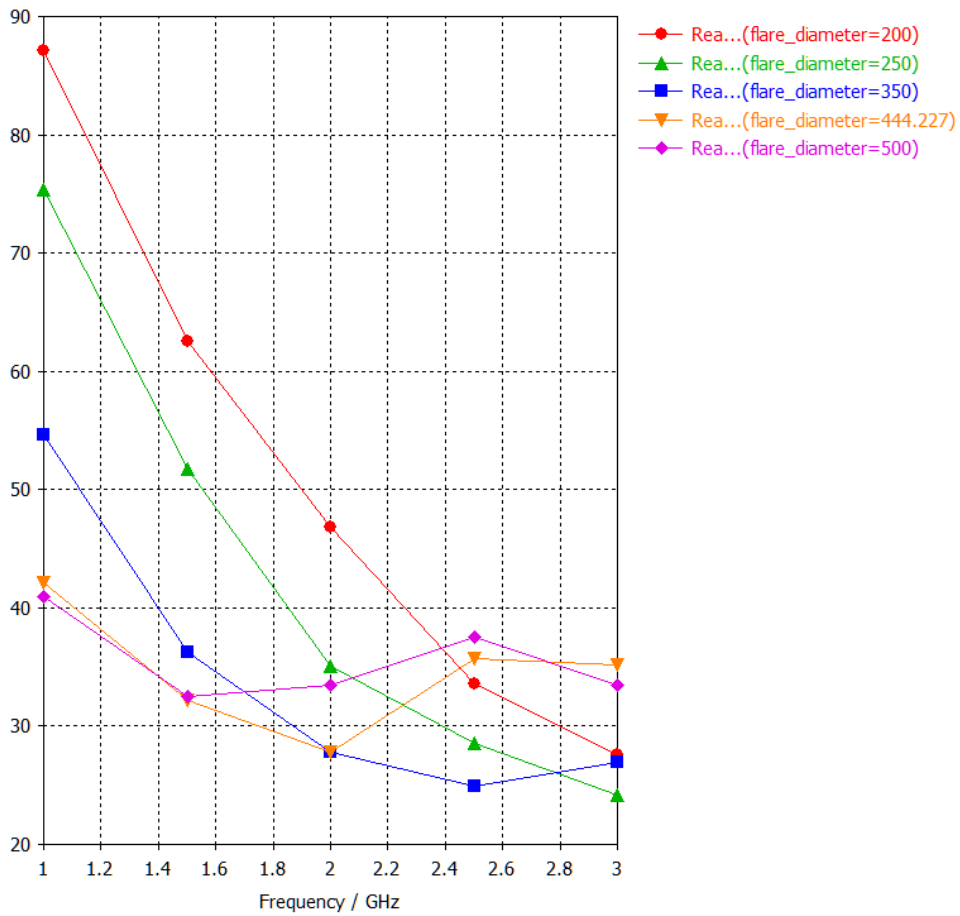


Figure 4-29: 3 dB beamwidth (elevation) vs flare diameter.

The 3 dB beamwidth (for the $\varphi = 90^\circ$ cut) vs frequency for the swept parameter of the flare diameter is shown in Figure 4-30. Again, for flare diameter = 445 mm, the optimum gain performance over frequency is demonstrated.

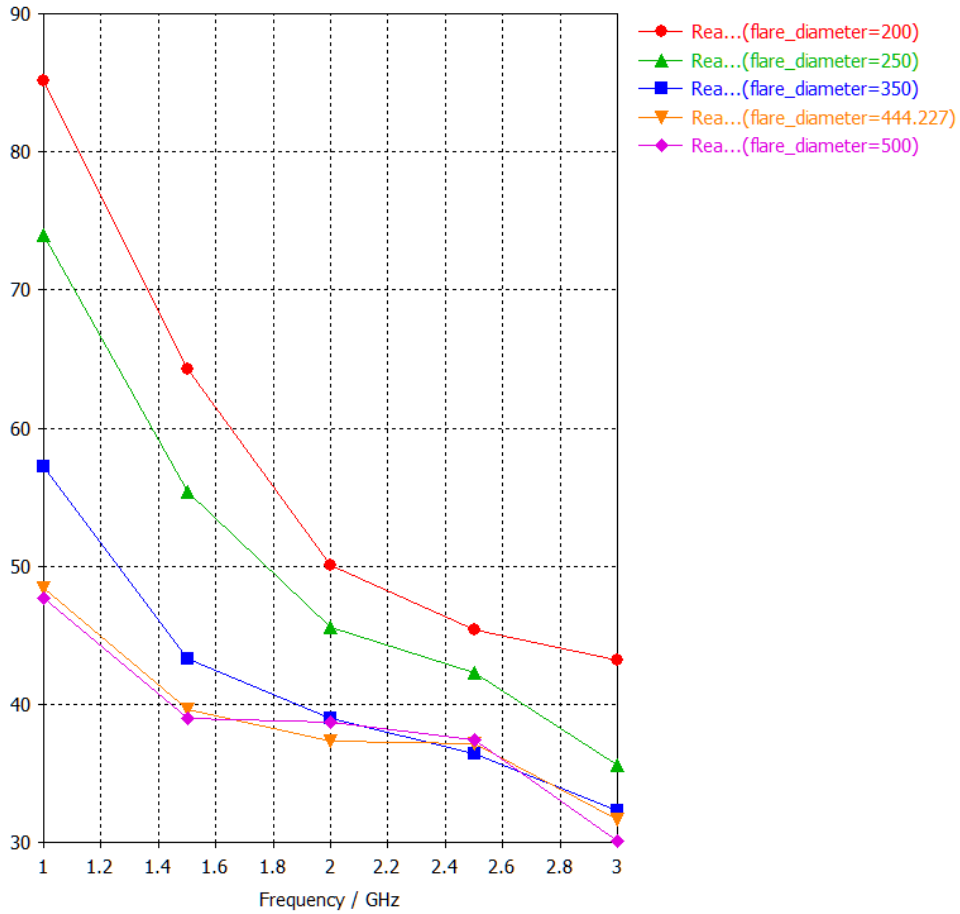


Figure 4-30: 3 dB beamwidth (azimuth) vs flare diameter.

The 12 dB beamwidth (for the $\varphi = 0^\circ$ cut) vs frequency for the swept parameter of the flare diameter is shown in Figure 4-31. Again, for flare diameter = 445 mm we have the optimum gain performance over frequency.

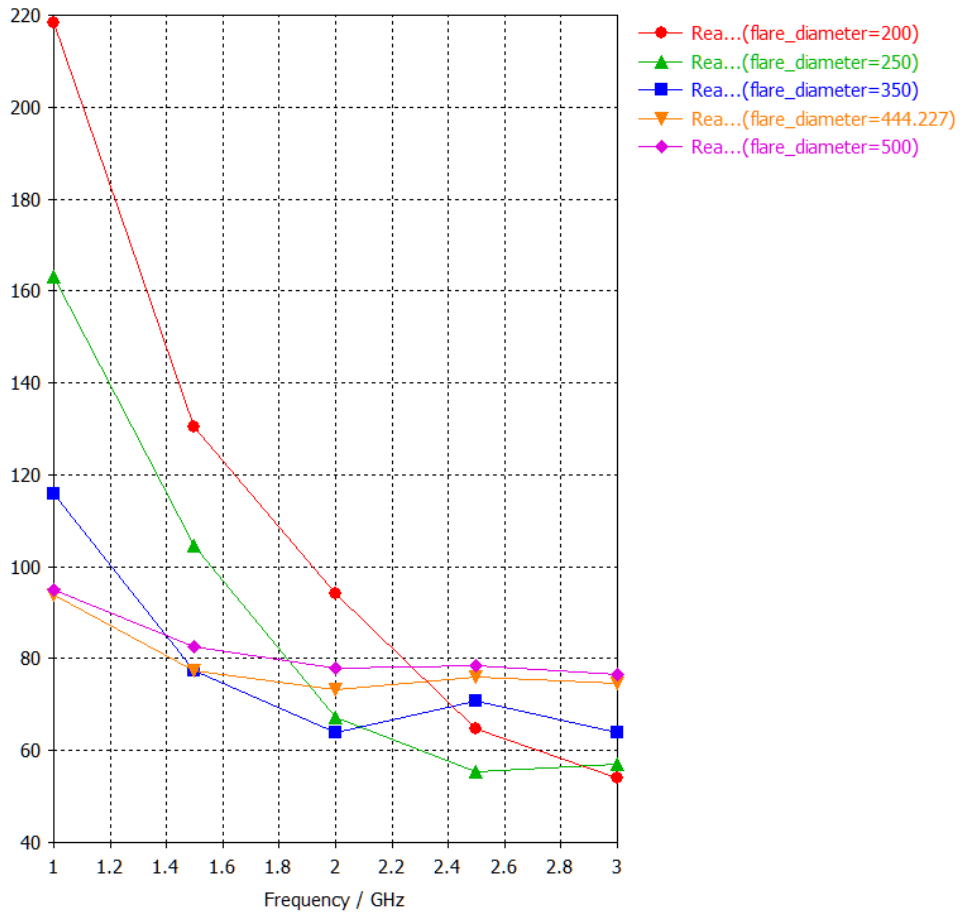


Figure 4-31: 12 dB beamwidth (elevation) vs flare diameter.

The 12 dB beamwidth (for the $\phi = 90^\circ$ cut) vs frequency for the swept parameter of the flare diameter is shown in Figure 4-32. Again, for flare diameter=445 mm we have the optimum gain performance over frequency (smaller values).

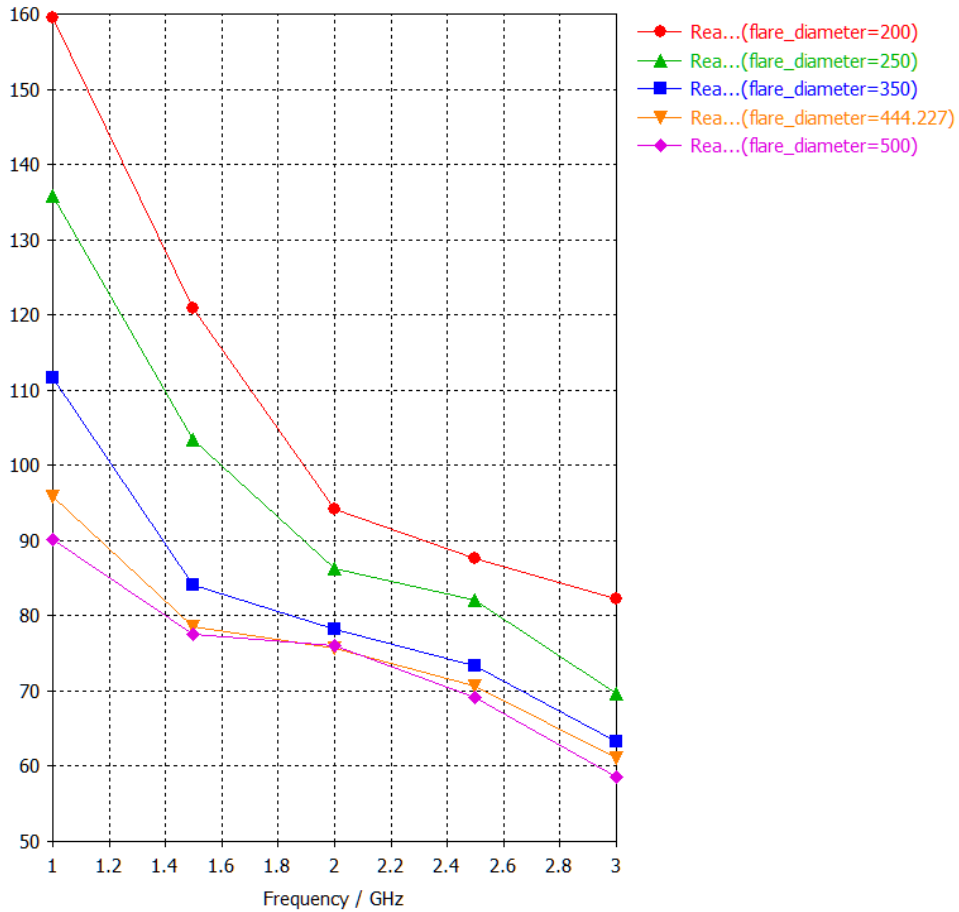


Figure 4-32: 12 dB beamwidth (azimuth) vs flare diameter.

The spill-over efficiency vs frequency for the swept parameter of the flare diameter is shown in Figure 4-33. Again, for flare diameter = 445 mm we have the optimum performance over frequency. In order to calculate the spill-over efficiency, firstly the calculation of the power flow inside the dish volume is done and secondly the power flow over the whole spherical space. The spill-over efficiency is the percentage of the fraction of the difference of the total radiated power minus the power flow inside the dish volume over the total radiated power.

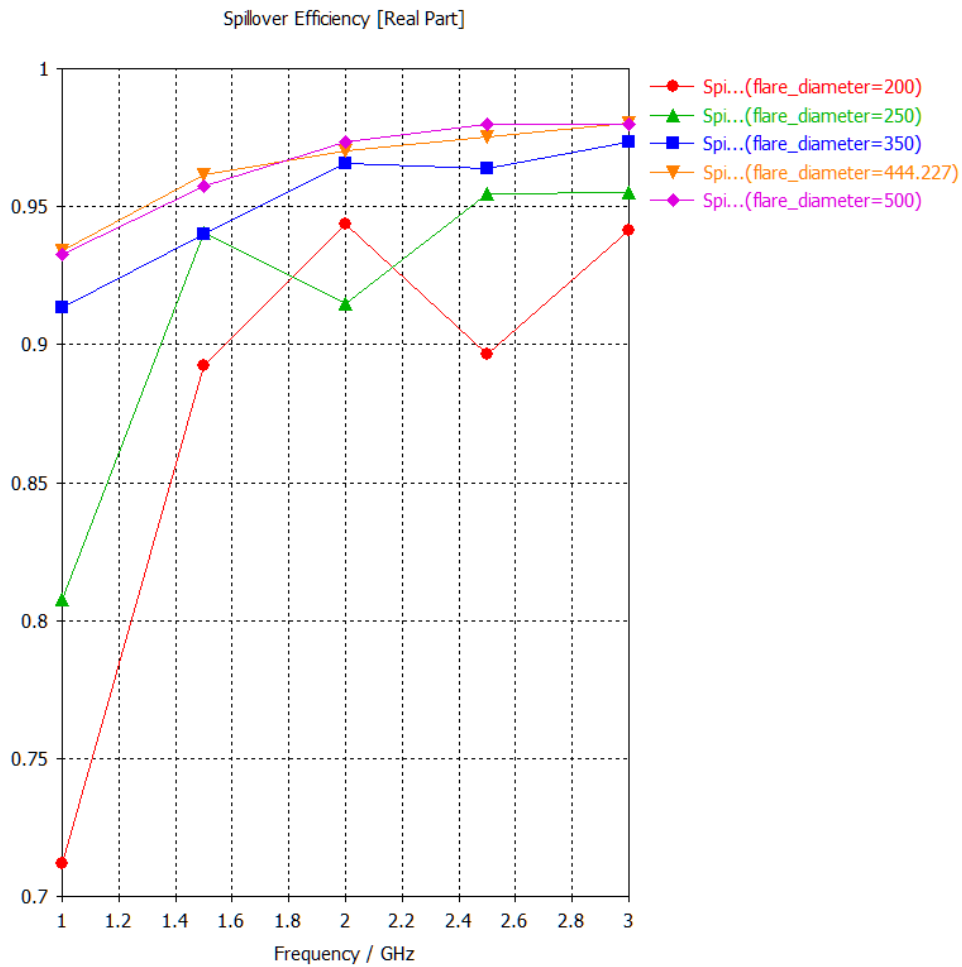


Figure 4-33: Spill-over efficiency percentage vs flare diameter.

In figures 4-34 and 4-35 the 3D radiation patterns for the realized gain over the frequency range 1-3 GHz (with 0.5 GHz step) for the bell-shaped flared horn antenna feed are shown.

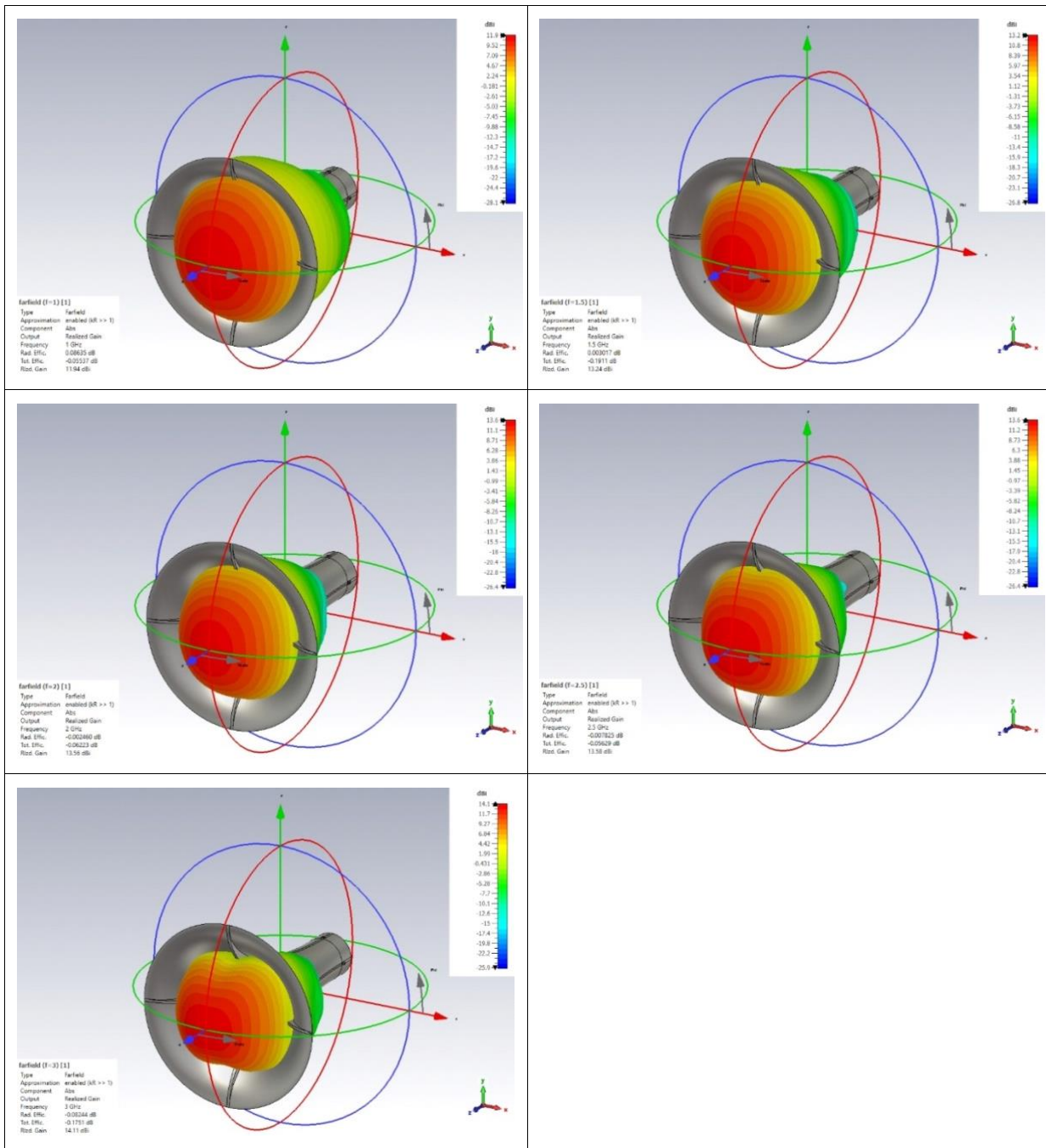


Figure 4-34: 3D Radiation patterns port 1.

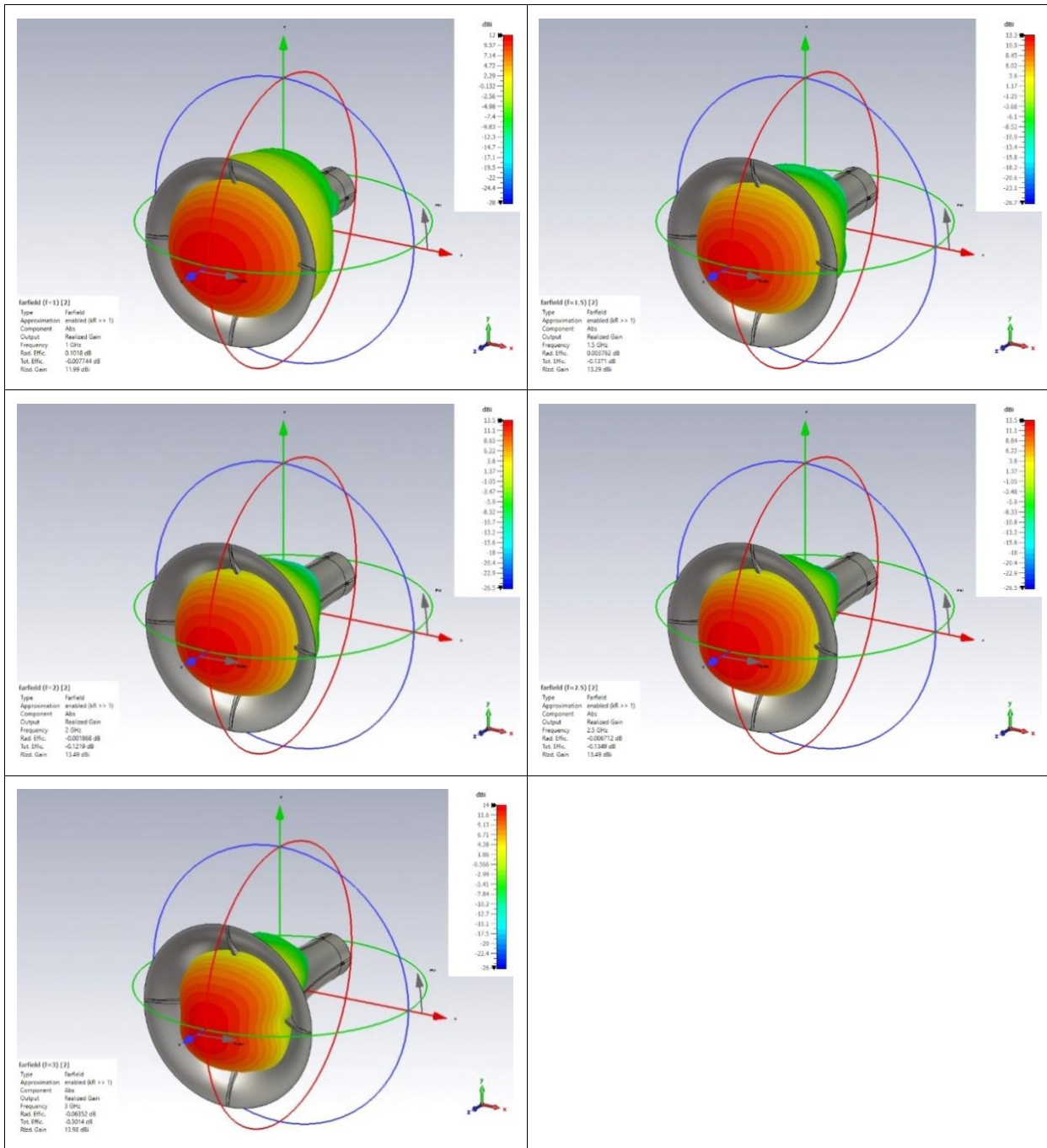


Figure 4-35: 3D Radiation patterns port 2.

5 Antenna dish reflector studies

5.1 Antenna dish reflector calculation procedures comparisons

In this section 3D EM simulation comparisons will be presented in order to understand which is the most beneficial with respect to computer resources and simulation time required in order to solve the antenna dish reflector with dual polarized horn feed problem. As feed horn the bell-shaped flared feed horn is chosen since it presents better RF performance over the straight flared horn feed antenna.

The simulations that will be presented are the following:

- Dish antenna with radiation source without blockage.
- Dish antenna with radiation source with blockage.
- Dish antenna with feeding antenna true geometries using SAM procedure (System Assembly modelling), unidirectional approach.
- Dish antenna with feeding antenna true geometries using SAM procedure (System Assembly modelling), bidirectional approach.

5.1.1 Antenna dish reflector with radiation source without blockage

In Figure 5-1 the gain performance over frequency of the complete dish/feed geometry is shown without taking into account any blockage. The feed is replaced by the equivalent far field source obtained by separate 3D EM simulation of the complete feed geometry.

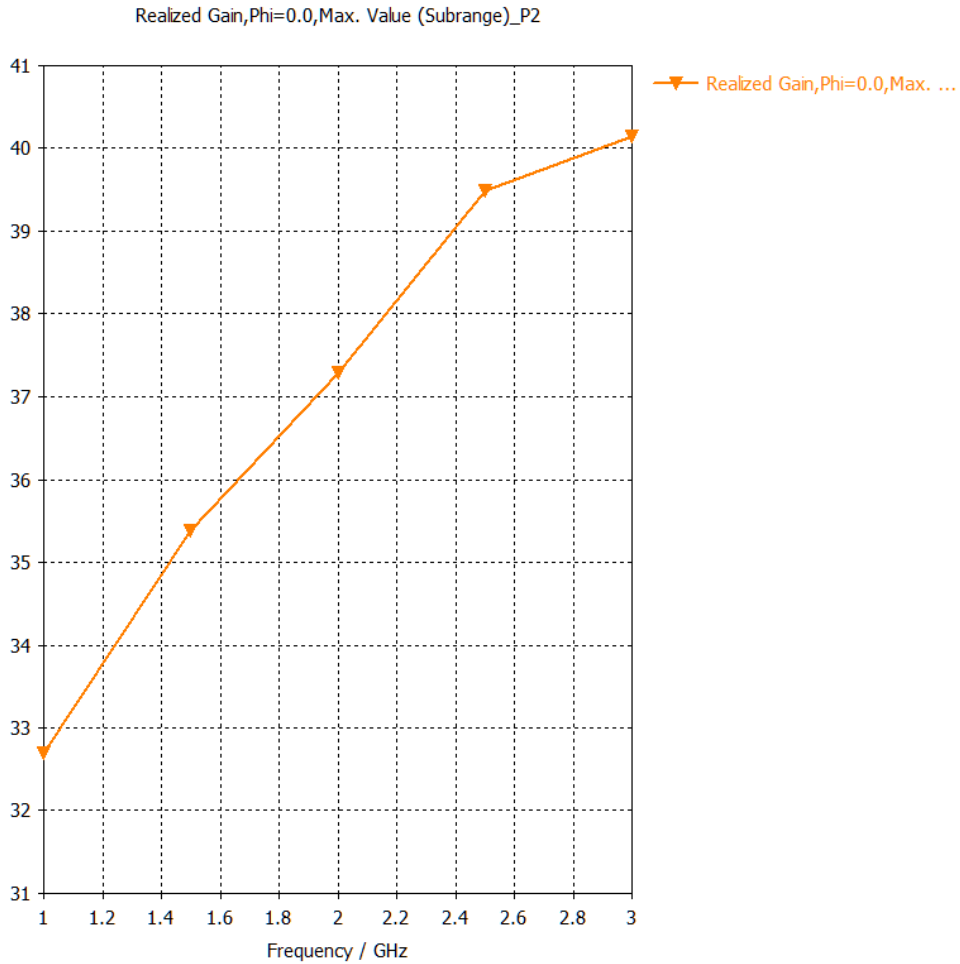


Figure 5-1: Gain variation over frequency.

In Figure 5-2 the 3dB beamwidth (for the $\phi = 90^\circ$ cut) vs frequency is presented for the case of no-blockage.

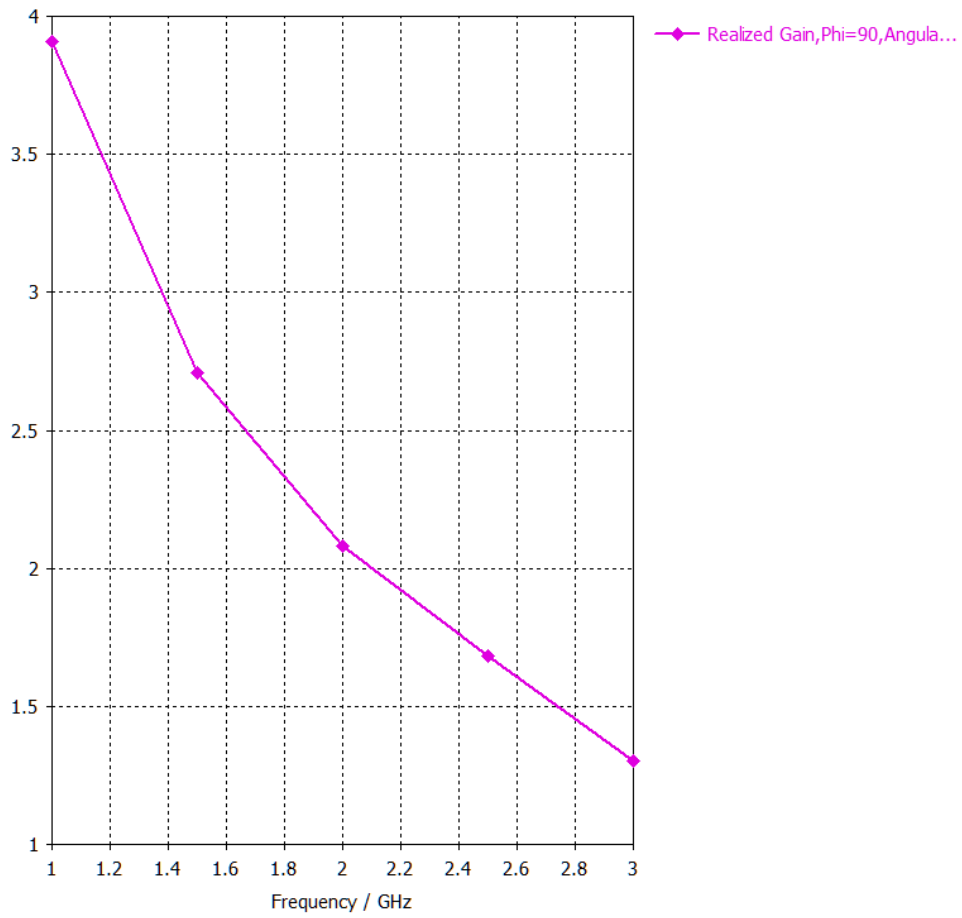


Figure 5-2: 3dB beamwidth variation over frequency.

In Figure 5-3 the cartesian plots for various frequency points in the frequency range 1-3 GHz are presented for the non-blockage case. In this plot we can see details for the sidelobe levels, front to back ratios and nulls.

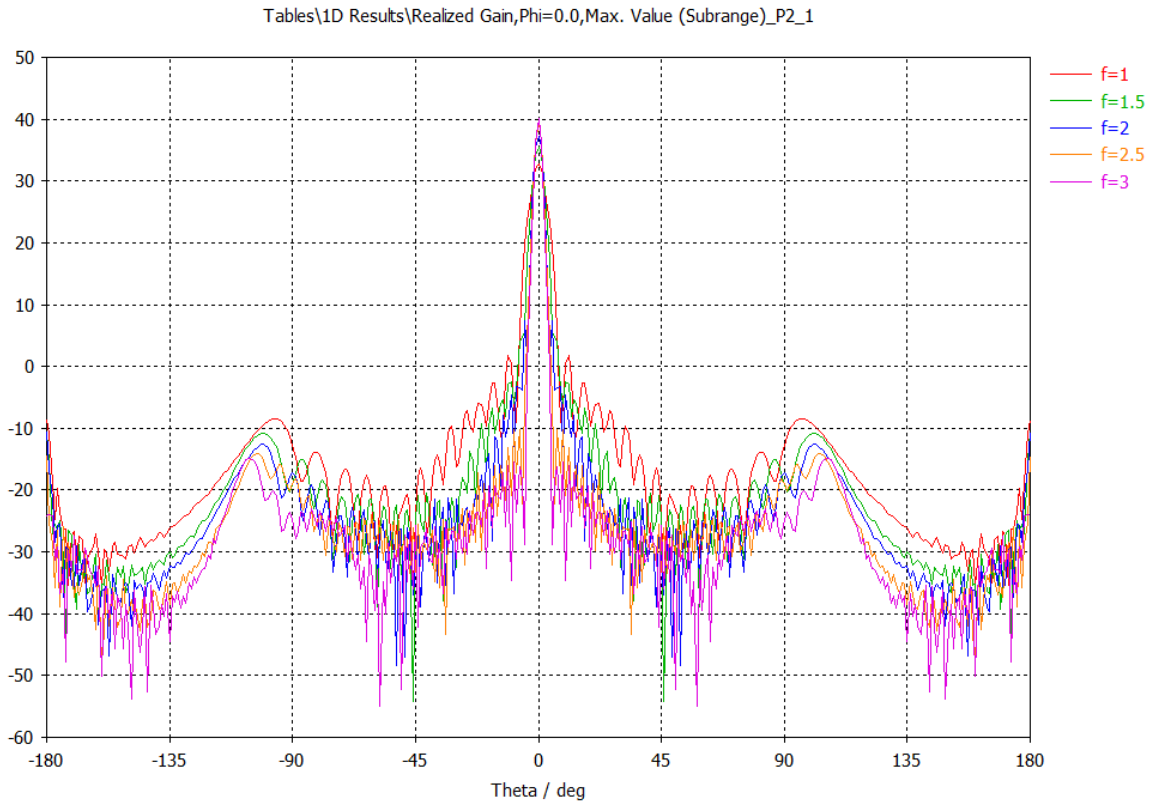


Figure 5-3: Radiation patterns over frequency.

5.1.2 Antenna dish reflector with radiation source with blockage

In Figure 5-4 the gain performance over frequency of the complete dish/feed geometry is shown taking into account the blockage effect. The blockage is emulated with a metallic disc of zero thickness with the same diameter as the flare diameter. The feed is replaced by the equivalent far field source obtained by separate 3D EM simulation of the complete feed geometry.

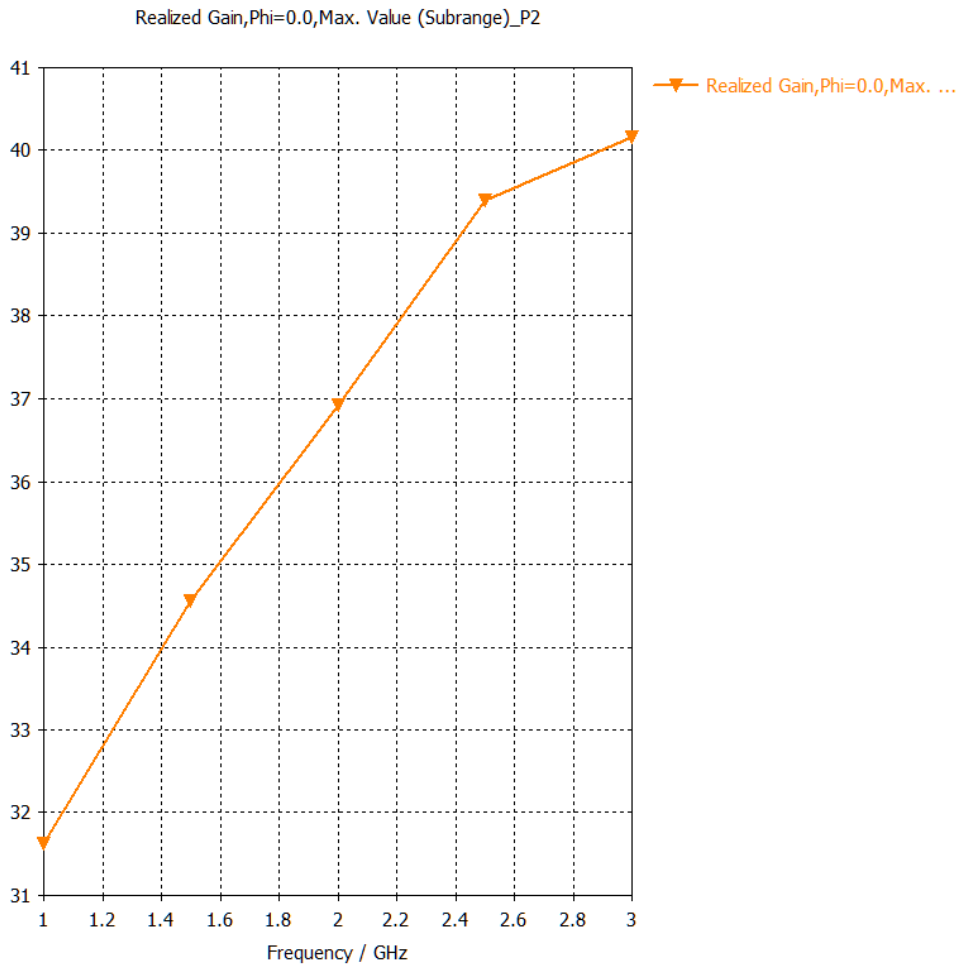


Figure 5-4: Gain variation over frequency.

In Figure 5-5 the 3dB beamwidth (for the $\phi = 90^\circ$ cut) vs frequency is presented for the case of blockage.

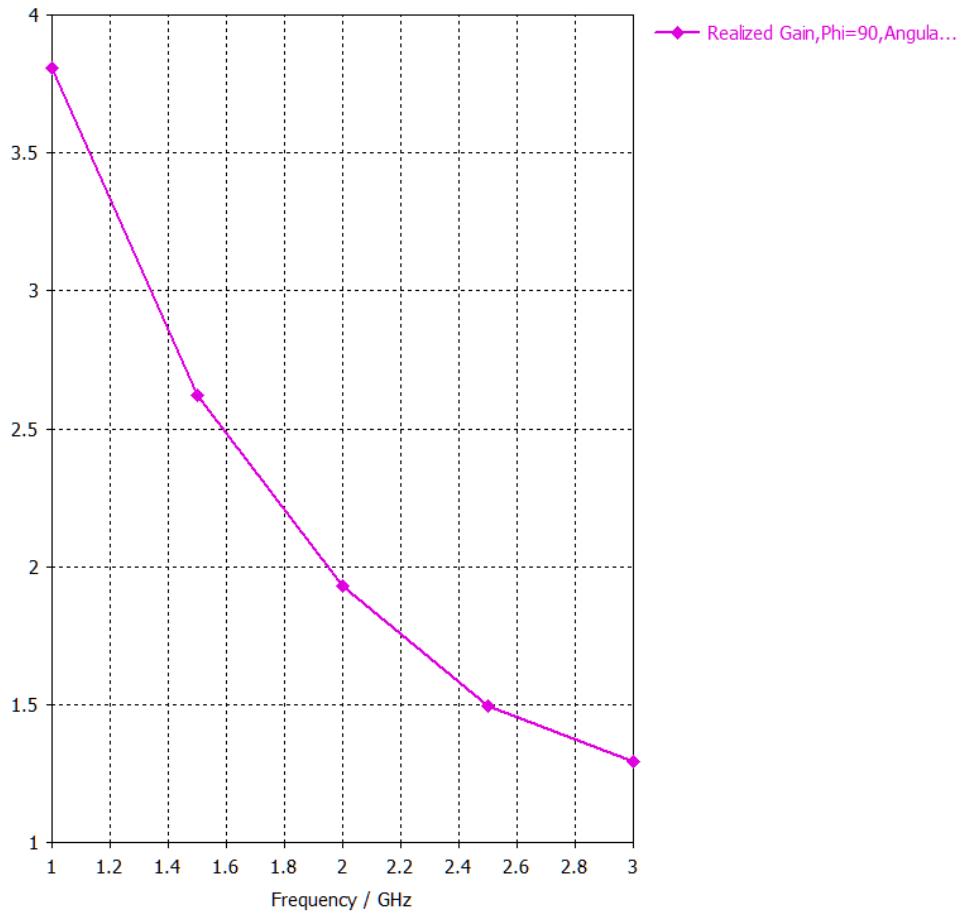


Figure 5-5: 3dB beamwidth variation over frequency.

In Figure 5-6 the cartesian plots for various frequency points in the frequency range 1-3 GHz are presented for the blockage case. In this plot we can see details for the sidelobe levels, front to back ratios and nulls.

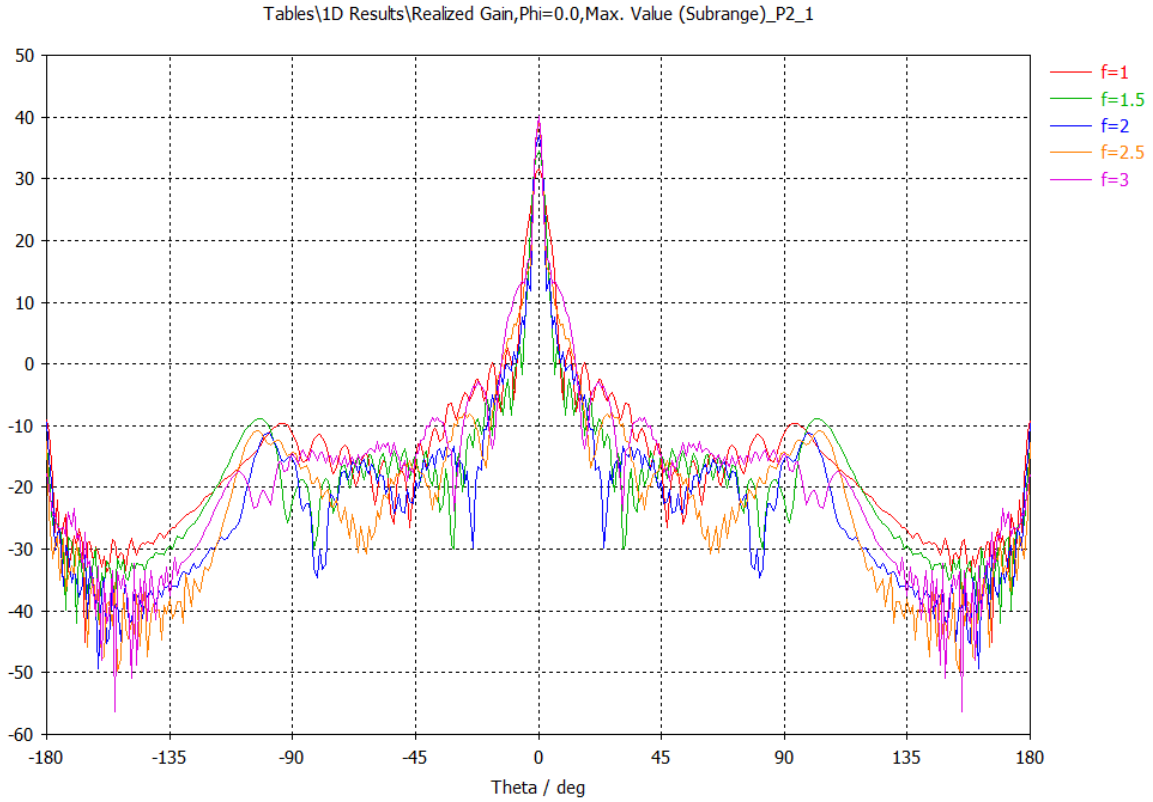


Figure 5-6: Radiation patterns over frequency.

5.1.3 Antenna dish reflector including feeding antenna true geometry using SAM procedure (System Assembly modelling), unidirectional approach.

In this section the System Assembly Modelling (SAM) procedure is used for the analysis of the complete geometric model of the antenna feed along with the 6 meters diameter dish. Specifically, the unidirectional approach is used. That means that the feed interacts with the dish but no blockage or spill-over phenomena are taken into account. The gain variation over frequency is plotted in Figure 5-7.

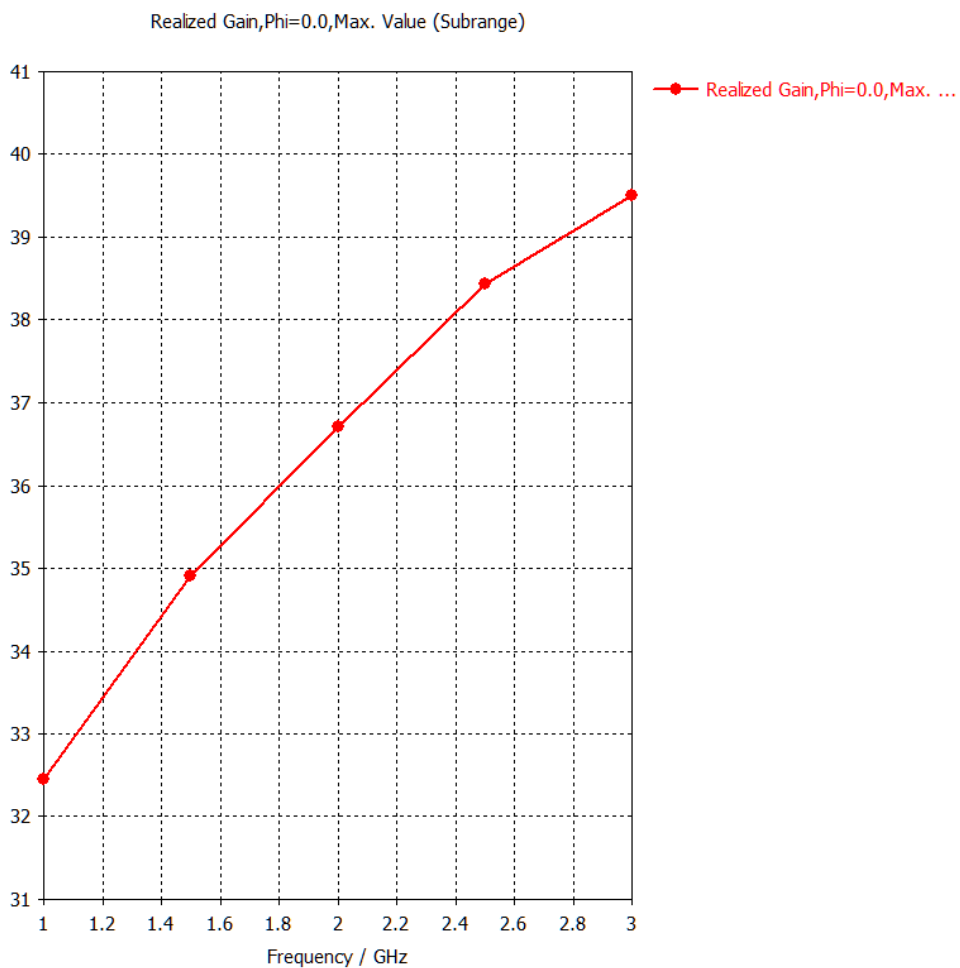


Figure 5-7: Gain variation over frequency.

If we compare Figure 5-7 with Figure 5-4, we see that there is a gain drop of about 0.5 dB. This difference probably happens due to mesh quality. The acceptable error percentage in the calculation is set to 2% in order to have a result in a realistic time duration.

In Figure 5-8 the 3 dB beamwidth (for the $\phi = 0^\circ$ cut) vs frequency is presented. If we compare it with Figure 5-5, it is obvious that the beamwidth is higher by 0.6 degrees again due to meshing issues.

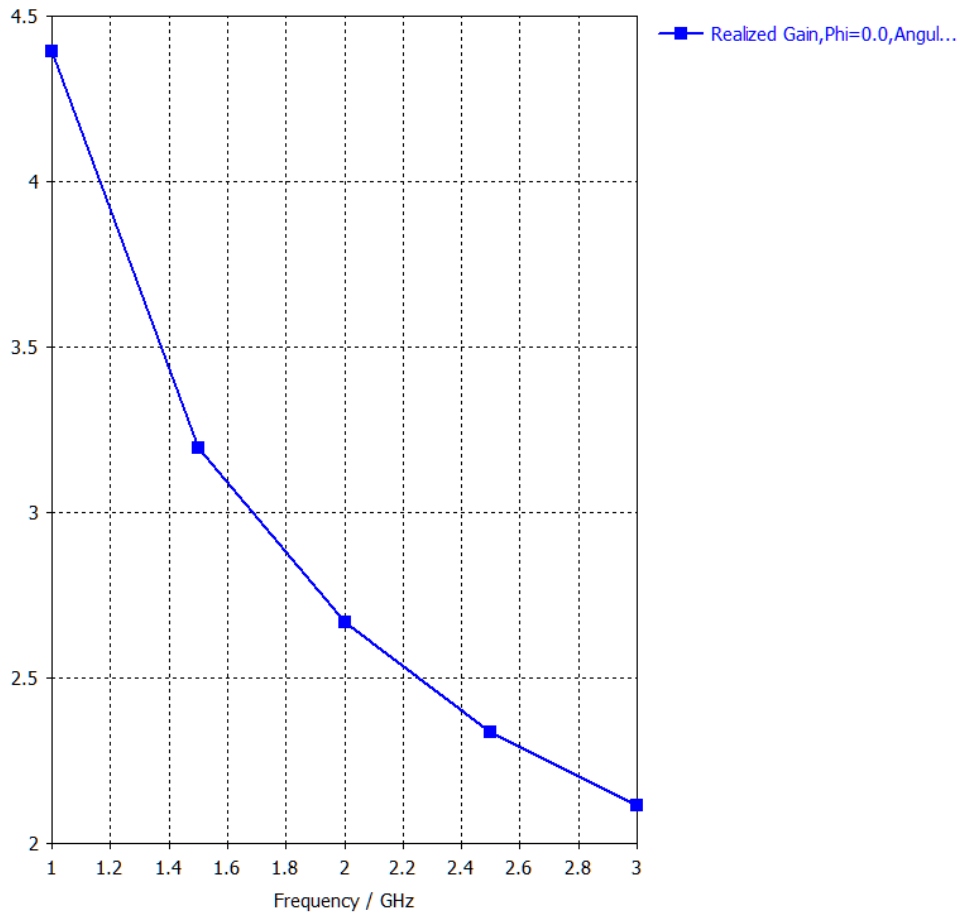


Figure 5-8: 3 dB beamwidth variation over frequency.

The cartesian plots of the radiation pattern for various frequencies in the range 1-3 GHz are depicted in Figure 5-9.

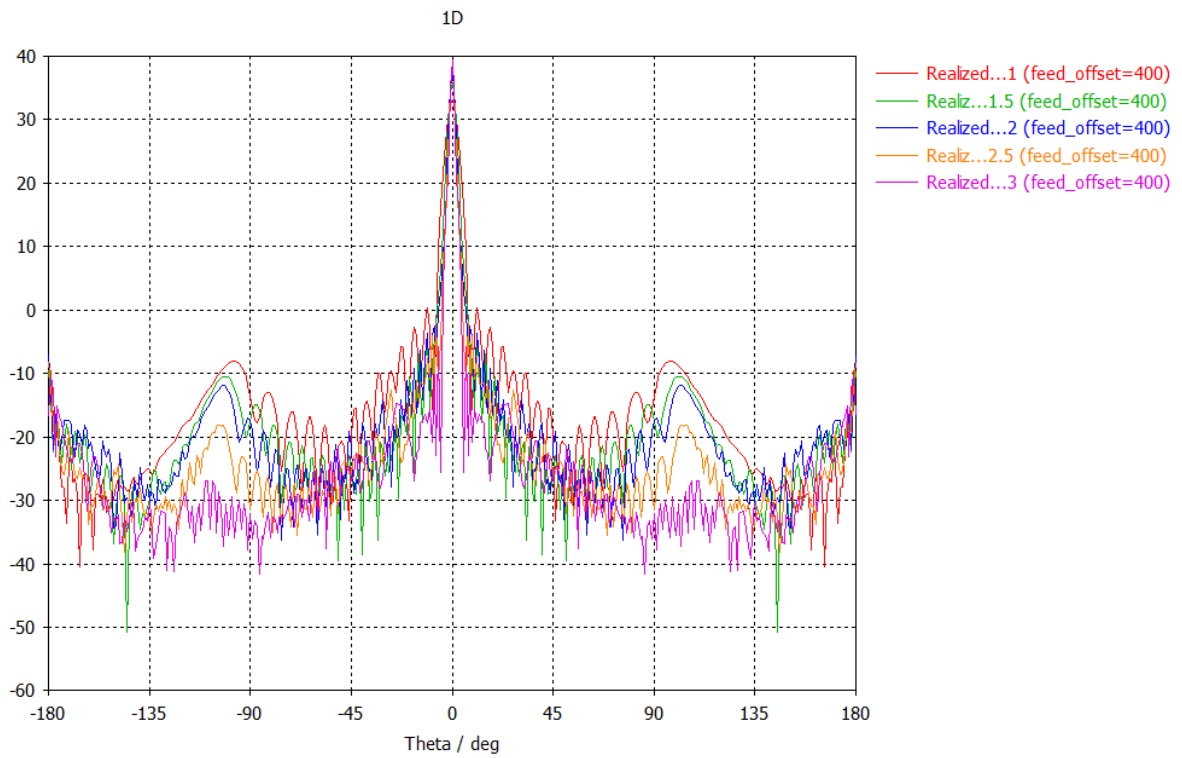


Figure 5-9: Radiation patterns over frequency.

5.1.4 Antenna dish reflector including feeding antenna true geometry using SAM procedure (System Assembly modelling), bidirectional approach.

In this section the System Assembly Modelling (SAM) procedure is employed for the analysis of the complete geometric model of the antenna feed along with the 6 meters diameter dish. Specifically, the bidirectional approach is used. That means that the feed interacts with the dish taking into account both blockage and spill-over phenomena. The gain variation over frequency is plotted in Figure 5-10.

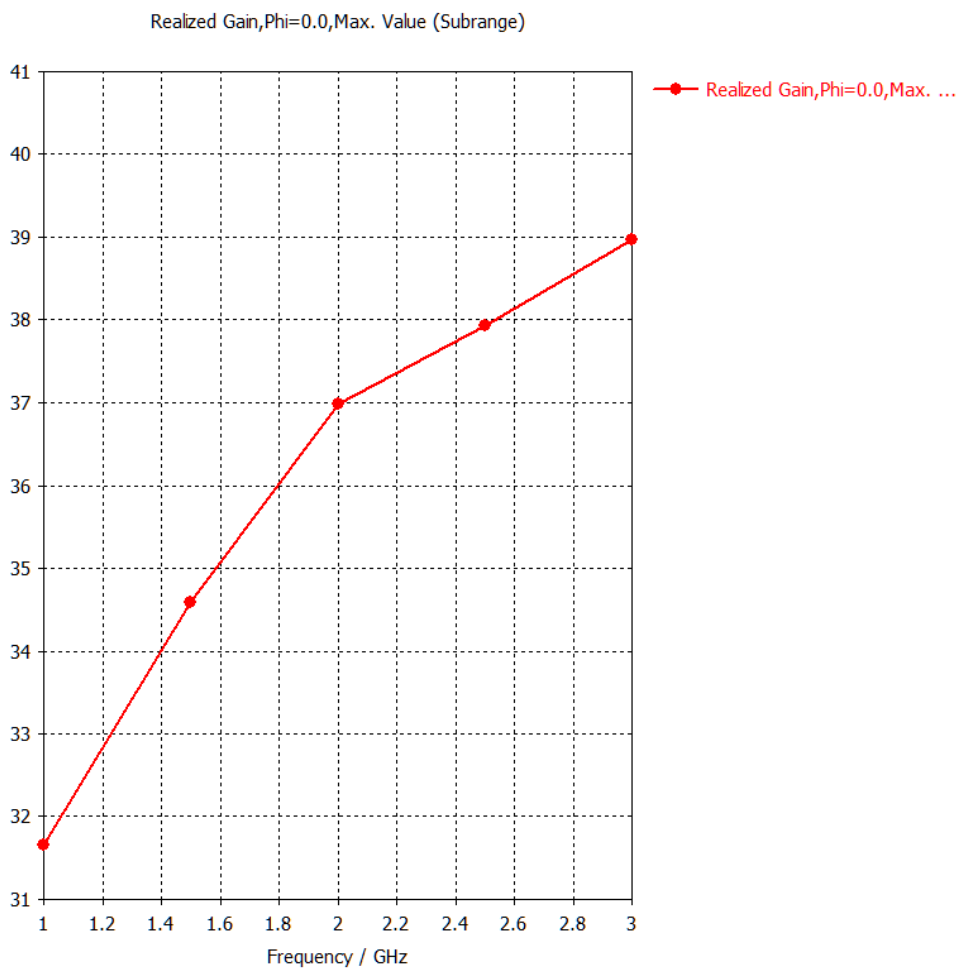


Figure 5-10: Gain variation over frequency.

If we compare Figure 5-10 with Figure 5-4, we see that is a gain drop of about 1 dB. This difference probably happens due to mesh quality. The acceptable error percentage in the calculation is set to 2% in order to have a result in a realistic time duration. There is also a small gain drop if we compare this figure with Figure 5-3.

In Figure 5-11 the 3dB beamwidth (for the $\phi = 0^\circ$ cut) vs frequency is presented. If we compare it with Figure 5-1, it is obvious that the beamwidth is higher by 0.4 degrees again due to meshing issues.

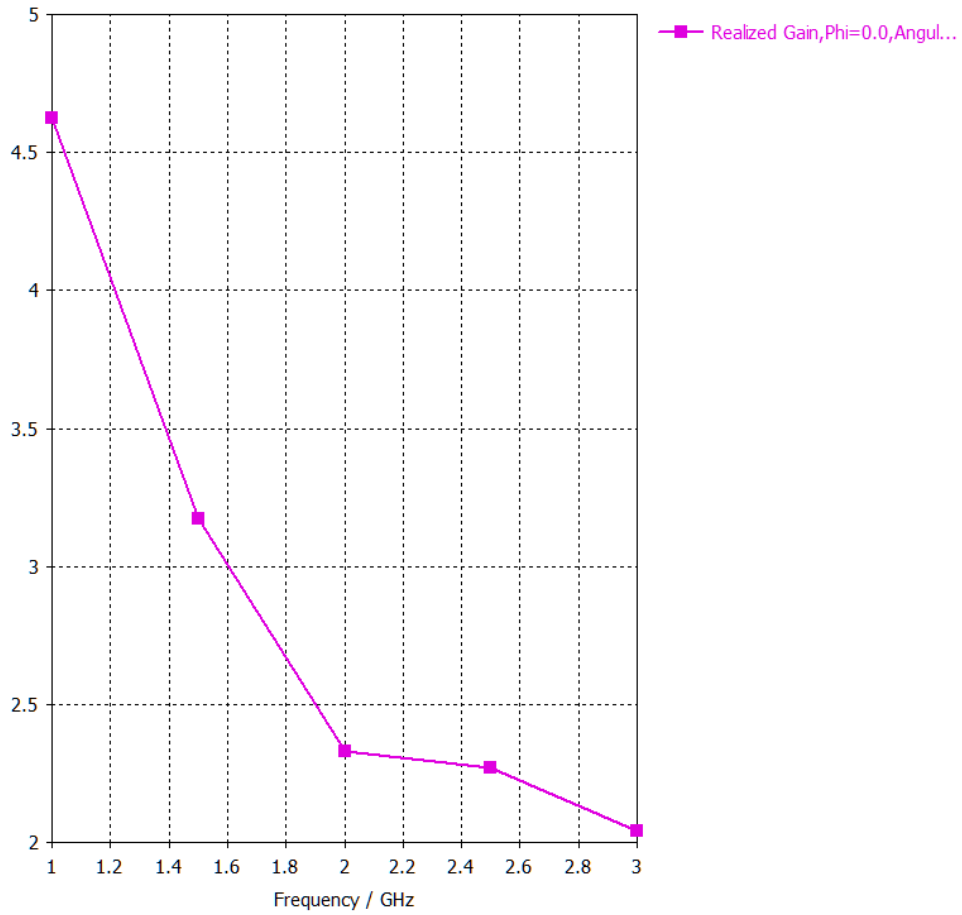


Figure 5-11: 3 dB beamwidth variation over frequency.

The cartesian plots of the radiation pattern for various frequency steps in the range 1-3 GHz is presented in Figure 5-12.

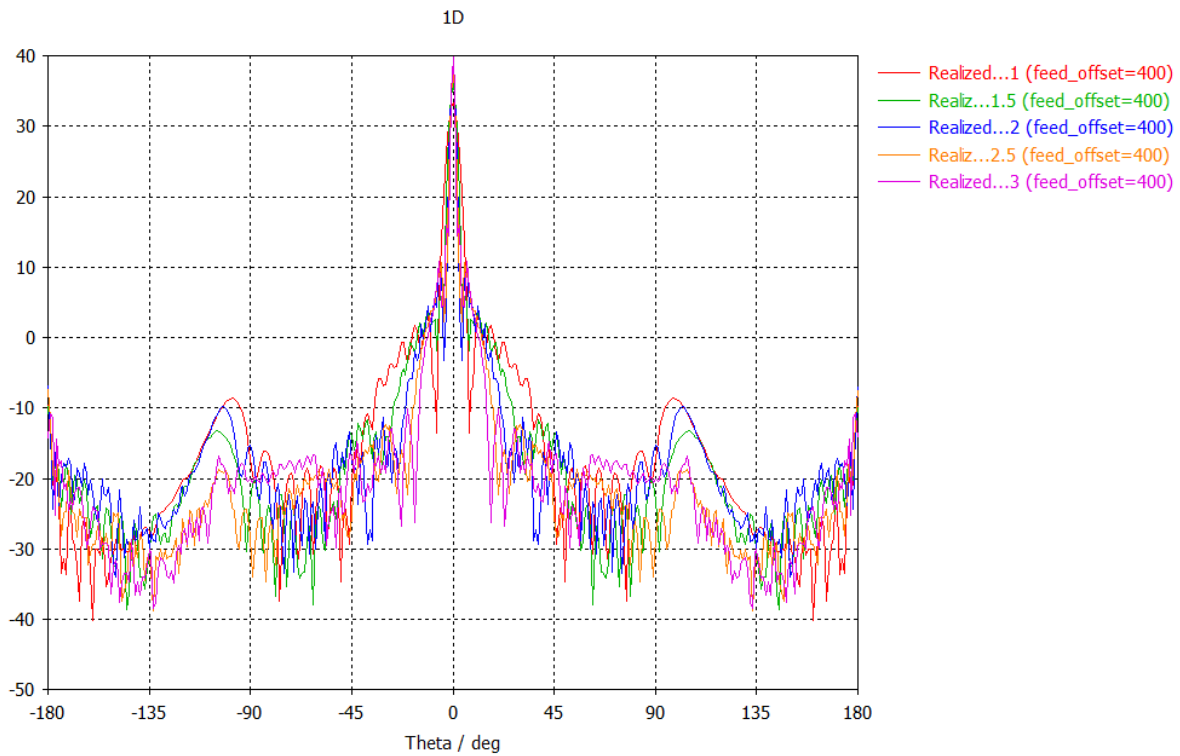


Figure 5-12: Radiation patterns over frequency.

5.2 Meshing approaches on SAM 3D EM Dish-Horn antenna simulations

5.2.1 Introduction

In this section different meshing methods of System Advanced Modelling (SAM) 3D electromagnetic simulation technique are presented. In all cases bi-directional coupling is used. For the dish simulation the Integral solver is used, where for the horn feed the time domain solver is employed. Both horn polarizations are taken into account, therefore no symmetry planes exist. Since for the high mesh (most accurate) due to computer memory limitations, a symmetry plane is assumed and only one port excitation is calculated. The general geometry of all simulations is shown in Figure 5-13:

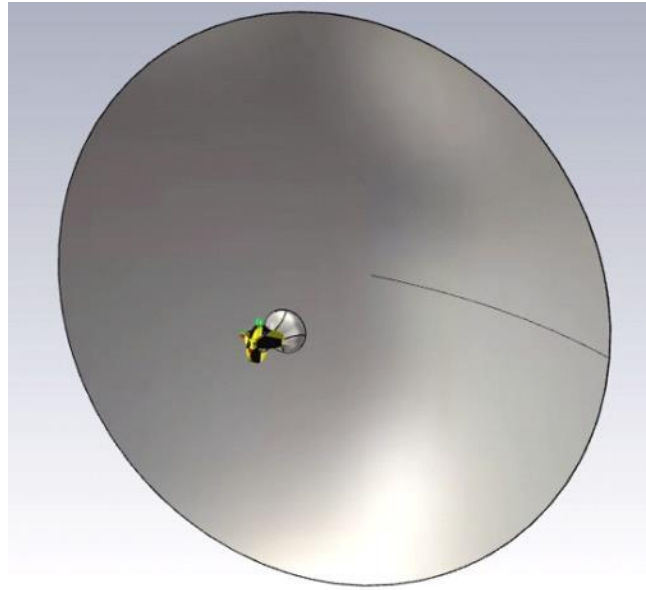


Figure 5-13: General dish-horn geometry.

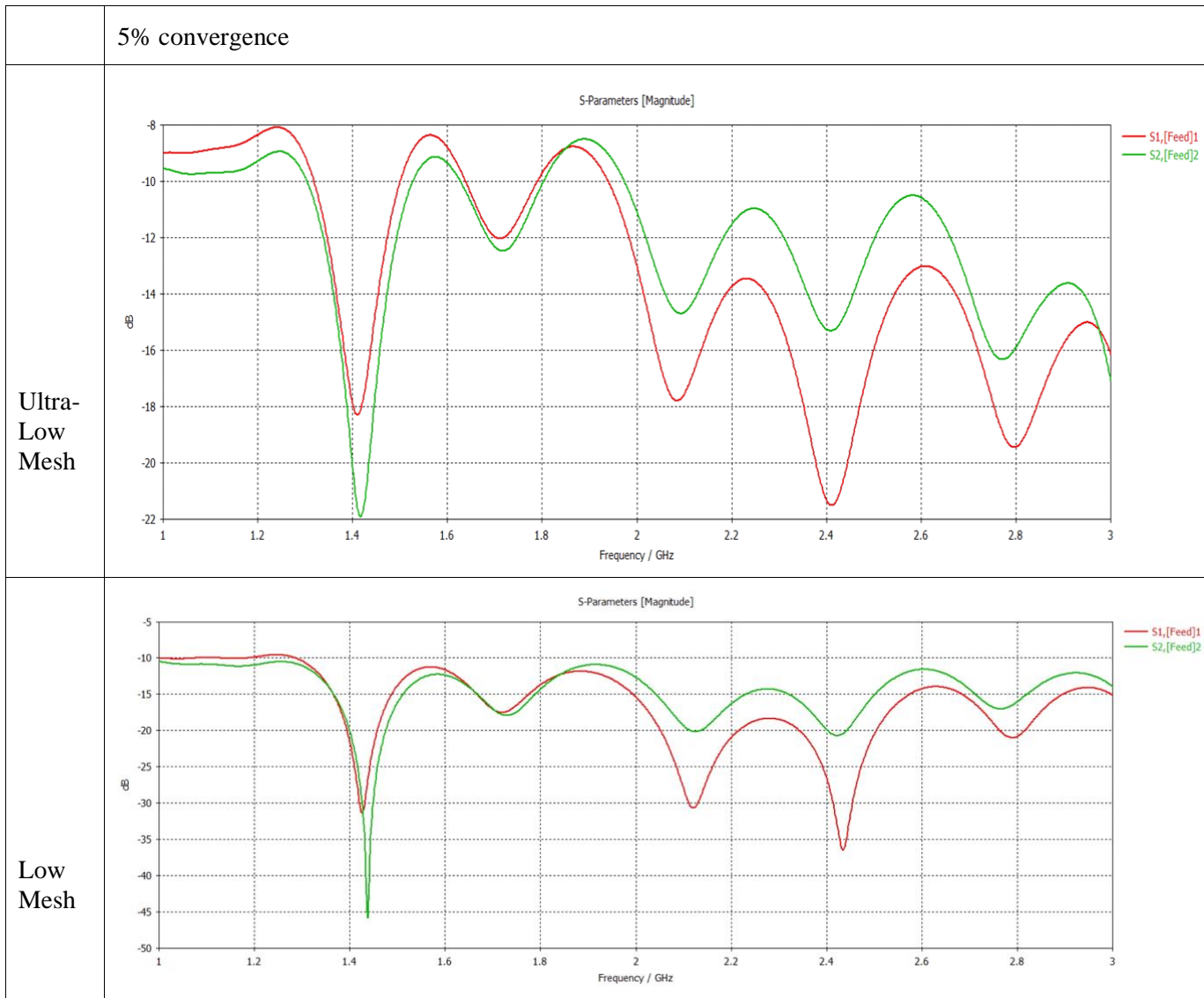
In table 5-14 the four valid simulation cases and their specifications are shown. The last two cases at the bottom of table 5-14 unfortunately have not succeeded in providing some results due to the fact that the simulation exceeded the computer resources.

<i>Simulation case</i>	<i>Convergence</i>	<i>Dish mesh surfaces</i>	<i>Feed mesh-cells</i>	<i>Simulation time</i>
<i>Dish-Feed ultra-low mesh 0.05</i>	<i>0.05</i>	<i>63.000</i>	<i>3.500.000</i>	<i>1h 8min</i>
<i>Dish-Feed ultra-low mesh 0.01</i>	<i>0.01</i>	<i>63.000</i>	<i>3.500.000</i>	<i>1h 29min</i>
<i>Dish-Feed low mesh 0.05</i>	<i>0.05</i>	<i>253.000</i>	<i>8.250.000</i>	<i>4h 30min</i>
<i>Dish-Feed low mesh 0.01</i>	<i>0.01</i>	<i>253.000</i>	<i>8.250.000</i>	<i>5h 55 min</i>
<i>Dish-Feed high mesh 0.05</i>	<i>0.05</i>	<i>480.000/2</i>	<i>23.000.000/2</i>	<i>Exceed memory limit, only possible using symmetry plane (6h 52min)</i>
<i>Dish-Feed high mesh 0.01</i>	<i>0.01</i>	<i>480.000/2</i>	<i>23.000.000/2</i>	<i>Exceed memory limit, only possible using symmetry plane (8h 45min)</i>

Table 5-14: Simulation cases.

5.2.2 Simulation results

In Figures 5-15 and 5-16 the S_{11} , S_{22} for the two polarization feed ports are shown for 1% and 5% convergence. The results in both convergence cases look quite the same.



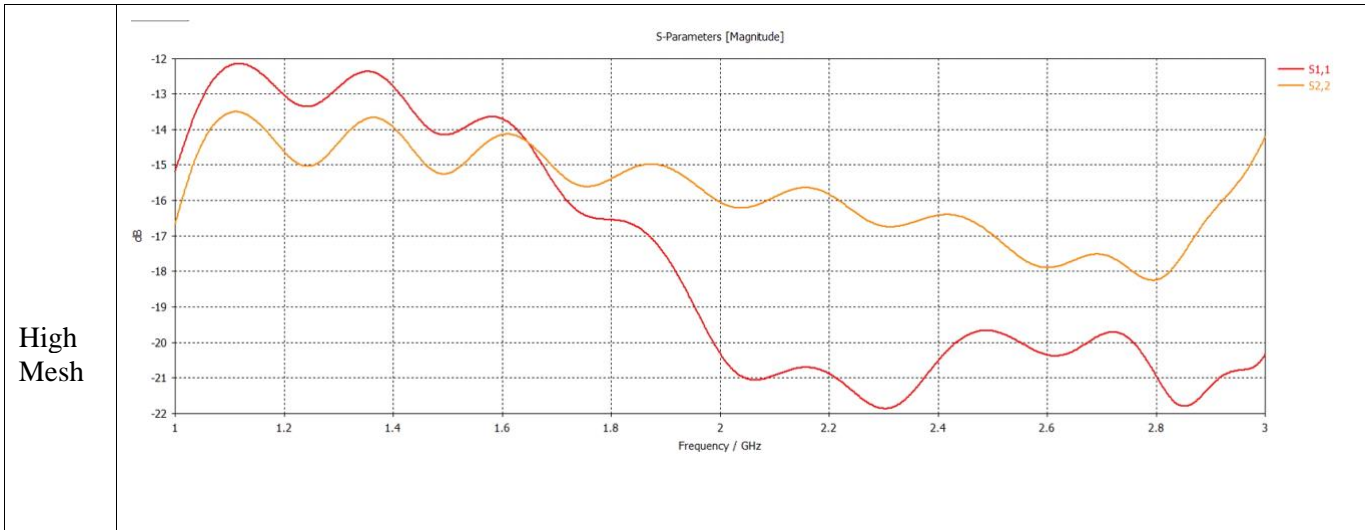


Figure 5-2: S_{11} , S_{22} simulation results over frequency, 5% convergence.

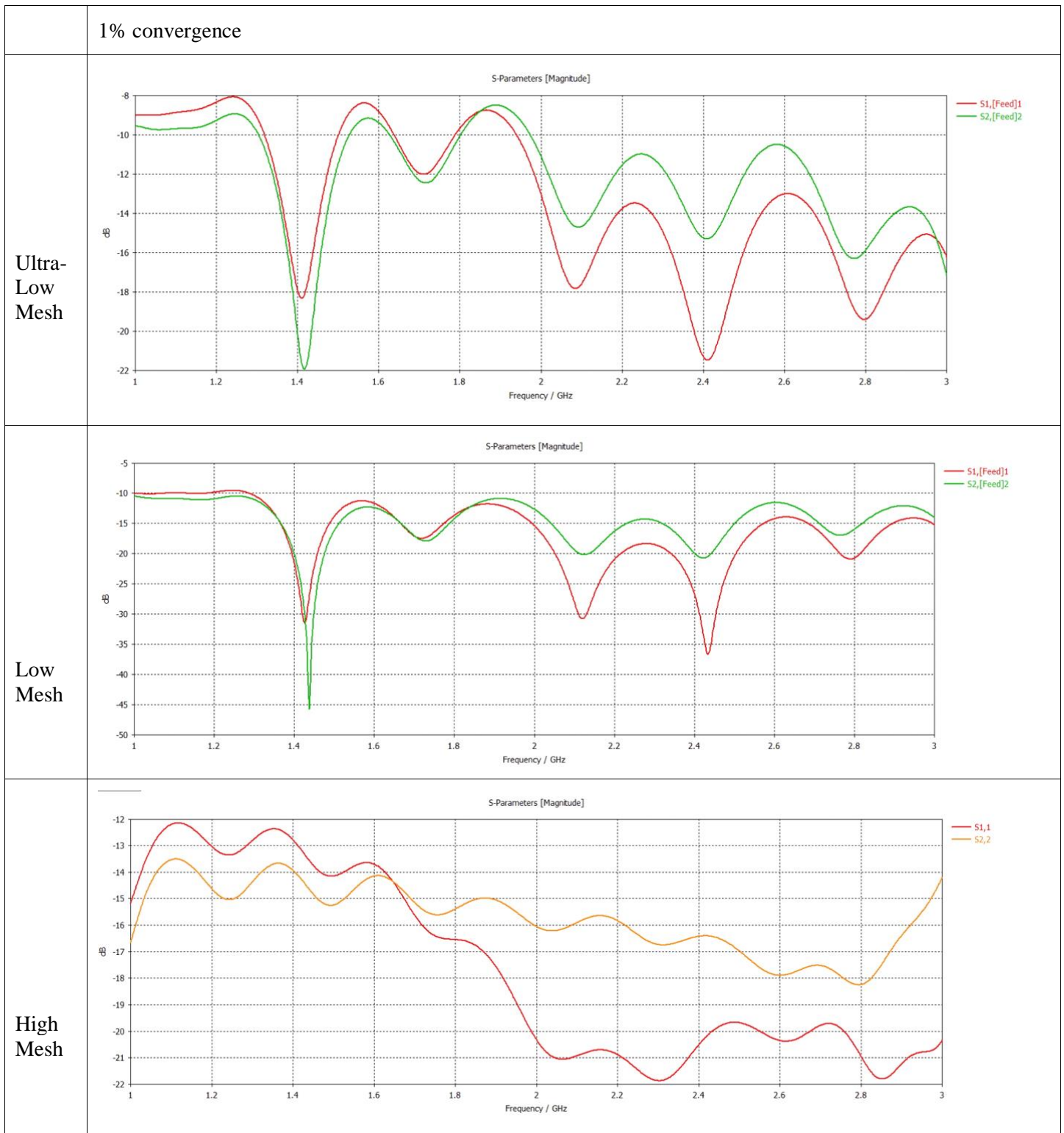
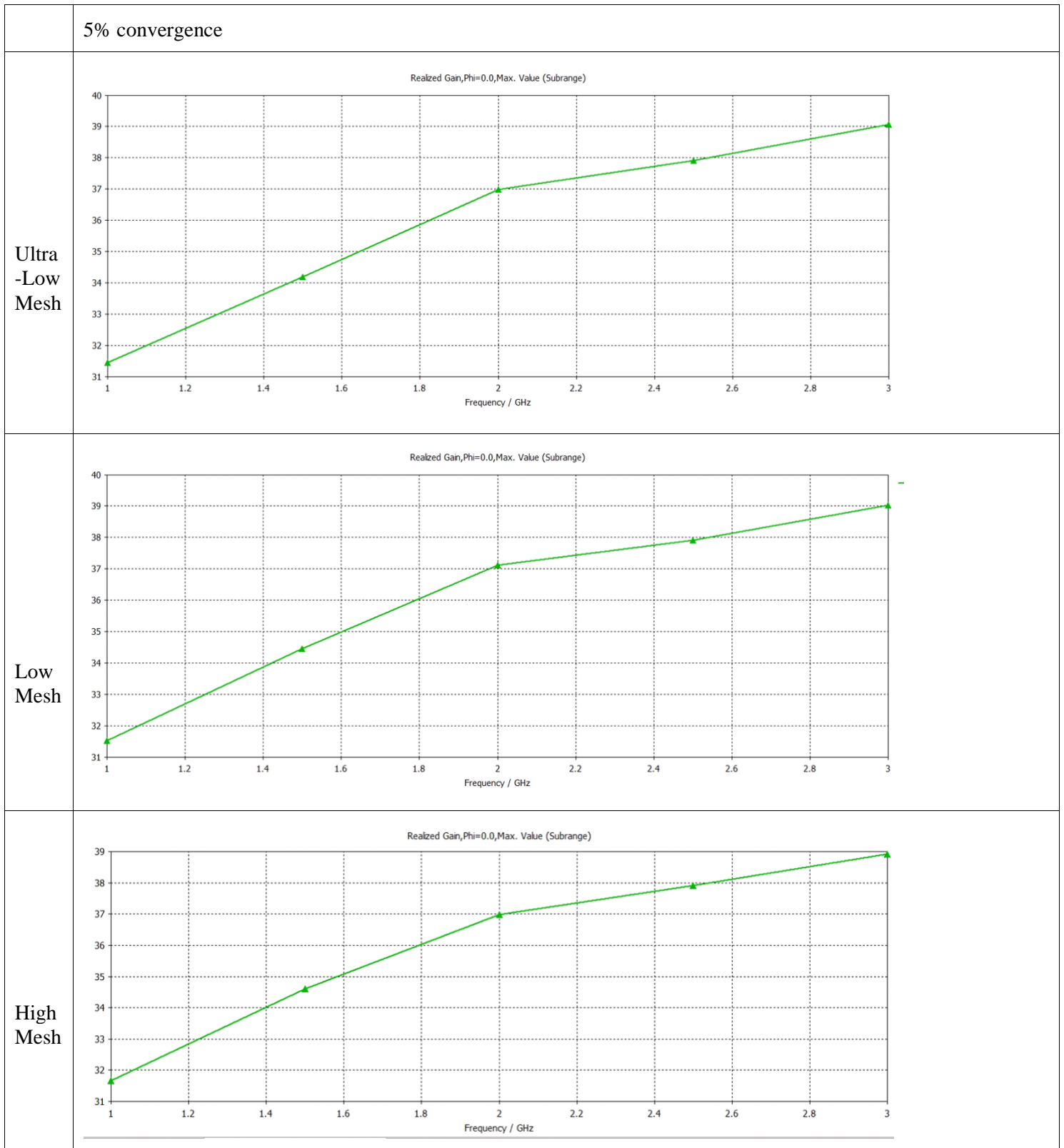


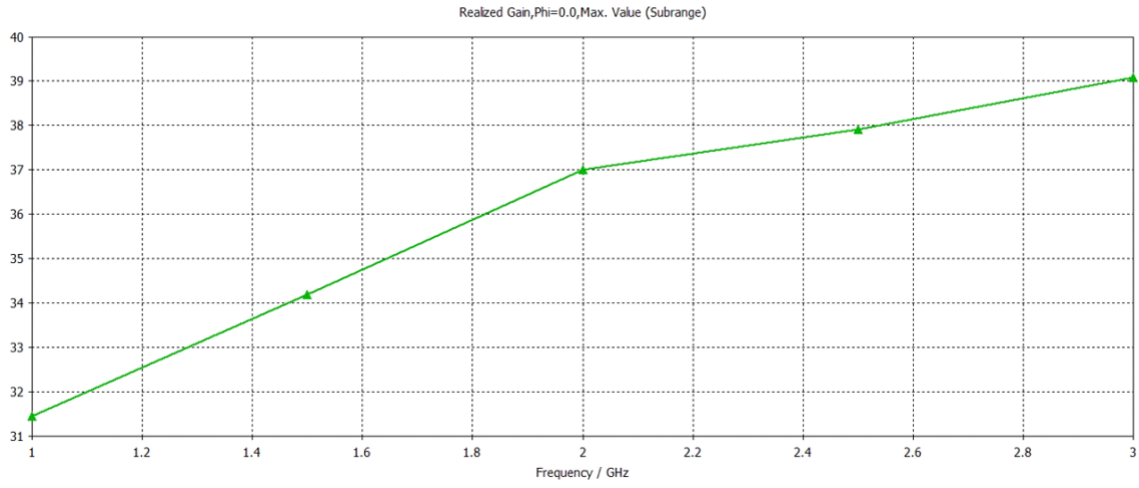
Figure 5-3: S_{11} , S_{22} simulation results over frequency, 1% convergence.

In Figure 5-17 the gain over frequency performance is shown for 1% and 5% convergence. The results in both convergence cases look quite the same.

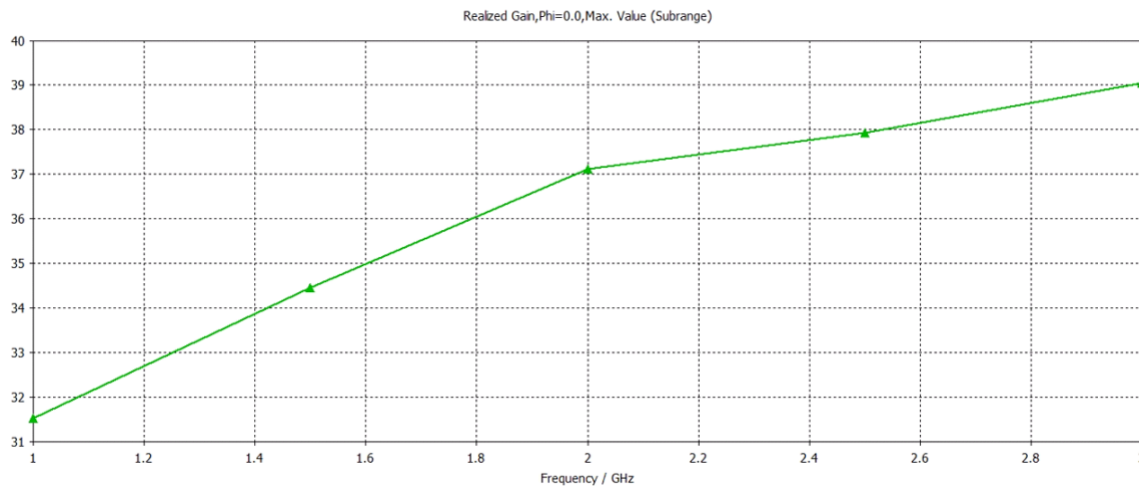


1% convergence

Ultra
-Low
Mesh



Low
Mesh



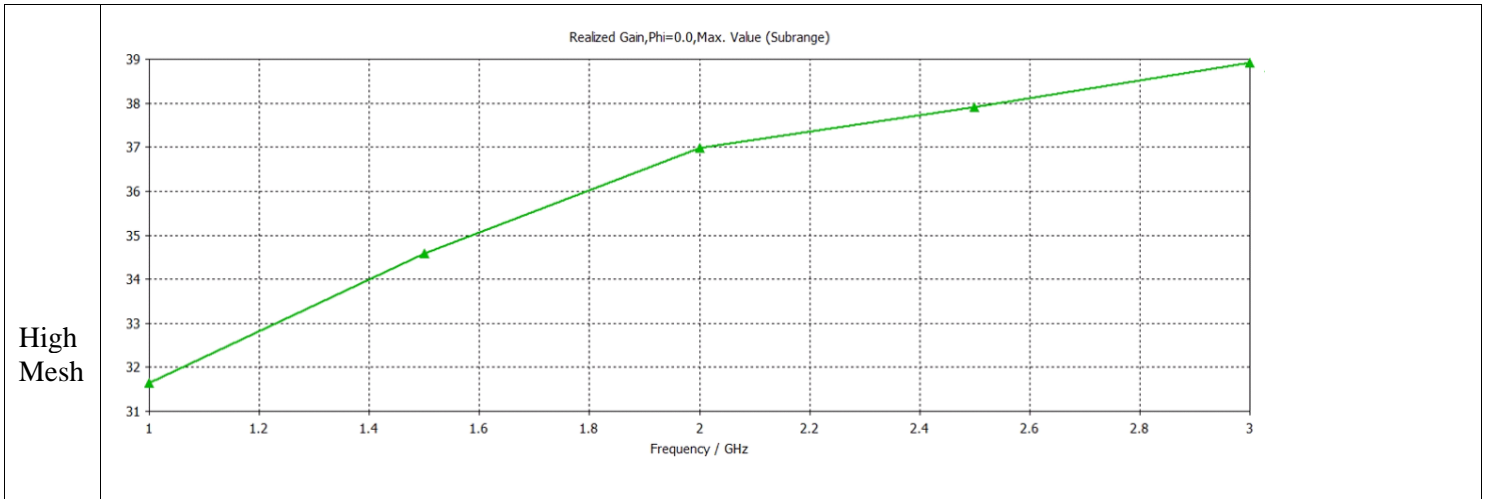
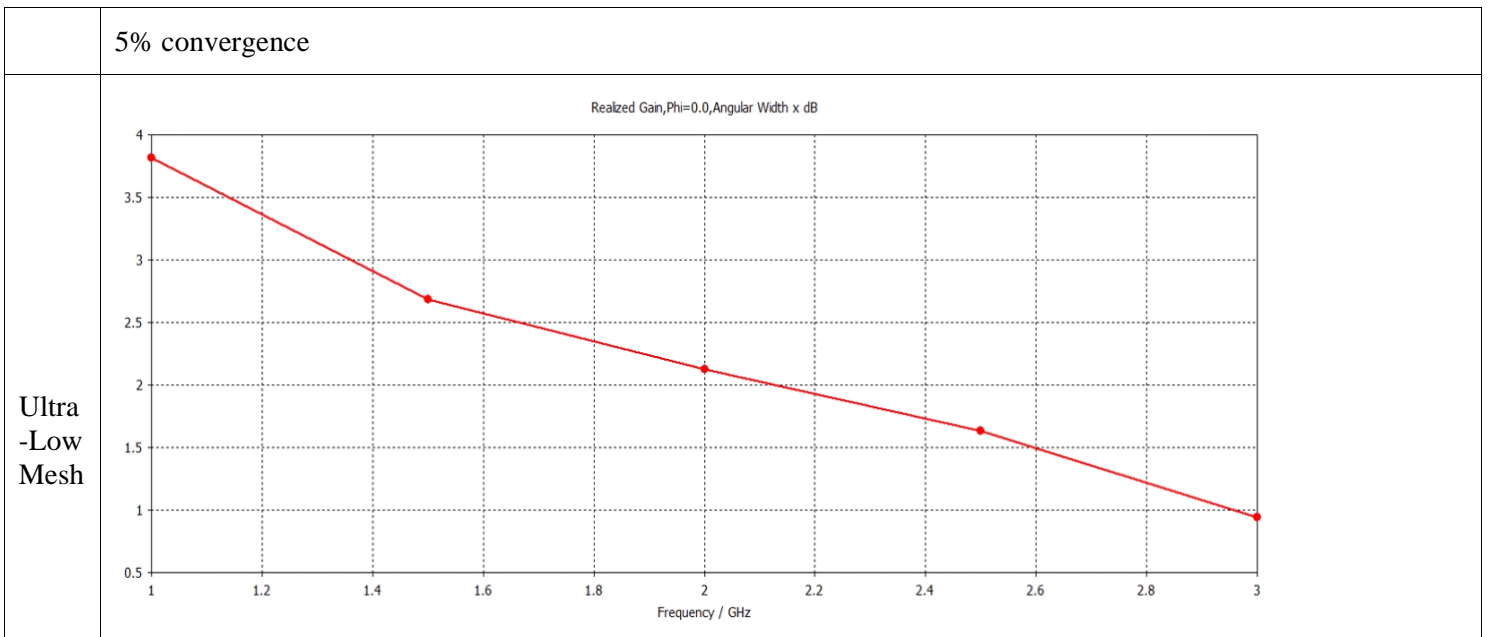
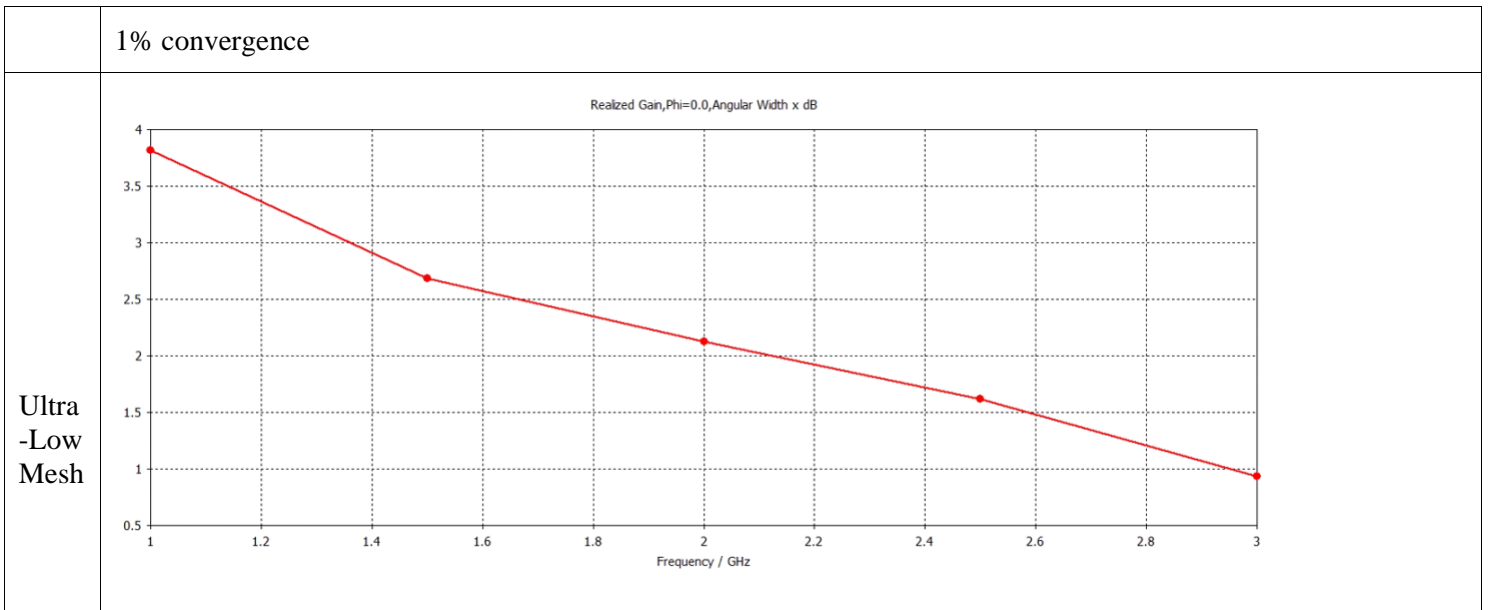
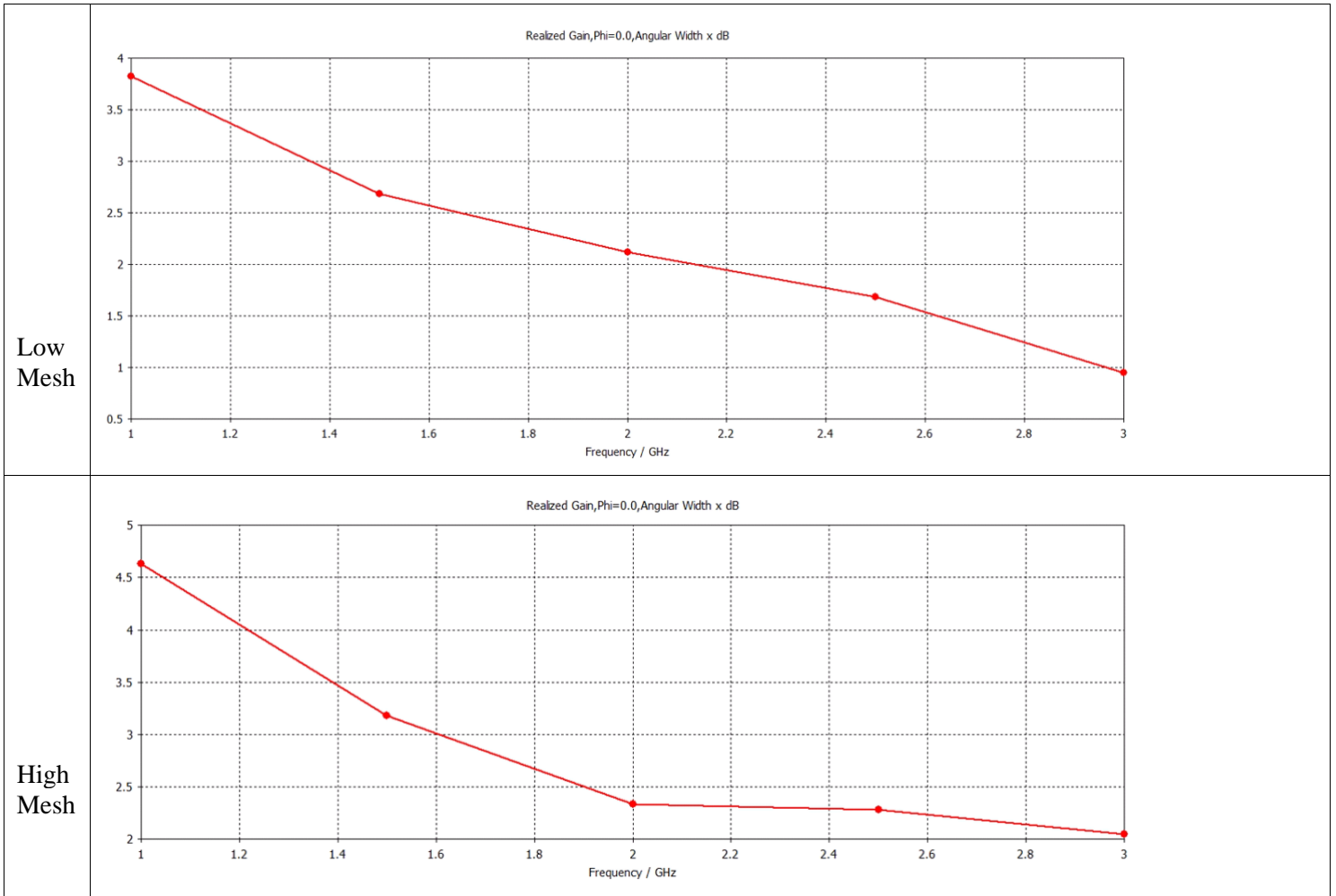


Figure 5-17: Dish antenna Gain over frequency, 5% and 1% convergence.

In Figure 5-18 the 3 dB beamwidth (for $\phi = 0^\circ$) over frequency performance is shown for 1% and 5% convergence. The results in both convergence cases look quite the same.





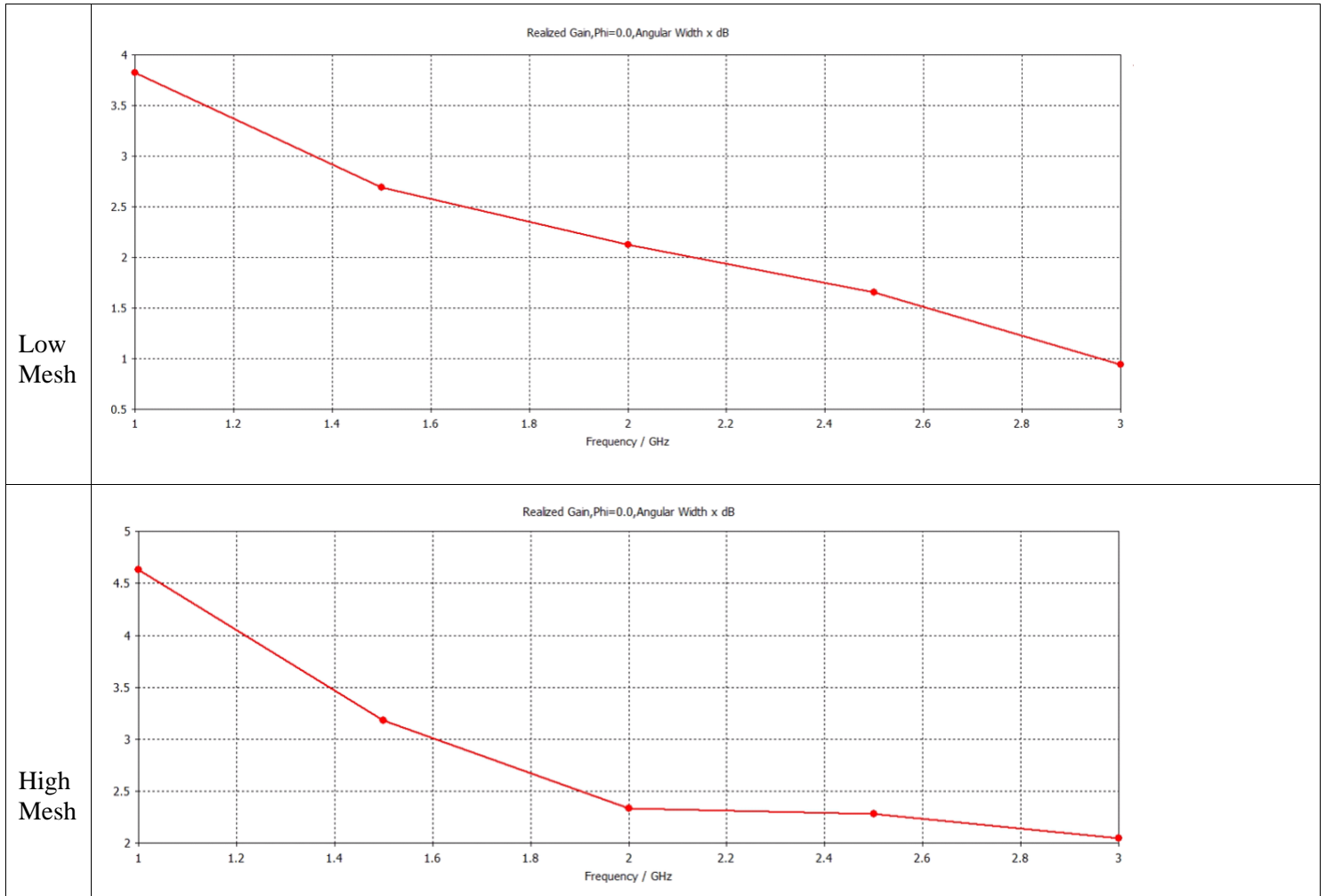


Figure 5-18: 3 dB beamwidth of dish antenna gain over frequency, 5% and 1% convergence.

In Figures 5-19 to 5-24, the cartesian radiation patterns over frequency performance is shown for 1% and 5% convergence. The results in both convergence cases look quite the same.

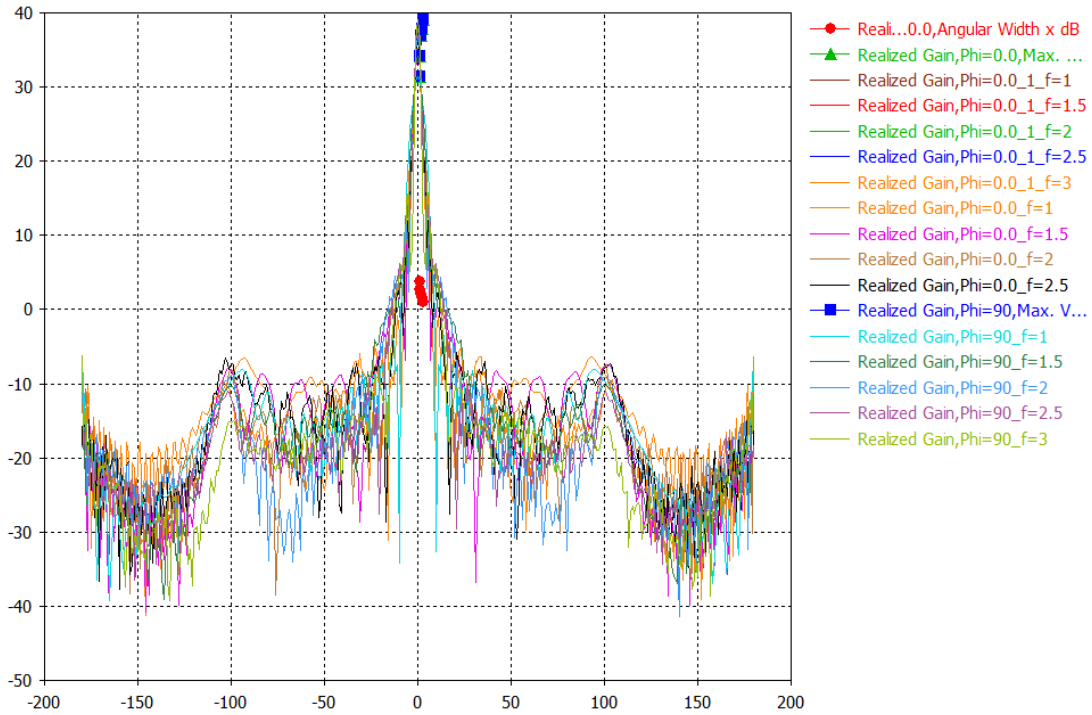


Figure 5-19: Ultra-Low Mesh 5% Convergence

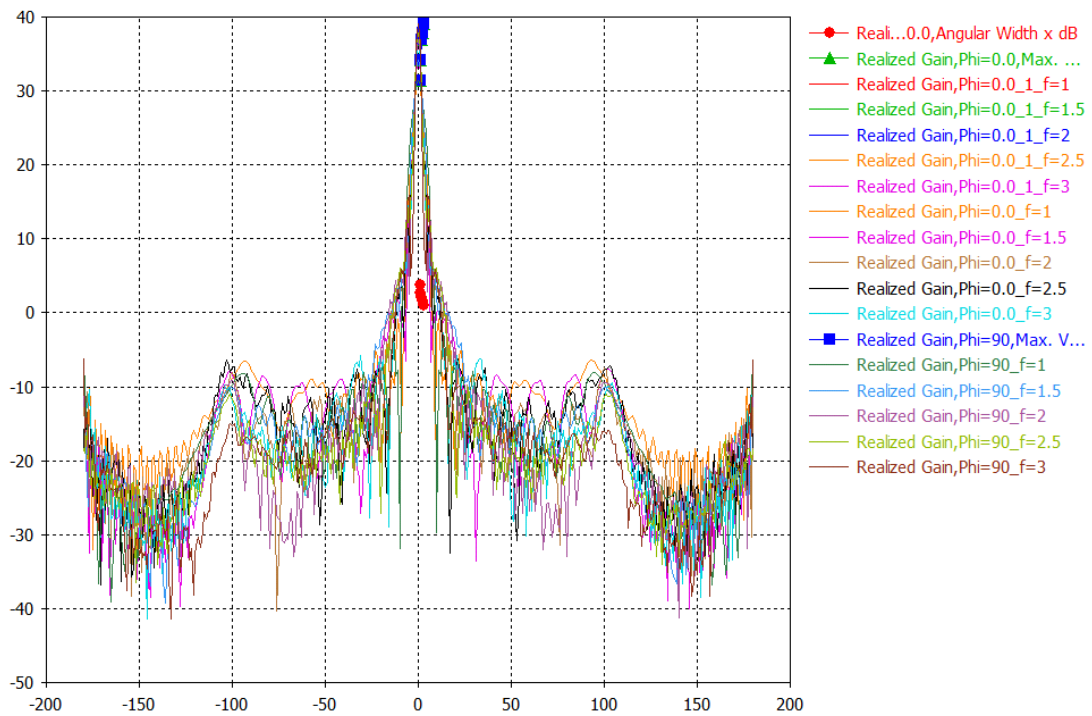


Figure 5-20: Ultra-Low Mesh 1% Convergence

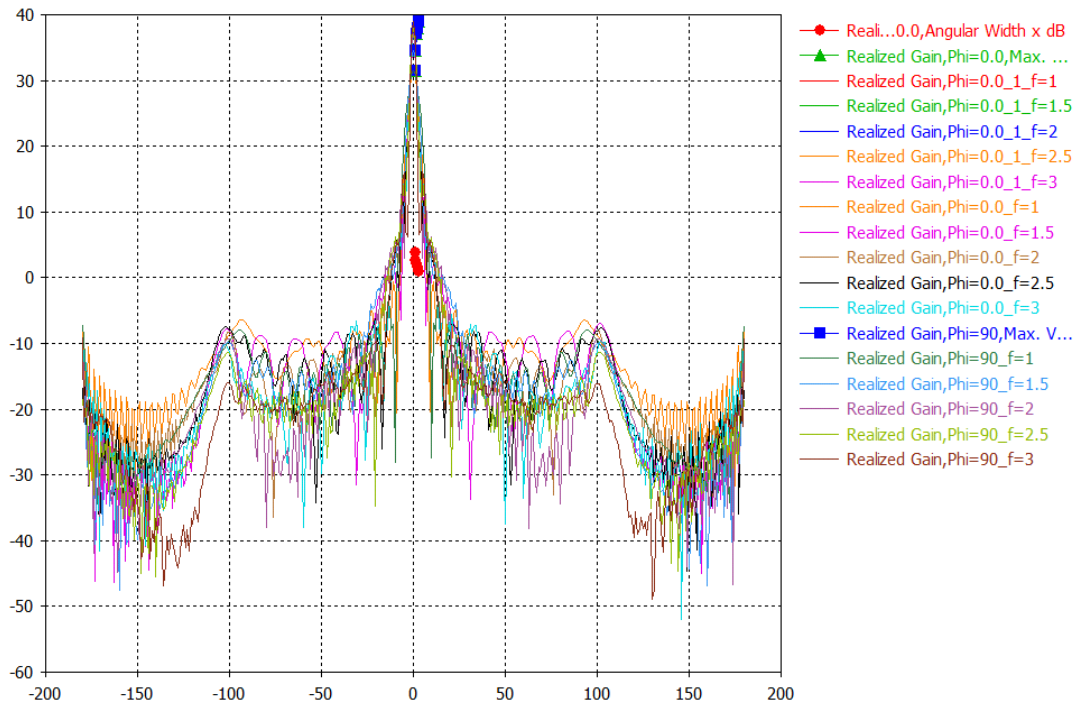


Figure 5-21: Low Mesh 5% Convergence

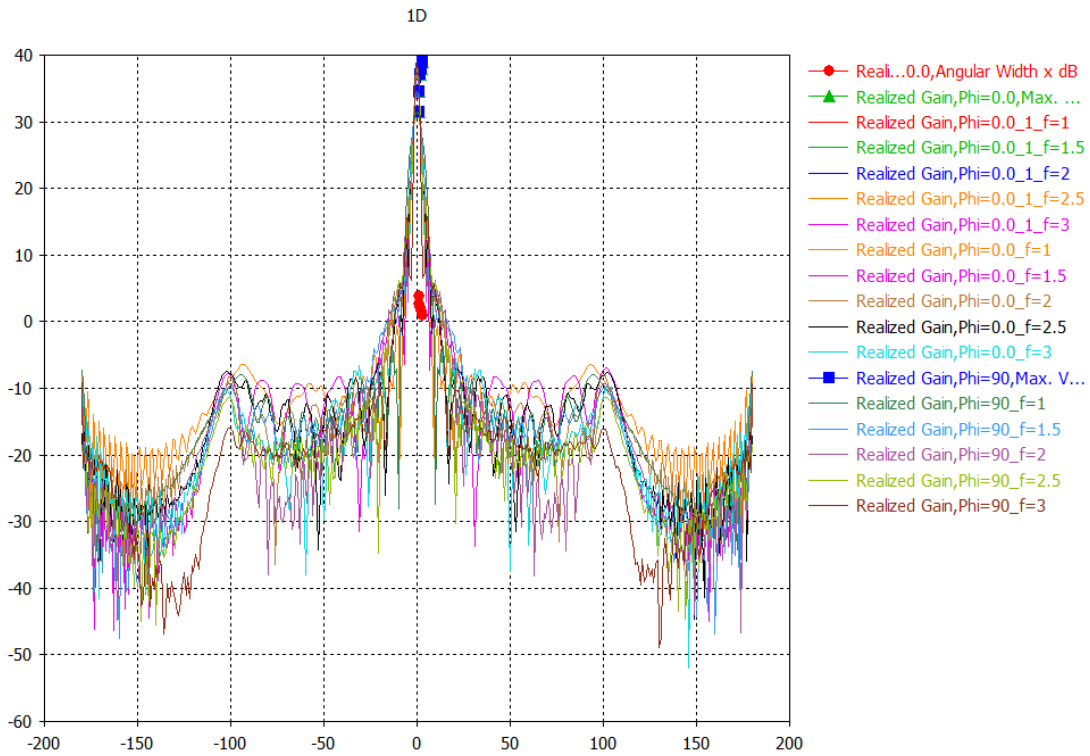


Figure 5-22: Low Mesh 1% Convergence

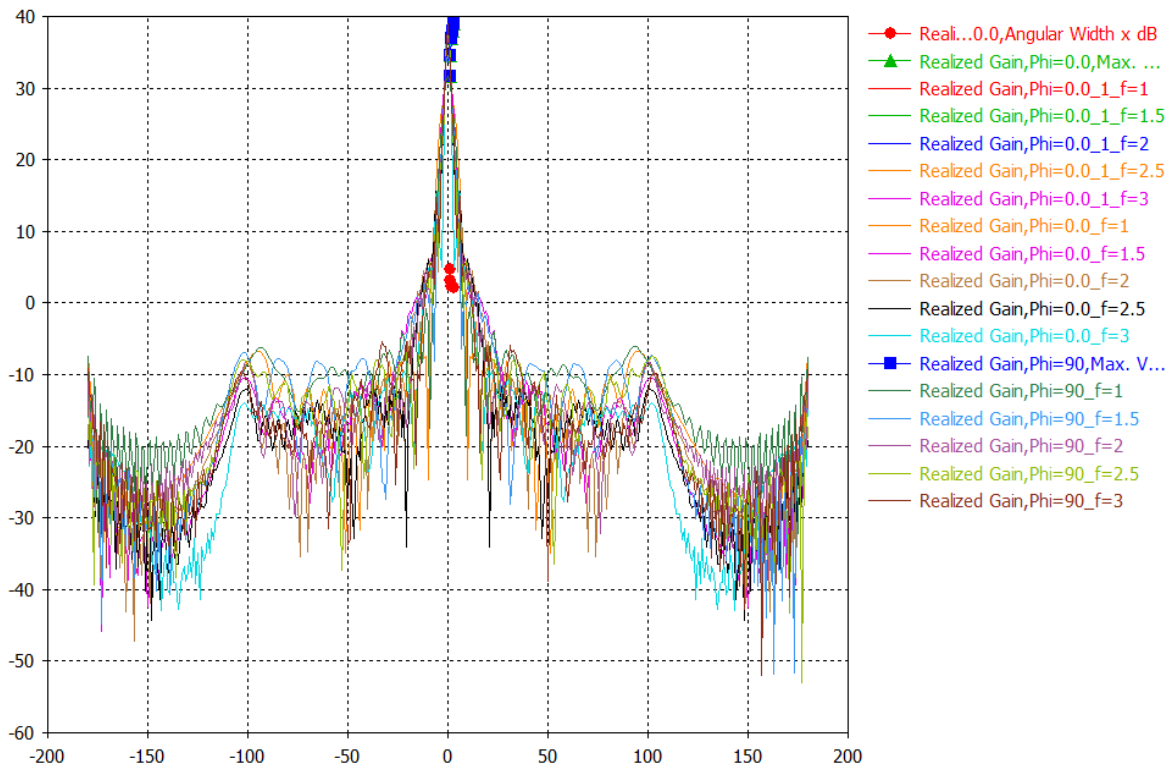


Figure 5-23: High Mesh 5% Convergence

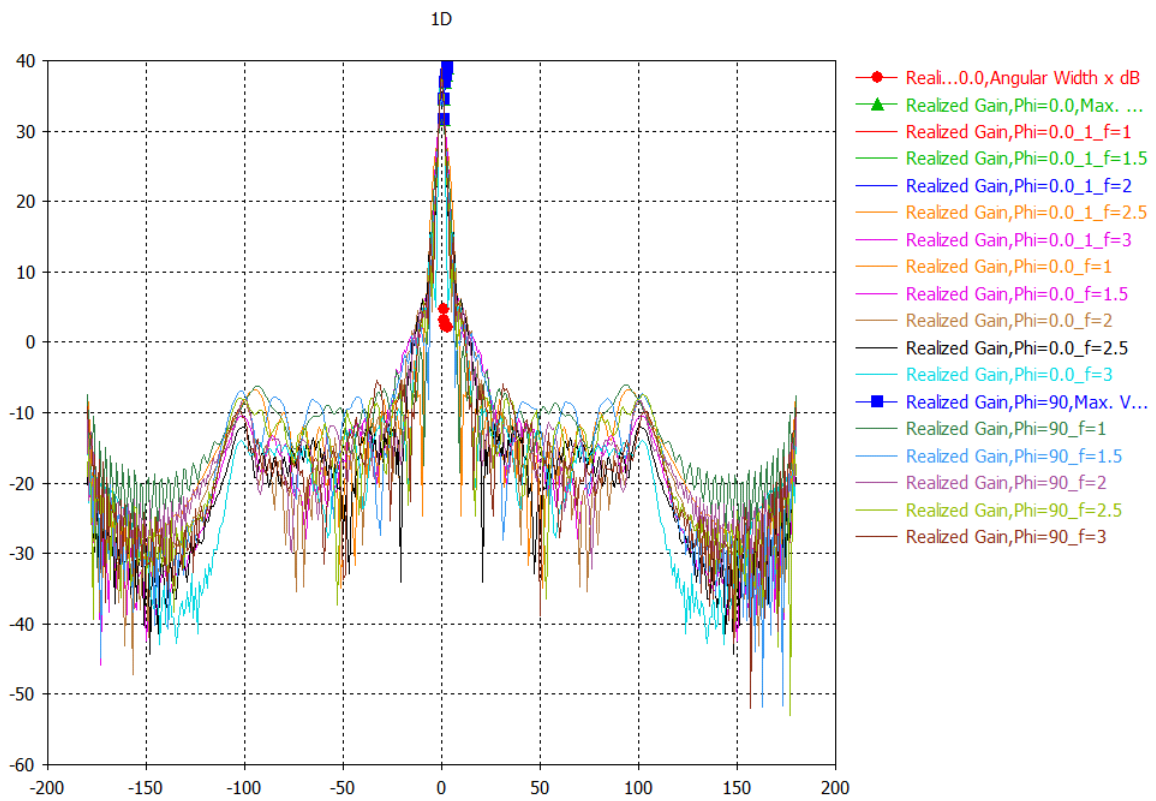


Figure 5-24: High Mesh 1% Convergence

In Figure 5-25, the 3D radiation patterns for the realized gain over the frequency range 1-3 GHz with 0.5 GHz step for the simple horn antenna feed are shown.

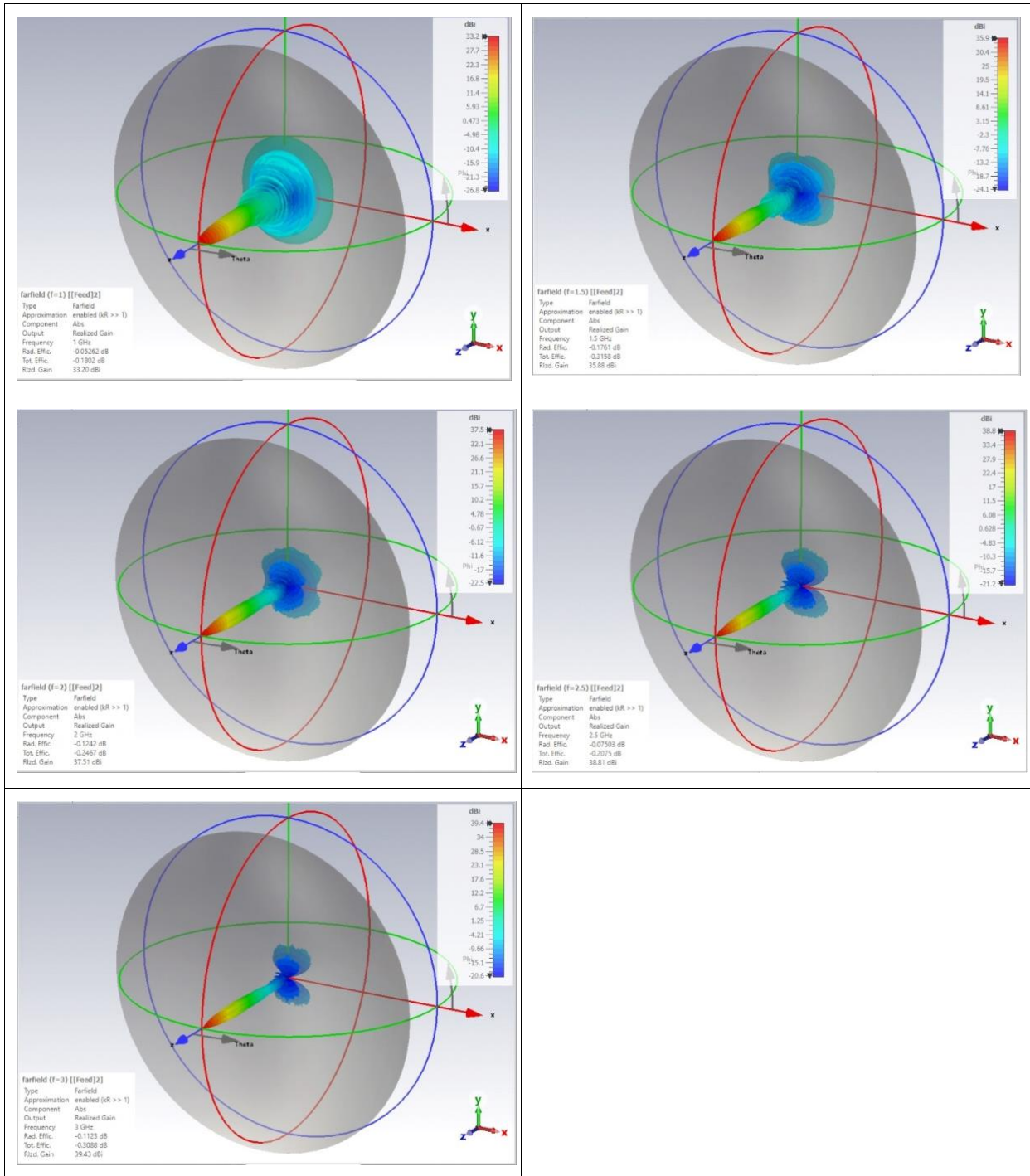


Figure 5-25: 3D Radiation patterns of the Dish antenna

5.3 Antenna dish reflector performance vs geometric anomalies

5.3.1 Introduction

In this report the performance of the 6 m dish antenna is studied versus various geometric anomalies that may be introduced during fabrication. The geometric anomalies taken into account are:

- Case 1: Hole at the center of the dish with radius varying in the range 1, 10, 20, 50, 100 mm.
- Case 2: Gap in the four quadrants of the parabolic dish both in “x” and “y” directions varying in the range 0.1, 1, 2, 5 mm.
- Case 3: Variation of the dish diameter +/- 10 mm.

5.4 Simulation results

5.4.1 Case 1

Due to the large diameter of the dish, its construction cannot be done as a whole from a single metal plate. Therefore, 4-8 sections of the plate that constitute the complete dish will be attached together in order to form it. From the mechanical / assembly point of view, a small hole at the center of the attachment of the separate sections may exist. In this case, this is exactly the simulation purpose in a swept manner with respect to the hole diameter.

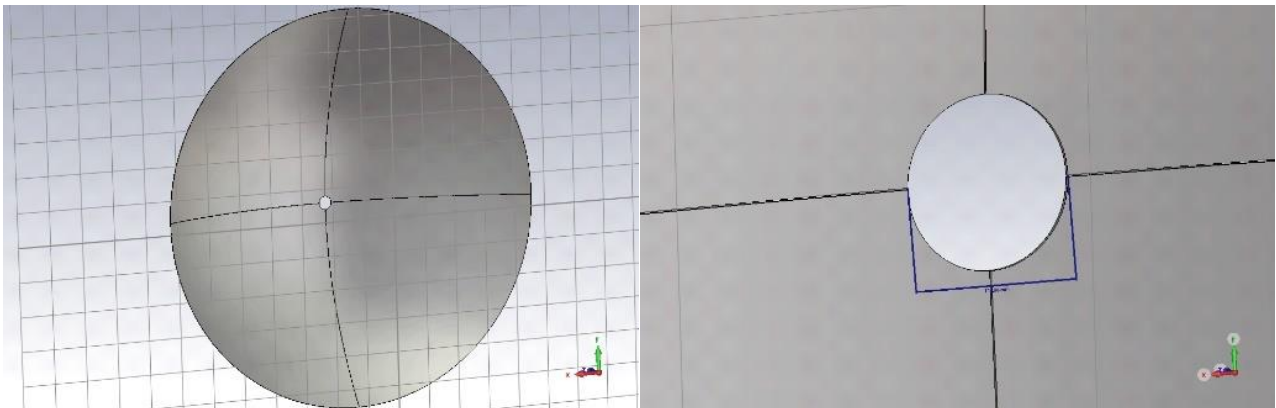


Figure 5-26: Parabolic dish geometry

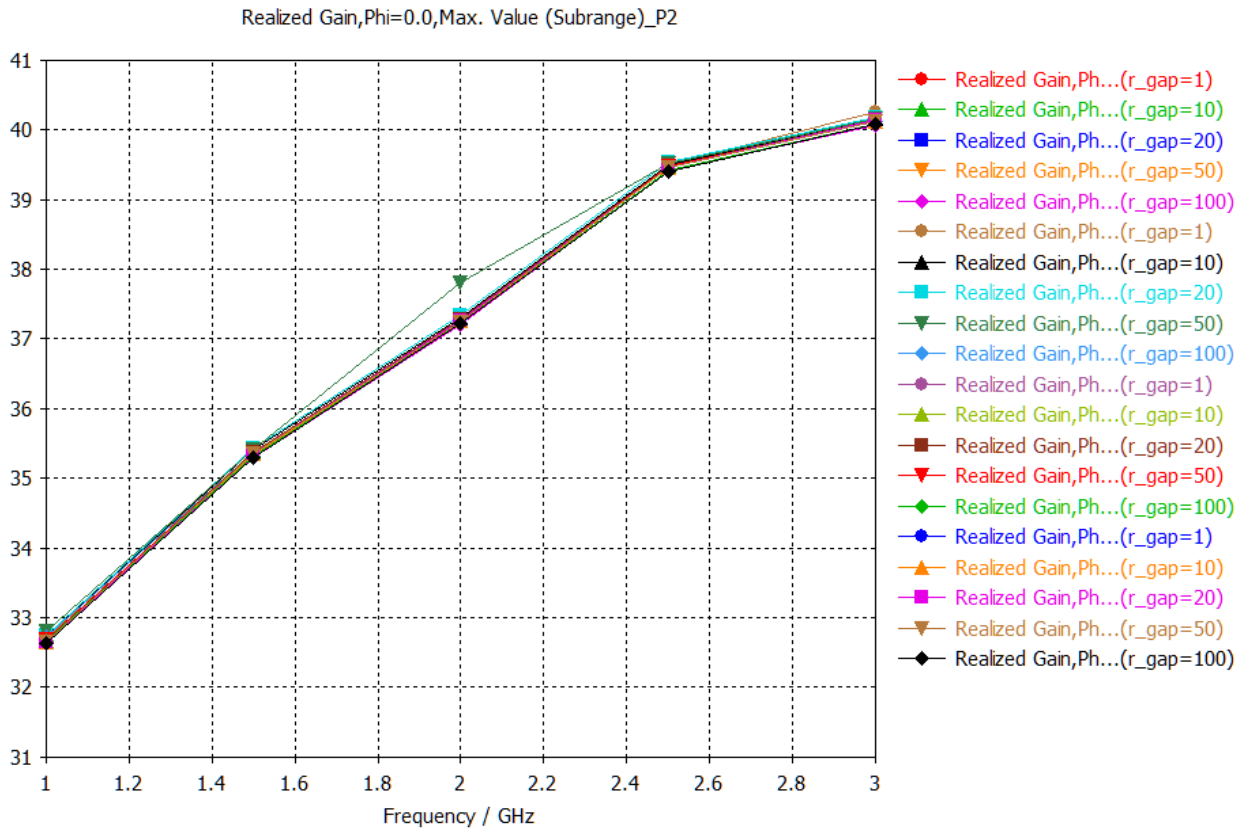
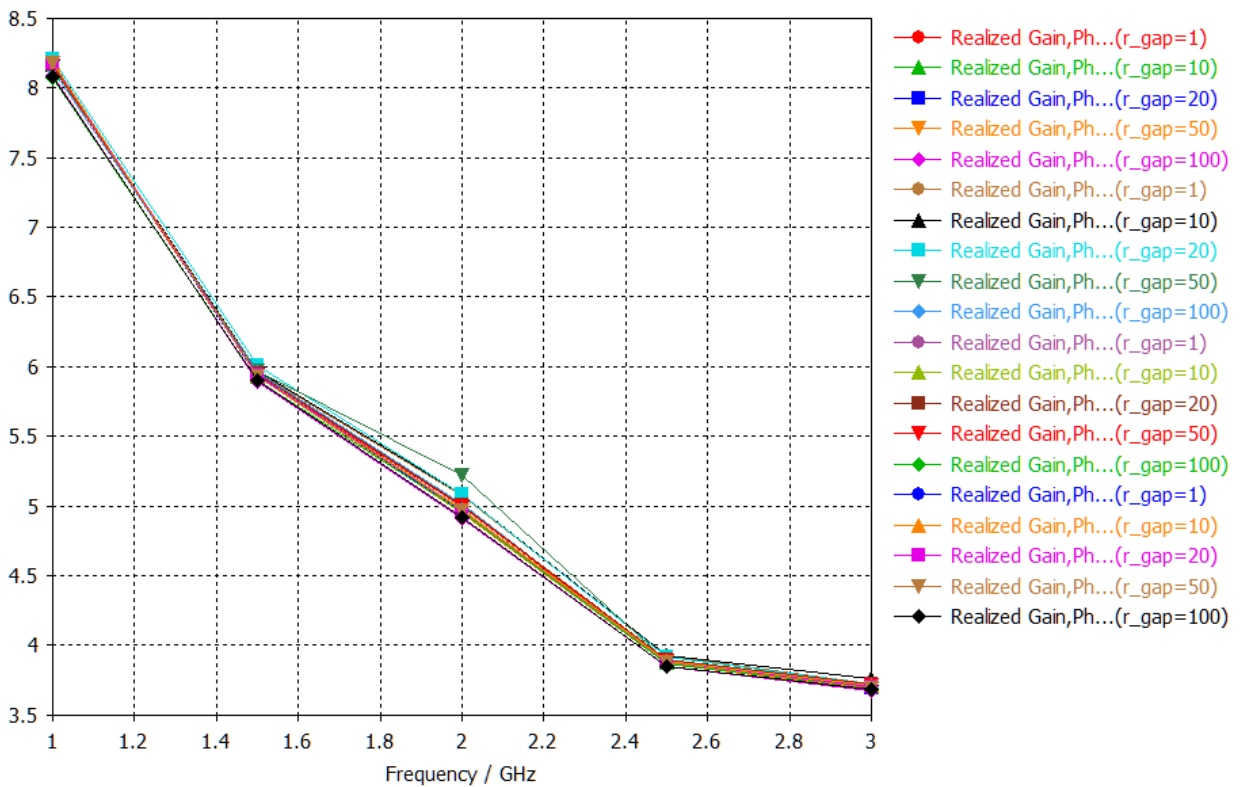


Figure 5-27: Gain variation vs frequency



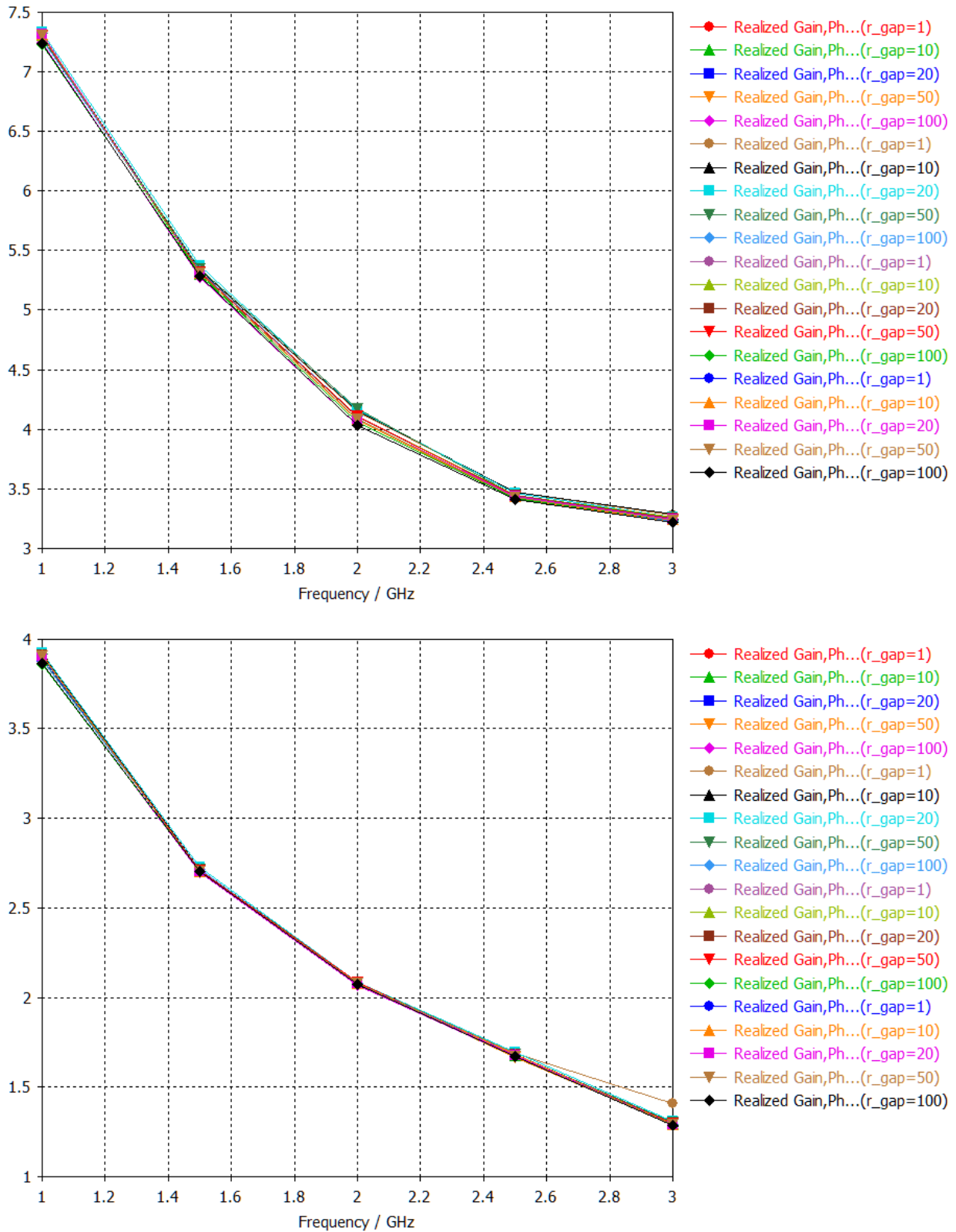


Figure 5-28: 12 dB, 10 dB, 3 dB beamwidths variation vs frequency

5.4.2 Case 2

Similarly, to Case 1 the separate metallic sections (in this example we assume four quadrants) may happen not to be attached ideally. Therefore, a small gap exists in between their junctions. In this case, this is exactly the simulation purpose in a swept manner with respect to the gap dimension.

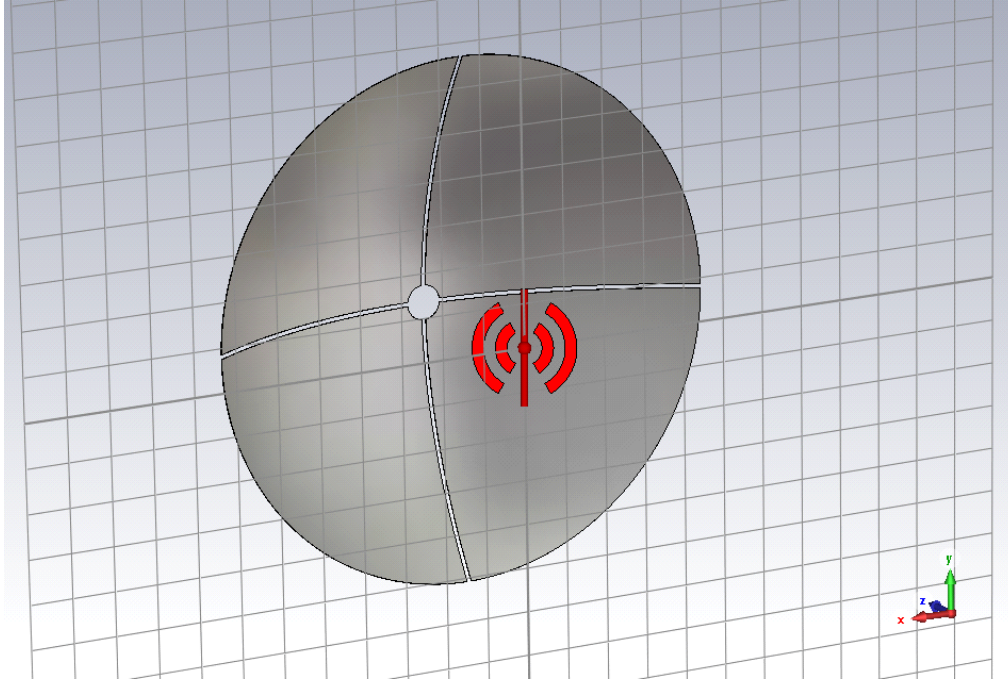


Figure 5-29: Parabolic dish geometry

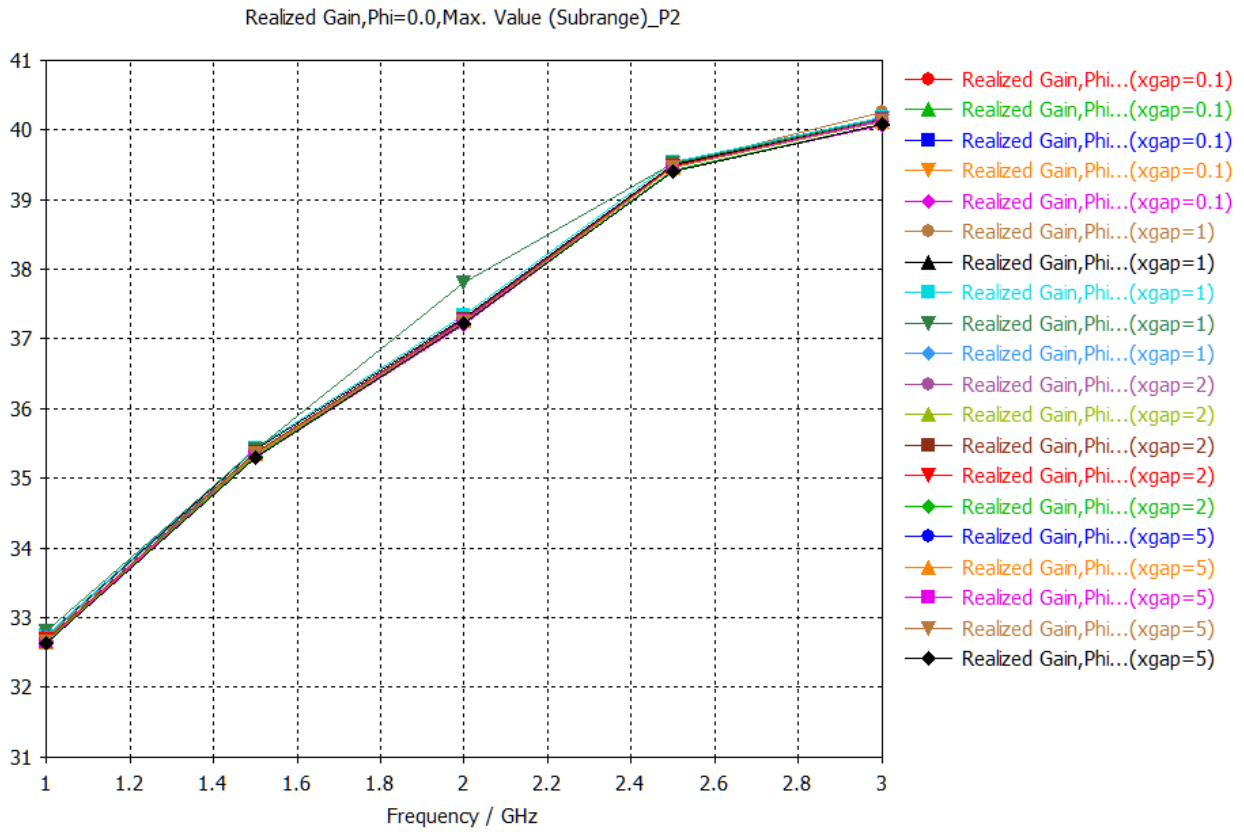
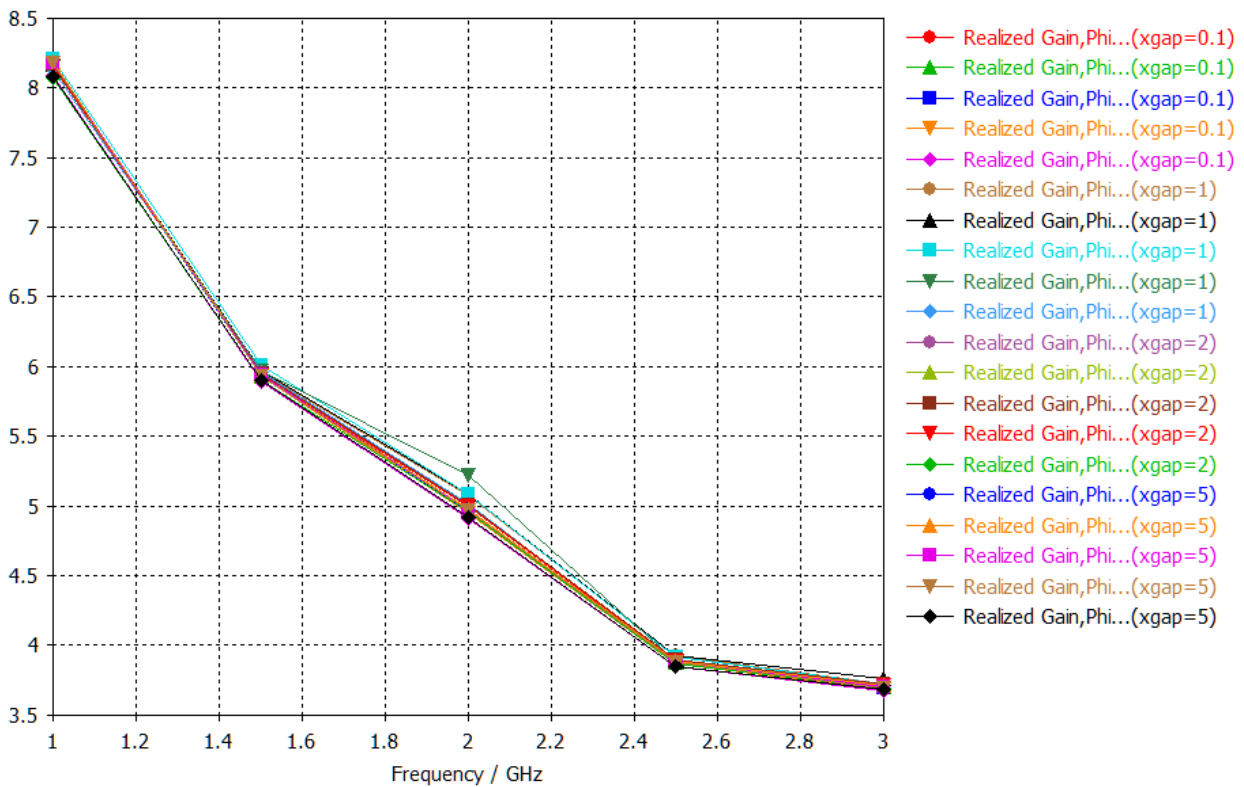


Figure 5-30a: Gain variation vs frequency



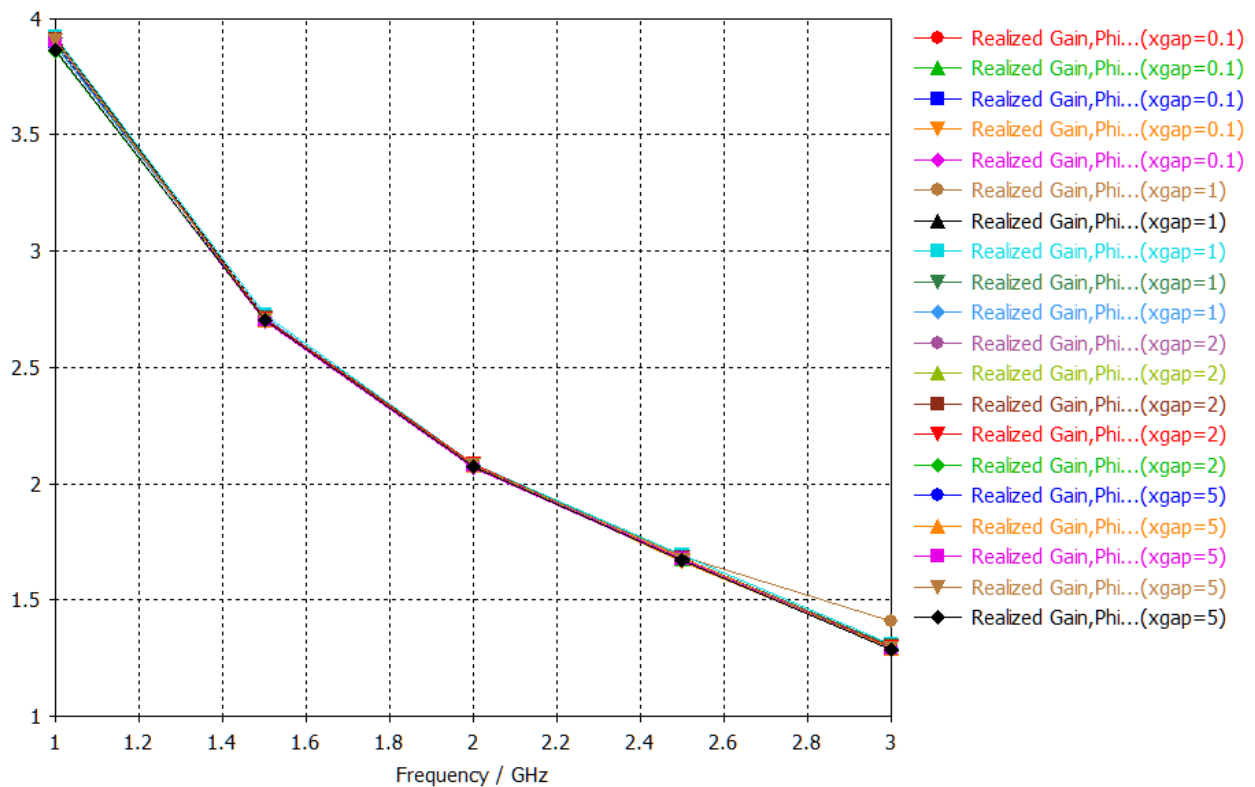
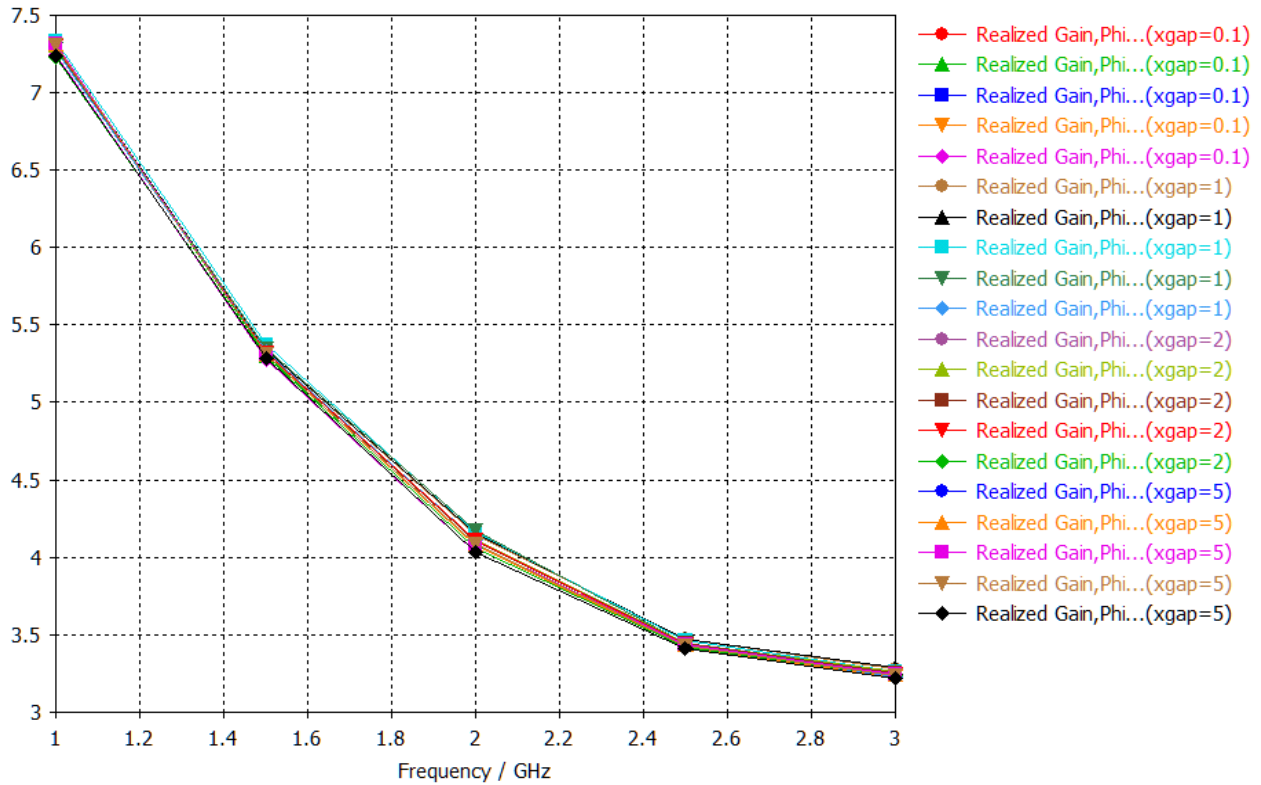


Figure 5-30b: 12 dB, 10 dB, 3 dB beamwidths variation vs frequency

5.4.3 Case 3

In this case the variation of the original dish diameter is taken into account. The mechanical tolerances are very small in this case, just +/-10 mm over a 6 meters dish diameter.

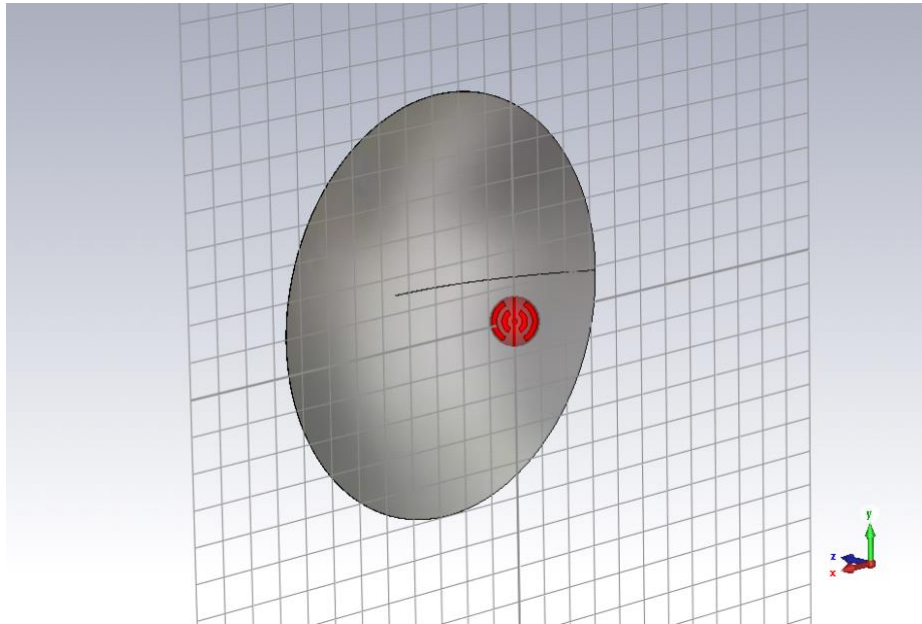


Figure 5-31: Parabolic dish geometry

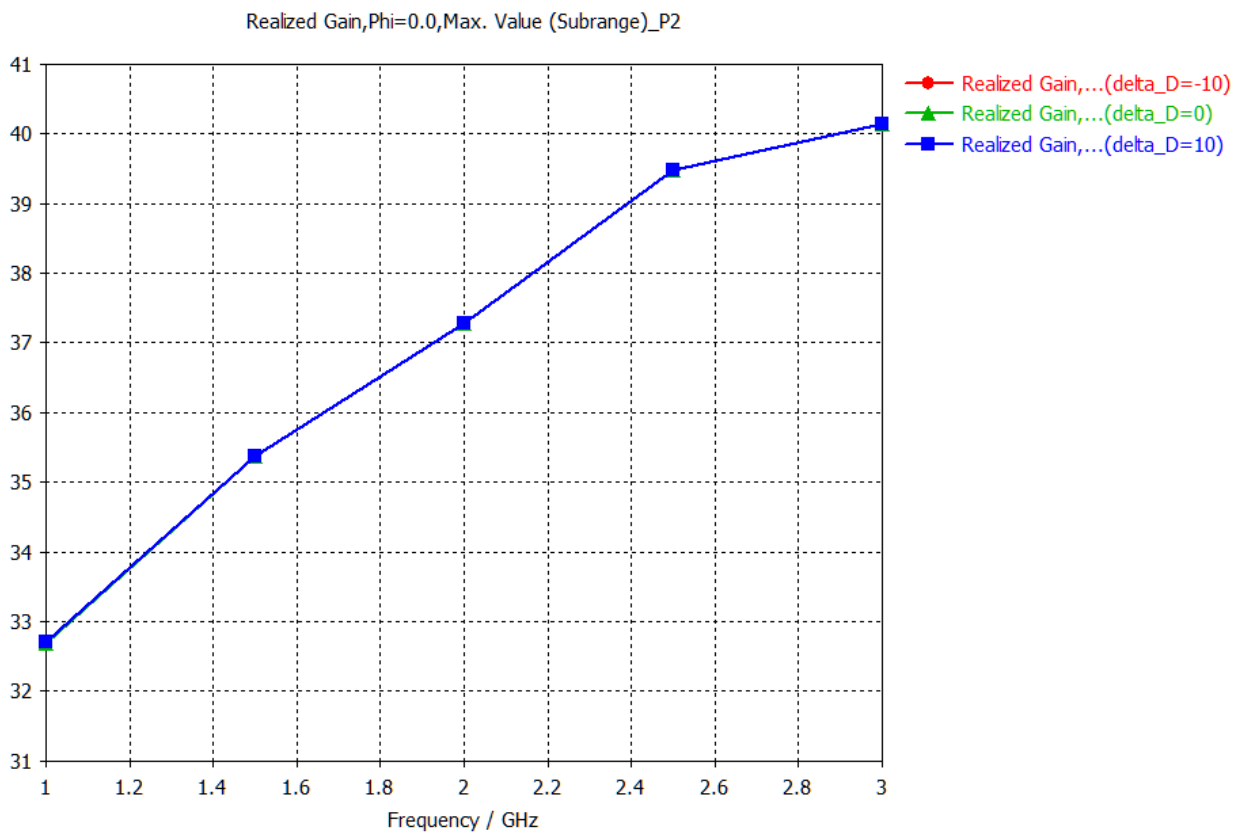
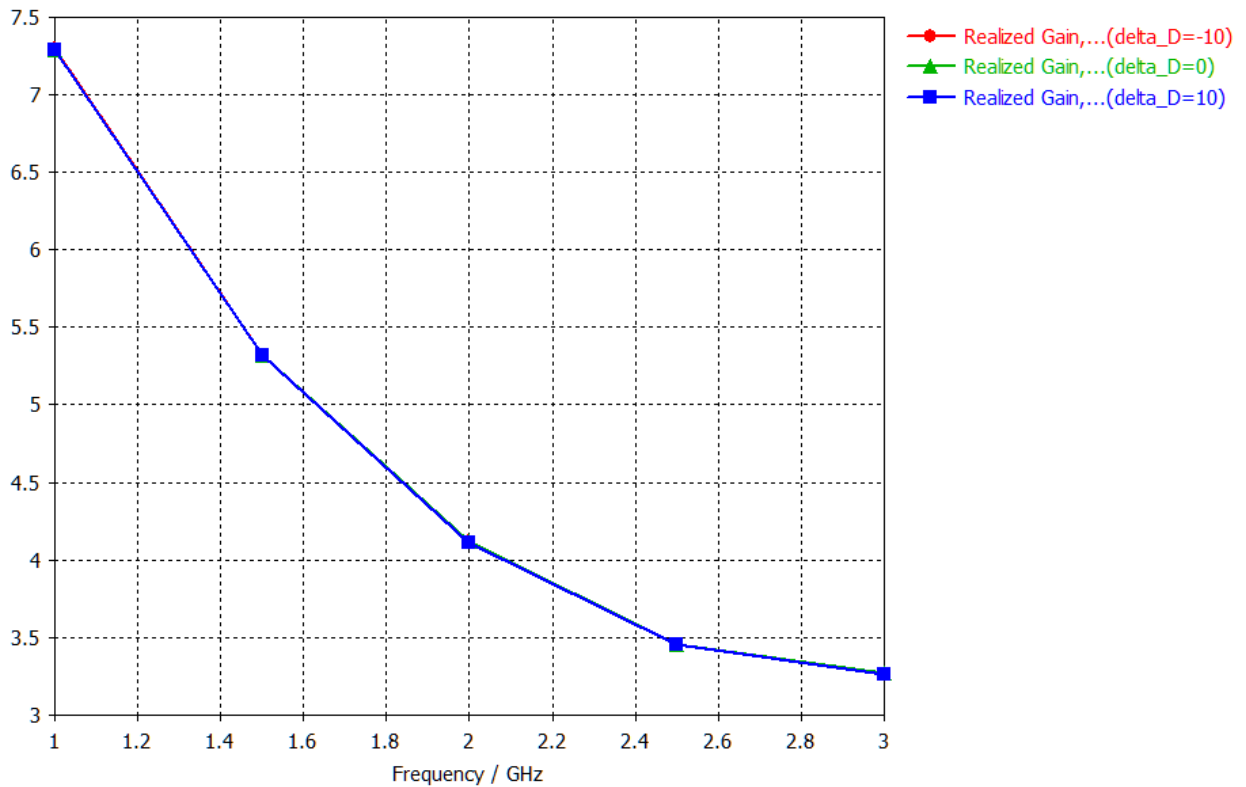
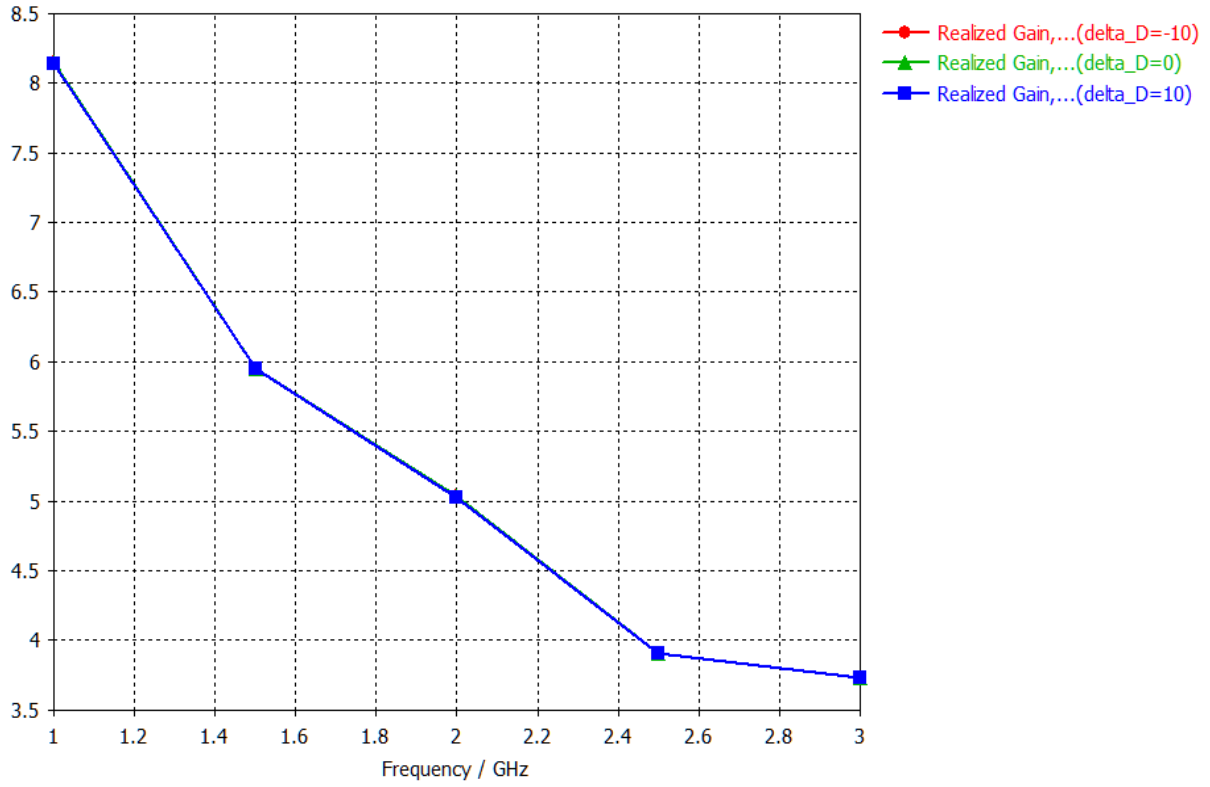


Figure 5-32: Gain variation vs frequency



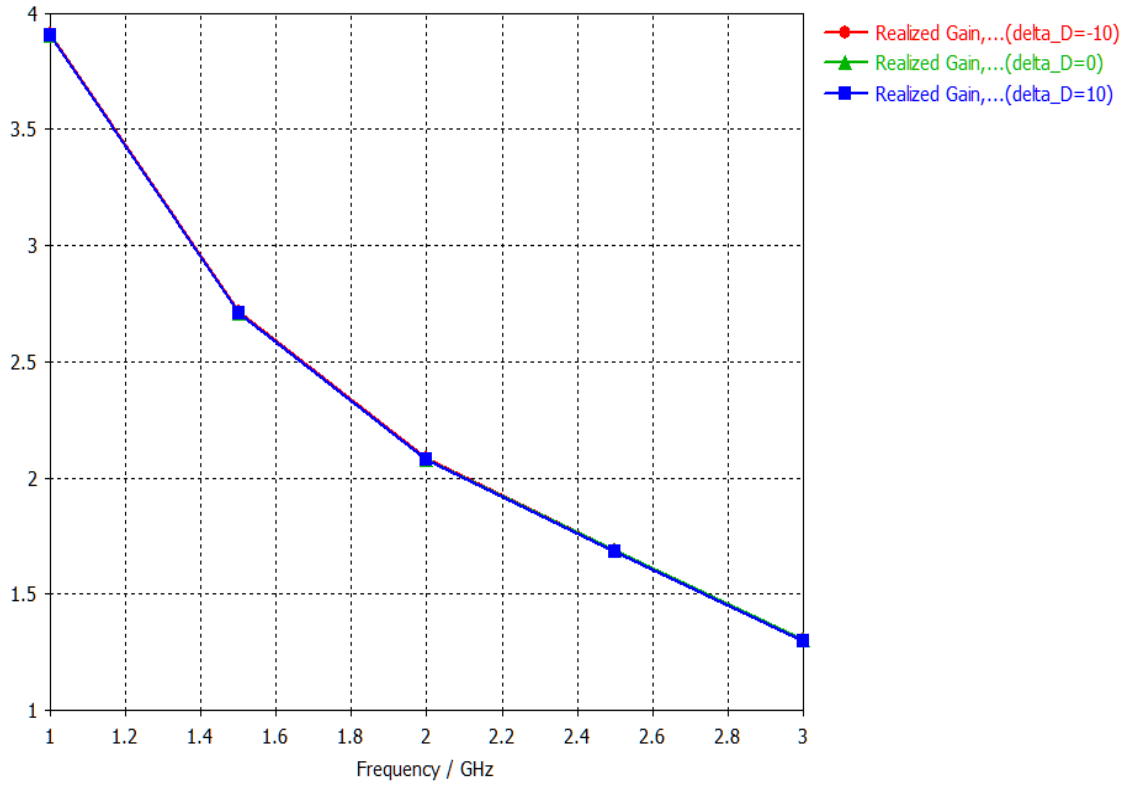


Figure 5-33: 12 dB, 10 dB, 3 dB beamwidths variation vs frequency

6 Additional Optimizations

An important aspect regarding the connection between the feed and the rest of the RF chain, is the connector type of the antenna feed. This component is used in order to connect the feed with the other parts of the chain (including the Low Noise Amplifiers and the filters). The connector is a coaxial waveguide consisting of a probe at the inner section of the connector, which transfers the signal, a dielectric medium in the middle and the ground shielding in the outer part. The outer part also comes with a thread in order to secure the connection with the rest of the RF chain.

There are numerous of RF connectors available in the market, however each of them has some very specific criteria, which reflect at the spectral efficiency of the system. That means that choosing a connector depends on the frequency range of the application. As it has been mentioned, the frequency range of ARGOS is 1-3 GHz based on the system requirements. The best quality connectors that could satisfy the system needs are the K-type and the N-type connectors.

6.1 K-type

K-type connectors, also known as 2.92mm connectors due to their diameter, are a niche category of RF connectors valued for their high-frequency performance and compact size. They offer a reliable connection for applications up to 40 GHz, making them suitable for various tasks in the microwave and millimeter wave range. Their small footprint allows for high-density packing in situations where space is limited, such as on circuit boards or within test equipment. While not as common as some other connector types like SMA, K-type connectors provide a valuable option for specific needs due to their combination of size, performance, and compatibility with certain other connector families like SMA and 3.5mm connectors.

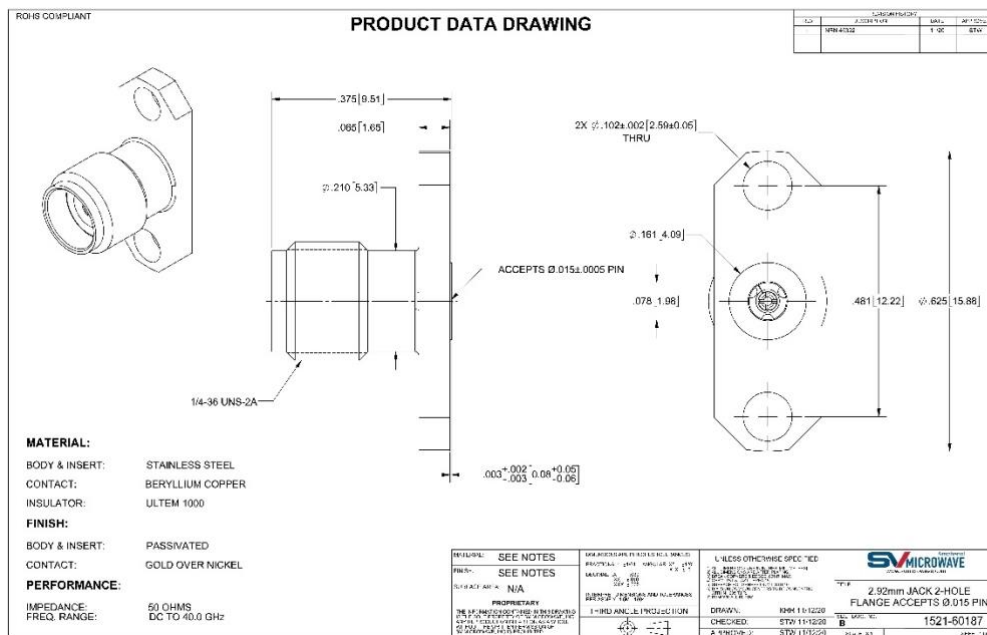


Figure 6-1: K-type Datasheet

6.2 N-type

N-type connectors are very common in RF applications, known for their durability, weather resistance, and reliable performance. Unlike K-type connectors designed for miniature applications, N-type connectors excel in medium-power handling and can operate effectively up to 11 GHz. Their secure threaded coupling mechanism ensures a vibration-resistant connection, making them ideal for outdoor environments or industrial settings. While not the most compact option, N-type connectors demonstrate low losses and offer a good balance between size and performance, accommodating various cable sizes like RG-8 and RG-58. Their widespread adoption across numerous industries, including broadcast, radar, and wireless communication systems, ensures easy availability and compatibility with existing equipment.

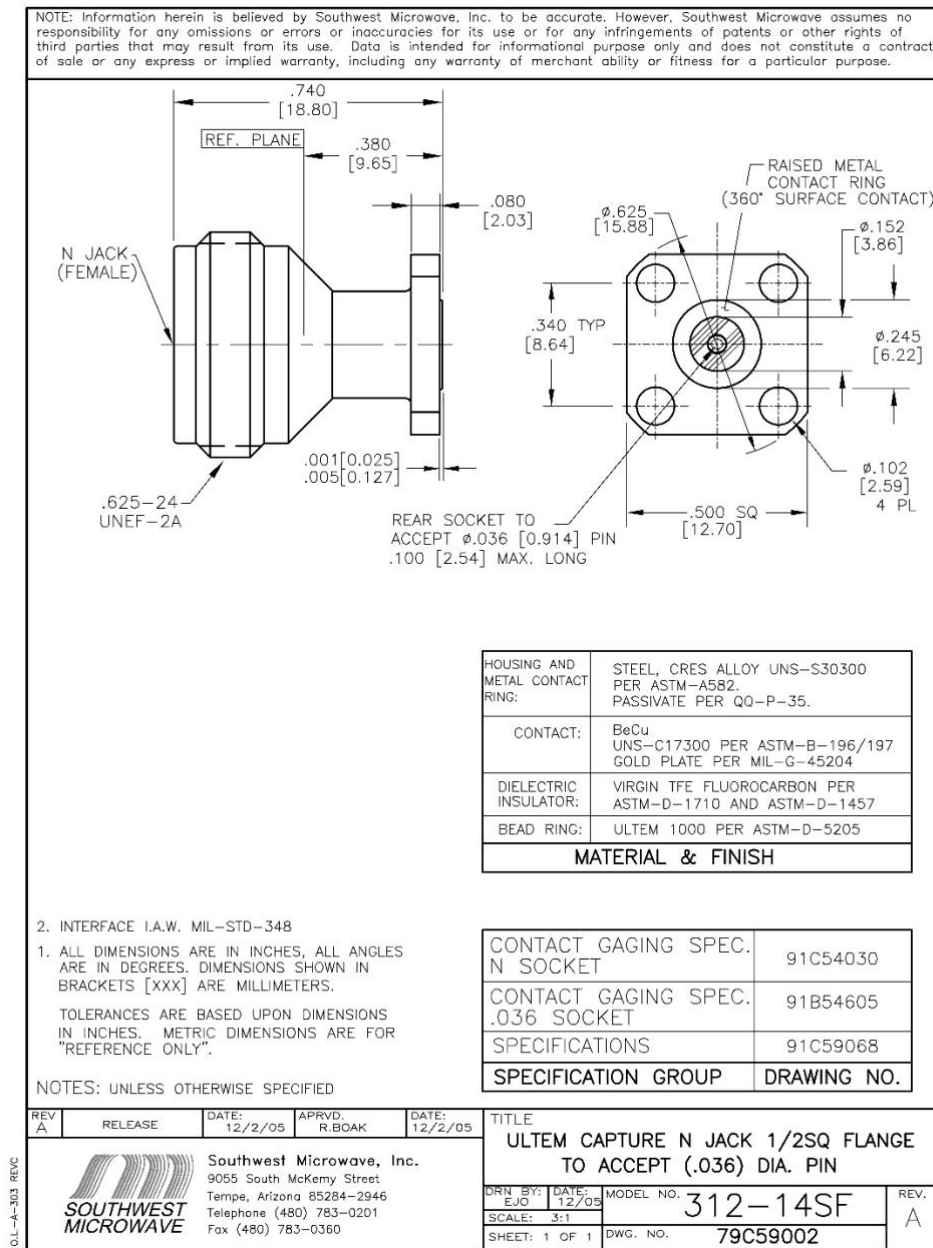


Figure 6-2: N-type Datasheet

6.3 Conclusions

In this report two alternative dual polarization wideband horn feeds have been studied and optimized by means of 3D electromagnetic simulation using the commercial software tool CST Microwave Studio. Both alternative feeds show good performance but the bell-shaped flared horn is slightly better with respect to radiation pattern metrics. The bell-shaped flared horn has been chosen to be the ARGOS antenna feed, because of the better characteristics in comparison with the straight flared horn, as presented in this report.

Several 3D electromagnetic comparisons have been presented in this report vs numerous parameters that affect either simulation accuracy or simulation time efficiency for both feeds and the complete dish antennas. Also, simulations have been presented concerning the effects on dish antenna performance versus mechanical tolerances.

Equipping an almost half-meter antenna such as ARGOS feed with the most suitable connector is crucial for ensuring reliable performance and long-term functionality.

N-type connectors are specifically designed for achieving lower levels of losses than the K-type connectors. Furthermore, the robust build and weatherproof design of N-type connectors make them ideal for outdoor systems like ARGOS. Their secure threaded coupling mechanism ensures a vibration-resistant connection, a vital factor for maintaining signal integrity. While K-type connectors boast a compact size, their limitations in power handling and durability may not be ideal for a half-meter antenna.

Finally, N-type connectors provide greater flexibility in cable selection. They are compatible with various cable sizes commonly used with antennas, offering more freedom to choose cables that optimize power handling and signal loss characteristics for your specific application. In conclusion, N-type connectors has been decided to equip ARGOS feed, because of their low losses, durability, and cable compatibility.